
Random Vibration Analysis of Deployable Solar Panels

Project Report
Yang-Che Lin

Aalborg University
Department of Mechanical and Manufacturing Engineering



AALBORG UNIVERSITY

STUDENT REPORT

Department of mechanical and manufacturing engineering

Aalborg University
Fibigerstraede 16
DK 9220 Aalborg øst
Tlf. 9940 9297
Fax 9815 1675

<http://www.m-tech.aau.dk/>

Title:

Random Vibration Analysis of Deployable Solar Panels

Theme:

Random Vibration

Project Period:

Spring Semester 2018

Project Group:

Fib 14

Participant(s):

Yang-Che Lin

Supervisor(s):

Sergey Sorokin

Copies: 0

Page Numbers: 67

Date of Completion:

20-08-2018

Abstract:

The folded solar panels will experience random vibration, which may cause fatigue problem, during the launch of a rocket. Thus, this project focuses on providing a basic understanding of random vibration and analytical solutions of several plate models in different condition. Random vibration analysis consists of two major parts, namely the analysis of vibration and random variable. The theories regarding vibration and random variable are reviewed and served as the basis of analytical analysis. The important method such as modal analysis and frequency domain analysis are also introduced. Finally, the plate model subjected to random excitation are presented with four different studies, namely study of mode, location, damping and material and discussed.

Contents

Preface	vii
1 Introduction	1
1.1 Problem Formulation and Approach	2
1.1.1 Random Excitation Study	4
2 Vibration Theory	7
2.1 Single Degree of Freedom System	7
2.2 Multiple Degree of Freedom System	11
2.2.1 Eigenvalue Problem	11
2.2.2 Orthogonality and Expansion Theorem	13
2.2.3 Modal Analysis	14
2.3 Plate Vibration	16
2.3.1 Equation of Motion and Boundary Condition	16
2.3.2 Free and Forced Vibration of Plate	18
3 Probability Theory	21
3.1 Random Variable	22
3.1.1 Expected Values	23
3.1.2 Moments of Random Variable	24
3.2 Time Domain Analysis	26
3.3 Frequency Domain Analysis	28
3.3.1 Power Spectral Density	29
3.3.2 Frequency Response Function	30
4 Analytical Analysis	31
4.1 Verification of Previous Study	32
4.2 Preliminary Study	35
4.3 Plate Model	37
4.3.1 Study of Mode Shape	39
4.3.2 Study of Location	40
4.3.3 Study of Damping	42
4.3.4 Study of Material	43
4.4 Summary and Discussion	43
5 Conclusion	45
Bibliography	47
A Beam Vibration	49
A.1 Equation of Motion and Boundary Condition	49
A.2 Free and Forced Vibration of Beam	50
A.2.1 Free Vibration	50
A.2.2 Forced Vibration	53

B Analytical Beam Model	55
B.1 Harmonic Base Excitation	55
B.2 White Noise Random Excitation	57
C Dirac Delta Function	63
C.1 Properties of Dirac Delta Function	63
C.2 Solution to Ordinary Differential Equation	64
D Reference Article	67

Preface

This project is conducted by student of Design of Mechanical Systems at Aalborg University from the 1st of February 2018 to 20th of August 2018. It is greatly appreciated for all the advice and assistance provided by the supervisors at Aalborg University and GOMSpace Denmark.

Aalborg University, August 20, 2018

Yang-Che Lin
<ylin16@student.aau.dk>

Chapter 1 Introduction

Satellite is a man-made machine which is launched into space and orbits around a body such as the Earth. It comes in various shapes and size and serves different purposes, for instance communication and navigation. For a satellite which is less than 10 kg, it is commonly referred as nano-satellite. During launching of a rocket, solar panels are folded into several layers and attached to the nano-satellite. Thereafter, the solar panels will unfold when they reach the correct orbit. A nano-satellite is shown in figure [1.1](#)



Figure 1.1: Nano-satellite with deployable solar panels [\[3\]](#)

The folded solar panels will experience random vibration, which may cause fatigue problem, during launching. Therefore, it is necessary to understand the characteristic of a solar panel subjected to random vibration in order to have a better design. This project focuses on providing a basic understanding of random vibration and analytical solutions of several relevant models. However, due to the limit of time, the scope of project is limited to linear analysis with stationary excitation. The problem formulation and approach can be found in section [1.1](#)

The random vibration analysis consists in two major parts, namely the analysis of vibration and random variable. The content of this project is structured in the same way. Firstly, the theory of vibration is reviewed in chapter [2](#) including single degree of freedom model, multiple degree of freedom model and plate vibration. The associate topic modal analysis plays an important role in the following analysis. Secondly, the theory of probability regarding random variable analysis is introduced in chapter [3](#). In random vibration, the excitation can not be modeled as a single time function and needs to be expressed by random variable. Thus, the idea of probability and corresponding time and frequency domain analysis method are introduced. Finally, the analytical analysis of several models based on the theories stated above is presented and discussed in chapter [4](#).

1.1 Problem Formulation and Approach

The sketch of deployable solar panel is shown in figure 1.2. The support pins are not bounded with the panel, which indicates that they may lose contact due to vibration during rocket launching process. If the contact is lost, it may cause damage on the solar panels through possible impacts. Therefore, a pretension force is applied at the center of panel to prevent this issue. However, it is difficult to determine if the pretension force is strong enough to hold the panels since the system response originated from random vibration still needs to be analyzed.

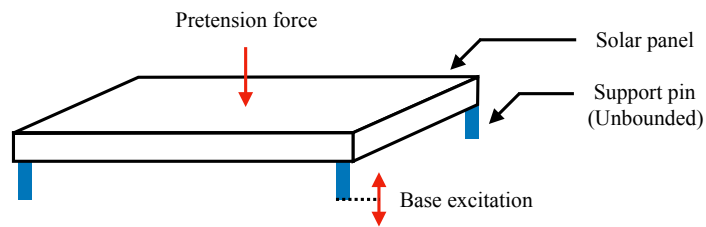


Figure 1.2: Sketch of deployable solar panel

The analysis is limited to linear analysis, therefore superposition principle is applicable. The approach for solving this problem is to divide the system into two subsystems as shown in figure 1.3. The first subsystem is subjected to the pretension force at center only, which leads to a certain level of displacement and force. The second subsystem is subjected to the random excitation only, which results in acceleration response and hence displacement and force. Thus, the level of force caused by random excitation is essential. If the resultant force caused by random excitation is larger than pretension force, the support pins might loss contact and the system needs to be adjusted.

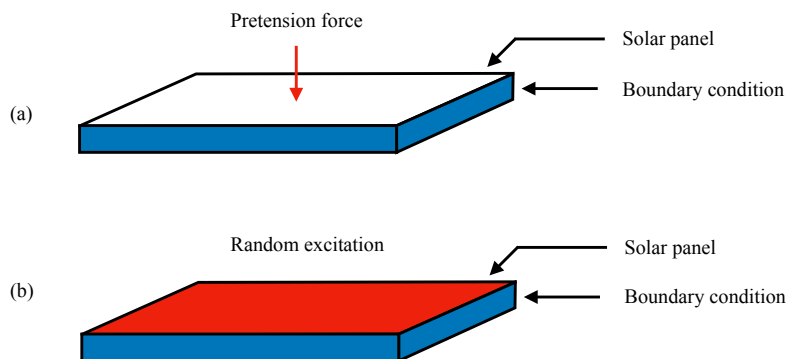


Figure 1.3: Sketch of (a) subsystem with pretension force (b) subsystem with random vibration

An overview on the approach used is illustrated in figure 1.4.

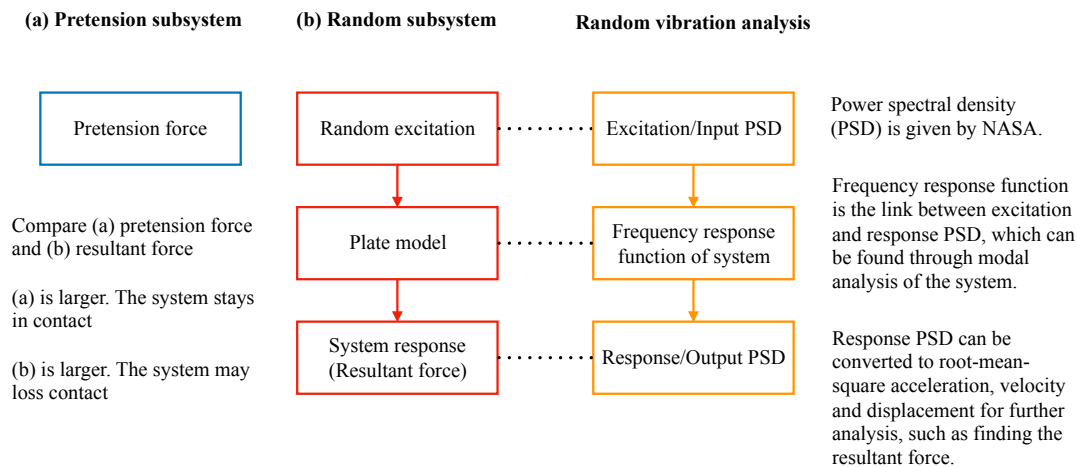


Figure 1.4: Illustration of approach

For the pretension subsystem, the pretension force is given by GOMSpace as 40 Newtons. This value is used as a reference in the following analysis. Since the project is focus on the characteristic of random vibration system, only the second subsystem response is studied in the following sections.

For the random subsystem, there are several elements need to be considered in order to conduct a random vibration analysis, such as the random excitation and plate model including boundary condition, material and damping. A brief explanation is shown in the list below. By making use of modal analysis, the system characteristic can be found and frequency response function can be formulated. Frequency response function is the link between random excitation PSD and response PSD. Once response PSD is found, the root-mean-square acceleration, velocity and displacement can also be known, and hence the resultant force. The detail regarding modal analysis can be found in chapter 2 and see chapter 3 for frequency response function and the relation with excitation and response PSD.

1. Excitation : Two random base excitation are considered in this project, namely 'white noise' and 'designed random excitation'. The white noise is used for a basic understanding of the system response and the designed random excitation is recommended by the company GOMSpace and NASA for nano-satellite. A more detailed study can be found in section 1.1.1
2. Model : The plate model is chosen for its better representation of a solar panel.
3. Boundary condition : The real boundary condition of solar panel is difficult to describe in a mathematical model. Through a brief inquiry with GOMSpace, the boundary condition of plate model is assumed to be simply supported along four edges.
4. Material : Due to confidentiality, the material used for analytical analysis is not the actual property of solar panels but aluminum.
5. Damping : According to GOMSpace, a damping ratio of 0.05 is commonly used for their projects. The real damping of the system is, however, difficult to determine. A damping ratio of 0.05 is considered as an initial start in this project. Additionally, a study of damping is also conducted in chapter 4

1.1.1 Random Excitation Study

There are two random excitation or input used in this project, both of them are studied in this section. The first one is known as white noise excitation, which has all components across a certain range of frequency contributed equally. That is, the auto-spectral density function can be expressed as a constant. Equation 1.1 shows the acceleration white noise used in the following sections. It should be noted that the unit is g^2/Hz , which is commonly used for acceleration random excitation.

$$S_{XX}(\omega) = S_0 = 0.1 \quad \text{for } f = 20 \text{ to } 2000 \text{ (Hz)} \quad (1.1)$$

The second one is referred as designed random excitation in the following sections. For an object less than 22.7 kg such as nano-satellite, the excitation acceleration spectral density (ASD) is given by 7 and shown in figure 1.5. The equations in this section are mainly based on 7 and 4.

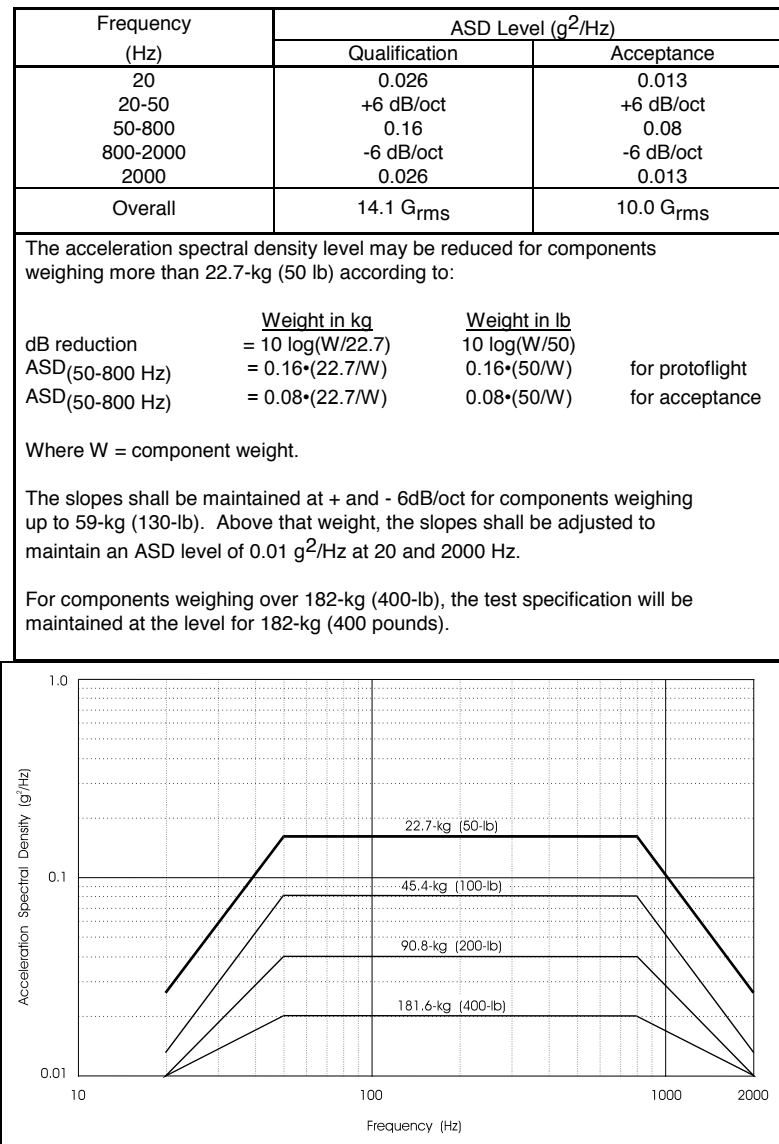


Figure 1.5: Generalized Random Vibration Test Levels Components (ELV) 7

where decibel dB is a dimensionless value commonly used to express the ratio of two values. If ASD_h and ASD_l represents the ASD value at higher and lower frequency, respectively, then the dB here can be defined as

$$dB = 10 \log \left(\frac{ASD_h}{ASD_l} \right) \quad (1.2)$$

According to the figure, the excitation can be categorized as three parts. The first part has positive slope, the second one is constant and the third one has negative slope. In order to take this ASD as input in analytical analysis, it is necessary to formulate the equations to describe its behavior. The constant part is not a problem, however the ones with slope given in dB/oct need to be reformulated.

Firstly, the number of octaves is found by

$$\text{Number of octaves : } \#Oct = \frac{\log \left(\frac{f_h}{f_l} \right)}{\log(2)} \quad (1.3)$$

where f_h and f_l represent the higher and lower frequency, respectively. Secondly, the level of dB is found by

$$dB = \text{Slope} \cdot \#Oct = 10 \log \left(\frac{ASD_h}{ASD_l} \right) \quad (1.4)$$

Thus, if s is used to denote the slope, the ASD magnitude of desired frequency can be found by

$$\begin{aligned} \frac{ASD_h}{ASD_l} &= 10 \left[\left(\frac{s}{10} \right) \left(\frac{\log \left(\frac{f_h}{f_l} \right)}{\log(2)} \right) \right] \\ &= \left(\frac{f_h}{f_l} \right)^{\frac{s}{10 \log(2)}} \end{aligned} \quad (1.5)$$

Finally, based on figure 1.5 and equation 1.5 the *Magnitude of ASD* (g^2/Hz) of designed random excitation can be expressed as

$$\text{Magnitude of ASD} = \begin{cases} (0.026) \cdot \left(\frac{f}{20} \right)^{\frac{6}{10 \log(2)}} & \text{for } f = 20 \text{ to } 50 \text{ (Hz)} \\ 0.16 & \text{for } f = 50 \text{ to } 800 \text{ (Hz)} \\ (0.16) \cdot \left(\frac{f}{800} \right)^{\frac{-6}{10 \log(2)}} & \text{for } f = 800 \text{ to } 2000 \text{ (Hz)} \end{cases} \quad (1.6)$$

Chapter 2 Vibration Theory

This chapter presents basic theory of vibration and provides the necessary theoretical background for the following chapters regarding random vibration and analytical analysis. The content, including theory and equation, is mainly based on [9], [10] and [2].

Firstly, the simplest vibration model, namely spring-mass system or single degree of freedom system, is introduced. Both undamped and damped model in free vibration are described. Thereafter, the multiple degree of freedom model along with one of the most commonly used method in finding system response, modal analysis, are introduced. Finally, the vibration of plate with various boundary conditions is presented. The beam vibration theory can also be found in appendix A.

2.1 Single Degree of Freedom System

An illustration of the simplest vibration system made by spring-mass system, also referred as single degree of freedom(SDOF) system, is shown in figure 2.1. The vibration system is said to experience free vibration if it oscillates due to the initial disturbance only and no external force acting on it. That is, if an initial displacement x is applied on the mass m then release it afterwards, the mass will undergo free vibration.

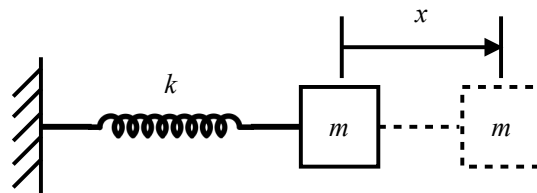


Figure 2.1: Single degree of freedom system

In order to find the equation of motion of the system, Newton's second law of motion is utilized. That is, the rate of change of momentum of a mass is equal to the force acting on it. Therefore, if a constant mass m is moved a distance $\vec{x}(t)$ by a force $\vec{F}(t)$ in the same direction, Newton's second law of motion gives

$$\vec{F}(t) = m \cdot \frac{d^2\vec{x}(t)}{dt^2} = m \cdot \ddot{\vec{x}}(t) \quad (2.1)$$

Figure 2.2 shows the free body diagram of the system. It can be seen that the force acting on the mass are $-k \cdot x(t)$ and $m \cdot \ddot{x}(t)$, which are caused by the spring elongation and mass acceleration, respectively. It should be noted that the negative sign indicates the direction of spring force is the opposite of the mass motion.

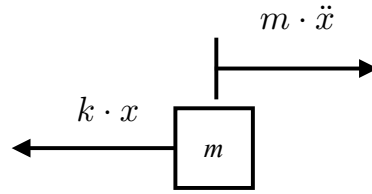


Figure 2.2: Free body diagram of single degree of freedom system

Therefore, the equation of motion for free vibration of undamped single degree of freedom system is given as

$$F(t) = -k \cdot x(t) = m \cdot \ddot{x}(t) \quad (2.2)$$

or

$$m \cdot \ddot{x}(t) + k \cdot x(t) = 0 \quad (2.3)$$

The response of the system can be obtained by assuming

$$x(t) = C \cdot e^{st} \quad (2.4)$$

where C and s are constants. By substituting equation 2.4 into 2.3, it yields

$$C(ms^2 + k) = 0 \quad (2.5)$$

Since C can not be zero, otherwise it would give a trivial solution, the rest part of the equation must be zero. Thus,

$$\begin{aligned} (ms^2 + k) &= 0 \\ \rightarrow s &= \pm \left(-\frac{k}{m}\right)^{\frac{1}{2}} \\ \rightarrow s &= \pm i\omega_n \end{aligned} \quad (2.6)$$

where $i = \sqrt{-1}$ and ω_n , known as natural frequency, is

$$\omega_n = \left(\frac{k}{m}\right)^{\frac{1}{2}} \quad (2.7)$$

Substitute the result of equation 2.6 into 2.4 gives

$$\begin{aligned} x(t) &= C_1 \cdot e^{s_1 t} + C_2 \cdot e^{s_2 t} \\ &= C_1 \cdot e^{i\omega_n t} + C_2 \cdot e^{-i\omega_n t} \end{aligned} \quad (2.8)$$

Equation 2.8 can be rewritten by making use of Euler's formula, which states for any real number x ,

$$e^{\pm ix} = \cos(x) \pm i \sin(x) \quad (2.9)$$

Hence,

$$x(t) = A_1 \cos(\omega_n t) + A_2 \sin(\omega_n t) \quad (2.10)$$

where A_1 and A_2 are new constants to be determined by initial condition of the system. If the initial conditions are given as

$$\begin{aligned} x(0) &= x_0 \\ \dot{x}(0) &= \dot{x}_0 \end{aligned} \quad (2.11)$$

A_1 and A_2 can be solved and equation [2.10](#) becomes

$$x(t) = x_0 \cos(\omega_n t) + \frac{\dot{x}_0}{\omega_n} \sin(\omega_n t) \quad (2.12)$$

However, if a model consists only spring-mass system, it would oscillate forever. Thus, it is necessary to consider energy dissipation term when modeling a real world system. The most common energy dissipation term is known as viscous damping force. An illustration of single degree of freedom system with damper is shown in figure [2.3](#).

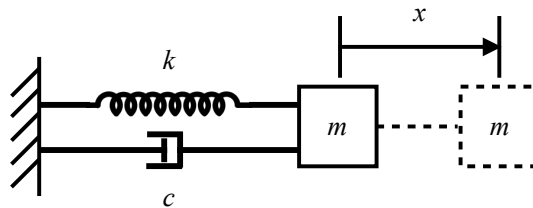


Figure 2.3: Single degree of freedom system with damper

The viscous damping force is proportional to velocity and acting on the opposite direction of velocity. It can be expressed as $F(t) = c \cdot \dot{x}$, where c is damping constant. The free body diagram is shown in figure [2.4](#).

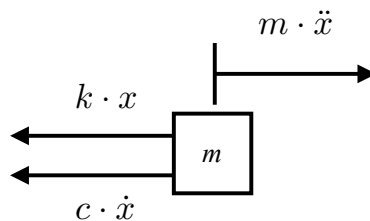


Figure 2.4: Free body diagram of single degree of freedom system with damper

By making use of Newton's second law, the equation of motion can be obtained as

$$m \cdot \ddot{x}(t) + c \cdot \dot{x}(t) + k \cdot x(t) = 0 \quad (2.13)$$

By following the similar procedure, the response of damped SDOF system can be found as

$$x(t) = C_1 \cdot e^{\left(-\frac{c}{2m} + \sqrt{\left(\frac{c}{2m}\right)^2 - \frac{k}{m}}\right)t} + C_2 \cdot e^{\left(-\frac{c}{2m} - \sqrt{\left(\frac{c}{2m}\right)^2 - \frac{k}{m}}\right)t} \quad (2.14)$$

Based on the expression of equation [2.14](#), the critical damping c_c and damping ratio ζ are defined as

$$\begin{aligned} \left(\frac{c_c}{2m}\right)^2 - \frac{k}{m} &= 0 \\ \rightarrow c_c &= 2\sqrt{km} = 2m\omega_n \\ \zeta &= \frac{c}{c_c} = \frac{c}{2m\omega_n} \end{aligned} \quad (2.15)$$

Equation [2.14](#) can be solved by considering three different cases, namely underdamped system ($\zeta < 1$), critically damped system ($\zeta = 1$) and overdamped system ($\zeta > 1$), with initial conditions. During the derivation of solution, sometimes damped natural frequency $\omega_d = \omega_n \cdot \sqrt{1 - \zeta^2}$ is used instead of natural frequency ω_n . A response comparison of three different cases are shown in figure [2.5](#).

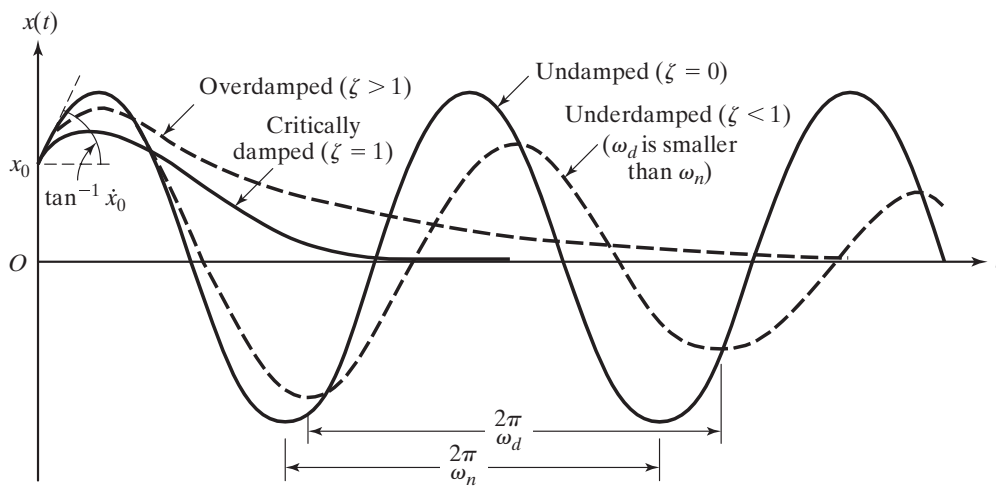


Figure 2.5: Response comparison of three different type of damping ratio [\[9\]](#)

2.2 Multiple Degree of Freedom System

For a multiple degree of freedom vibration system, the equation of motion would be a set of coupled ordinary differential equations. The solution can be very complicated when considering a high number of degree of freedom. Therefore, a method known as modal analysis is often used to solve this type of problem.

In modal analysis, the response is expressed as a linear combination of the normal modes of the system. It results in a set of uncoupled ordinary differential equations. Thus, it is equivalent as solving a number of single degree of freedom system. The procedure of modal analysis is demonstrated in this section.

2.2.1 Eigenvalue Problem

Consider the equation of motion of a multiple degree of freedom undamped vibration system.

$$[m] \cdot \ddot{\vec{x}} + [k] \cdot \vec{x} = 0 \quad (2.16)$$

where \vec{x} and $\ddot{\vec{x}}$ are the vector of displacement and acceleration, respectively. Matrix $[m]$ and $[k]$ consists the corresponding mass and spring constant. The solution can be found by assuming

$$x_i(t) = X_i \cdot T(t), \quad i = 1, 2, \dots, n \quad (2.17)$$

where X_i is a constant and $T(t)$ is a function of time. The vector \vec{X} , which known as mode shape, is the combination of X_i . Substituting equation [2.17](#) into [2.16](#), it becomes

$$[m] \vec{X} \ddot{T}(t) + [k] \vec{X} T(t) = 0 \quad (2.18)$$

Equation [2.18](#) can be rearranged and rewritten in scalar form of n separated equations.

$$-\frac{\ddot{T}(t)}{T(t)} = \frac{\left(\sum_{j=1}^n k_{ij} X_j \right)}{\left(\sum_{j=1}^n m_{ij} X_j \right)}, \quad i = 1, 2, \dots, n \quad (2.19)$$

Since the left hand side of equation [2.19](#) only depends on time t and the right hand side only depends on the index i , both sides must be equal to a constant. The constant is assumed to be ω^2 . Thus the left hand side of the equation becomes

$$\ddot{T}(t) + \omega^2 T(t) = 0 \quad (2.20)$$

and the solution can be found as

$$T(t) = C_1 \cos(\omega t + \phi) \quad (2.21)$$

where C_1 and ϕ are constants and represent the amplitude and phase angle, respectively. While the right hand side of equation 2.19 becomes

$$\sum_{j=1}^n (k_{ij} - \omega^2 m_{ij}) X_j = 0, \quad i = 1, 2, \dots, n \quad (2.22)$$

or

$$([k] - \omega^2 [m]) \vec{X} = 0 \quad (2.23)$$

Equation 2.23 is known as eigenvalue problem. ω is the natural frequency and ω^2 is the eigenvalue. In order to find the non-trivial solution, the determinant Δ of coefficient matrix must be zero. Thus,

$$\Delta = |[k] - \omega^2 [m]| = 0 \quad (2.24)$$

To solve equation 2.24, it is in fact finding the roots of a polynomial equation, which gives n values of eigenvalue ω_i^2 and natural frequencies ω_i . That is, $\omega_1, \omega_2, \dots$, and ω_n .

Once the eigenvalues are found, the corresponding mode shapes $\vec{X}^{(i)}$ can also be determined. It should be noted that the mode shapes are arbitrary chosen, therefore it actually represents the shape instead of the real displacement. An illustration of mode shapes of three degree of freedom system is shown in figure 2.6. Different mode corresponds different eigenvalue.

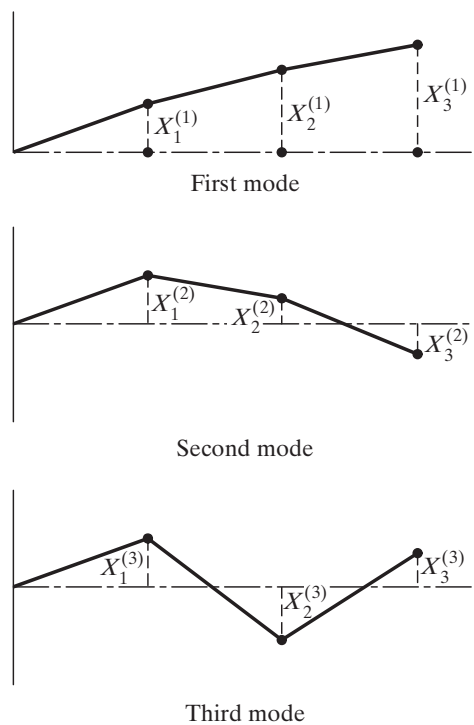


Figure 2.6: Mode shapes of three degree of freedom system. [9]

2.2.2 Orthogonality and Expansion Theorem

One of the most important property of mode shape is orthogonality. For two vectors $\vec{X}^{(i)}$ and $\vec{X}^{(j)}$, they are said to be orthogonal if $\vec{X}^{(i)} \cdot \vec{X}^{(j)} = 0$. Consider equation [2.23](#) and rewritten with two different natural frequencies ω_i and ω_j as

$$\begin{aligned}\omega_i^2 [m] \vec{X}^{(i)} &= [k] \vec{X}^{(i)} \\ \omega_j^2 [m] \vec{X}^{(j)} &= [k] \vec{X}^{(j)}\end{aligned}\quad (2.25)$$

By considering the symmetry of $[m]$ and $[k]$ and premultiplying the first part of equation [2.25](#) with $\vec{X}^{(j)T}$ and the second part with $\vec{X}^{(i)T}$, the equation becomes

$$\begin{aligned}\omega_i^2 \vec{X}^{(j)T} [m] \vec{X}^{(i)} &= \vec{X}^{(j)T} [k] \vec{X}^{(i)} \equiv \vec{X}^{(i)T} [k] \vec{X}^{(j)} \\ \omega_j^2 \vec{X}^{(i)T} [m] \vec{X}^{(j)} &\equiv \omega_j^2 \vec{X}^{(j)T} [m] \vec{X}^{(i)} = \vec{X}^{(i)T} [k] \vec{X}^{(j)}\end{aligned}\quad (2.26)$$

By subtracting the second part of equation [2.26](#) from the first part, it becomes

$$\left(\omega_i^2 - \omega_j^2\right) \vec{X}^{(j)T} [m] \vec{X}^{(i)} = 0 \quad (2.27)$$

In the general situations, ω_i^2 is not equal to ω_j^2 , therefore

$$\vec{X}^{(j)T} [m] \vec{X}^{(i)} = 0, \quad i \neq j \quad (2.28)$$

By substituting equation [2.28](#) into [2.26](#), it can be found that

$$\vec{X}^{(j)T} [k] \vec{X}^{(i)} = 0, \quad i \neq j \quad (2.29)$$

The two equations [2.28](#) and [2.29](#) indicate that the mode shapes $\vec{X}^{(i)}$ and $\vec{X}^{(j)}$ are orthogonal with respect to both mass matrix $[m]$ and stiffness matrix $[k]$. When $i = j$, they yield to so called generalized mass and stiffness equations of the i th mode. That is

$$\begin{aligned}M_{ii} &= \vec{X}^{(i)T} [m] \vec{X}^{(i)}, & i &= 1, 2, \dots, n \\ K_{ii} &= \vec{X}^{(i)T} [k] \vec{X}^{(i)}, & i &= 1, 2, \dots, n\end{aligned}\quad (2.30)$$

or in matrix form

$$\begin{aligned}[\curvearrowleft M \curvearrowright] &= \begin{bmatrix} M_{11} & 0 & \dots & 0 \\ 0 & M_{22} & \dots & 0 \\ \vdots & \vdots & \ddots & \vdots \\ 0 & 0 & \dots & M_{nn} \end{bmatrix} = [X]^T [M] [X] \\ [\curvearrowleft K \curvearrowright] &= \begin{bmatrix} K_{11} & 0 & \dots & 0 \\ 0 & K_{22} & \dots & 0 \\ \vdots & \vdots & \ddots & \vdots \\ 0 & 0 & \dots & K_{nn} \end{bmatrix} = [X]^T [K] [X]\end{aligned}\quad (2.31)$$

$[X]$ is the modal matrix, which is given by

$$[X] = \begin{bmatrix} \vec{X}^{(1)} & \vec{X}^{(2)} & \dots & \vec{X}^{(n)} \end{bmatrix} \quad (2.32)$$

If the mode shapes $\vec{X}^{(i)}$ is normalized with respect to mass $[m]$ such that

$$\vec{X}^{(i)T} [m] \vec{X}^{(i)} = 1, \quad i = 1, 2, \dots, n \quad (2.33)$$

Then $[\diagdown M \diagdown]$ would be equal to identity matrix $[I]$ and $[\diagdown K \diagdown]$ would reduce to $[\diagdown \omega_i^2 \diagdown]$.

The expansion theorem shows that any vector in the n -dimensional space can be expressed by a linear combination of the n linearly independent vector. Since the eigenvectors has the property of orthogonality and linear independence, they are also applicable for expansion theorem. Thus, for an arbitrary vector \vec{x} in n -dimensional space, it can be expressed as

$$\vec{x} = \sum_{i=1}^n c_i \vec{X}^{(i)} \quad (2.34)$$

where c_i are constants. By premultiplying the equation with $\vec{X}^{(i)T} [m]$ and considering $\vec{X}^{(i)}$ is normalized, the constant c_i can be found as

$$c_i = \vec{X}^{(i)T} [m] \vec{x}, \quad i = 1, 2, \dots, n \quad (2.35)$$

Equation [2.35](#) is known as expansion theorem.

2.2.3 Modal Analysis

Consider the equation of motion of a multiple degree of freedom undamped vibration system with external force as shown in equation [2.36](#). When external force is applied, the system undergoes forced vibration. The solution can be obtained by making use of modal analysis as follows

$$[m] \cdot \ddot{\vec{x}} + [k] \cdot \vec{x} = \vec{F} \quad (2.36)$$

Firstly, the eigenvalue problem as shown in equation [2.23](#) needs to be solved. Thereafter, the natural frequencies $\omega_1, \omega_2, \dots, \omega_n$ and corresponding mode shapes $\vec{X}^{(1)}, \vec{X}^{(2)}, \dots, \vec{X}^{(n)}$ can be obtained. By expansion theorem as shown in equation [2.35](#), the solution of equation [2.36](#) can be expressed as a linear combination of mode shapes as

$$\vec{x}(t) = q_1(t) \vec{X}^{(1)} + q_2(t) \vec{X}^{(2)} + \dots + q_n(t) \vec{X}^{(n)} \quad (2.37)$$

or

$$\vec{x}(t) = \vec{q}(t) [X] \quad (2.38)$$

where $q_i(t)$ are time-dependent generalized coordinates. By substituting equation 2.38 into equation 2.36, it becomes

$$[m] [X] \ddot{\vec{q}} + [k] [X] \vec{q} = \vec{F} \quad (2.39)$$

Premultiplying equation 2.39 by $[X]^T$ and considering the normalized normal modes as shown in equation 2.33, it yields

$$\begin{aligned} [X]^T [m] [X] \ddot{\vec{q}} + [X]^T [k] [X] \vec{q} &= [X]^T \vec{F} \\ \rightarrow [I] \ddot{\vec{q}} + [\omega^2] \vec{q} &= [X]^T \vec{F} \\ \rightarrow [I] \ddot{\vec{q}} + [\omega^2] \vec{q} &= \vec{Q}(t) \end{aligned} \quad (2.40)$$

where $\vec{Q}(t)$ is the generalized force. Equation 2.40 can be rewritten as

$$\ddot{q}_i(t) + \omega_i^2 q_i(t) = Q_i(t), \quad i = 1, 2, \dots, n \quad (2.41)$$

As it can be seen from equation 2.41, the original coupled equation of motion is now transferred to a set of uncoupled equations. Thus, it is equivalent as solving a number of single degree of freedom system. The solution can be found by the same method described in section 2.1. The initial conditions for generalized coordinates are given as

$$\begin{aligned} \vec{q}(0) &= [X]^T [m] \vec{x}(0) \\ \dot{\vec{q}}(0) &= [X]^T [m] \dot{\vec{x}}(0) \end{aligned} \quad (2.42)$$

2.3 Plate Vibration

The previous sections 2.1 and 2.2 only introduced the vibration of discrete system. That is, the system is only modeled by simple mass, damper and spring elements. In this section, one of the continuous vibration system, namely plate vibration, is presented. Details regarding another commonly seen continuous system, beam, can be found in appendix A.

The fundamental difference between discrete and continuous system is that the previous one had finite degree of freedom, while the later one has infinite degree of freedom. Additionally, the governing equation for discrete system is ordinary differential equation, on the other hand, it is partial differential equation for continuous system. Despite the equations for discrete system seems easier to solve, it may not give the accurate solution compare to the continuous solution.

The equation of motion of plate is firstly given and followed by a description of various boundary conditions in this section. The boundary condition is not introduced in the previous sections since it only influences the discrete system in an indirect way. Finally, the analysis of free and forced vibration of plate is demonstrated. The plate considered in this project follows the assumptions made in classical plate theory, Kirchhoff–Love plate theory. The assumptions are summarized as follows

1. The thickness of plate h is small compared to plate length and width
2. The transverse deflection w is small compared to thickness h
3. The middle plane is neutral plane and does not experience in-plane deformation
4. The effect of transverse shear deformation and rotary inertial are neglected, that is, the lines normal to the middle plane remains normal after deformation

It can be seen from the assumptions that the classical plate theory is very similar to Bernoulli-Euler beam theory. While in plate theory, the transverse deflection w depends not only on x but also on y , that is, the transverse deflection of plate is expressed as $w(x, y, t)$.

2.3.1 Equation of Motion and Boundary Condition

Figure 2.7 shows the stresses, forces and induced moment in a plate element.

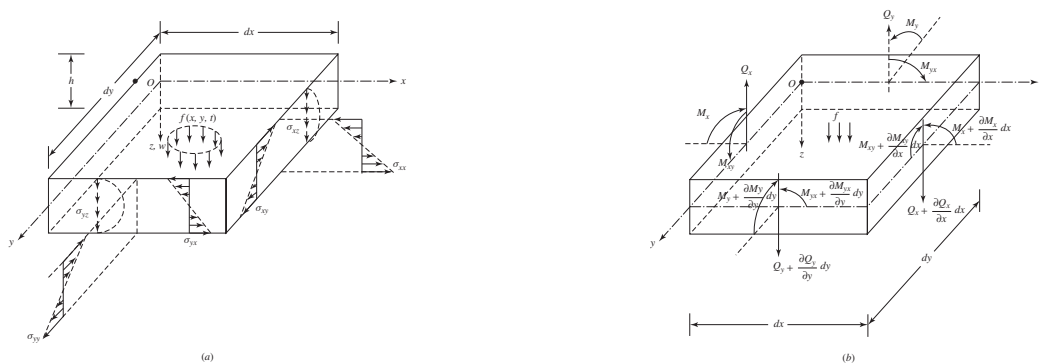


Figure 2.7: (a) Stresses in a plate; (b) forces and induced moment resultants in an element of a plate [10]

The equation of motion for plate is given by

$$D \left(\frac{\partial^4 w}{\partial x^4} + 2 \frac{\partial^4 w}{\partial x^2 \partial y^2} + \frac{\partial^4 w}{\partial y^4} \right) + \rho h \frac{\partial^2 w}{\partial t^2} = f(x, y, t) \quad (2.43)$$

or

$$D \nabla^4 w(x, y, t) + \rho h \frac{\partial^2 w(x, y, t)}{\partial t^2} = f(x, y, t) \quad (2.44)$$

where

$$D = \frac{Eh^3}{12(1-\nu^2)} \quad (2.45)$$

For a plate with damping, the equation of motion is given as

$$D \nabla^4 w(x, y, t) + c \frac{\partial w(x, y, t)}{\partial t} + \rho h \frac{\partial^2 w(x, y, t)}{\partial t^2} = f(t) \quad (2.46)$$

E , ν , ρ , c and h represents the plate Young's modulus, Poisson's ratio, mass density, damping coefficient and thickness, respectively. ∇^4 is also known as biharmonic operator in Cartesian coordinate. The equation of motion for free vibration can be obtained by assuming $f(x, y, t) = 0$ in equation [2.44](#).

Instead of using two boundary conditions to solve equation of motion in beam vibration, four boundary conditions are needed in plate vibration. Consider a plate with four edges, $x = 0$, $x = a$, $y = 0$ and $y = b$. The commonly used boundary conditions are listed below. It should be noted that the examples below are taken for the edge $x = a$, while for the other edges of plate such as $y = b$ it should be adjusted accordingly.

1. Free end :

(a) Bending moment : $M_x = -D \left(\frac{\partial^2 w}{\partial x^2} + \nu \frac{\partial^2 w}{\partial y^2} \right) \Big|_{x=a} = 0$

(b) Shear force : $V_x = Q_x + \frac{\partial M_{xy}}{\partial y} = -D \left[\frac{\partial^3 w}{\partial x^3} + (2-\nu) \frac{\partial^3 w}{\partial x \partial y^2} \right] \Big|_{x=a} = 0$

2. Simply supported (pinned) end :

(a) Deflection : $w \Big|_{x=a} = 0$

(b) Bending moment : $M_x = -D \left(\frac{\partial^2 w}{\partial x^2} + \nu \frac{\partial^2 w}{\partial y^2} \right) \Big|_{x=a} = 0$

3. Fixed (clamped) end :

(a) Deflection : $w \Big|_{x=a} = 0$

(b) Slope (angle) : $\frac{\partial w}{\partial x} \Big|_{x=a} = 0$

2.3.2 Free and Forced Vibration of Plate

Free Vibration

Consider a plate with edges at $x = 0, a$ and $y = 0, b$. The equation of motion for plate in free vibration is given as

$$D\nabla^4 w + \rho h \frac{\partial^2 w}{\partial t^2} = 0 \quad (2.47)$$

The solution can be assumed as

$$w(x, y, t) = W(x, y) \cdot T(t) \quad (2.48)$$

Substitute equation [2.48](#) into [2.47](#) and rearrange it, the equation becomes

$$\begin{aligned} \frac{d^2 T(t)}{dt^2} + \omega^2 T(t) &= 0 \\ \nabla^4 W(x, y) - \lambda^4 W(x, y) &= 0 \end{aligned} \quad (2.49)$$

where

$$\lambda^4 = \frac{\rho h \omega^2}{D} \quad (2.50)$$

The general solution of equation [2.49](#) is given as

$$\begin{aligned} T(t) &= A \cos(\omega t) + B \sin(\omega t) \\ W(x, y) &= C_1 \sin(\alpha x) \sin(\beta y) + C_2 \sin(\alpha x) \cos(\beta y) + \\ &C_3 \cos(\alpha x) \sin(\beta y) + C_4 \cos(\alpha x) \cos(\beta y) + \\ &C_5 \sinh(\theta x) \sinh(\phi y) + C_6 \sinh(\theta x) \cosh(\phi y) + \\ &C_7 \cosh(\theta x) \sinh(\phi y) + C_8 \cosh(\theta x) \cosh(\phi y) \end{aligned} \quad (2.51)$$

where A, B and $C_n, n = 1, 2, \dots, 8$ are constants to be determined by initial and boundary conditions. Additionally,

$$\lambda^2 = \alpha^2 + \beta^2 = \theta^2 + \phi^2 \quad (2.52)$$

For a plate with all boundaries simply supported, equation [2.51](#) yields

$$\begin{aligned} \sin(\alpha a) &= 0 \\ \sin(\beta b) &= 0 \end{aligned} \quad (2.53)$$

In addition, only C_1 is not zero. Equation [2.53](#) is known as frequency equation, the solution is given as

$$\begin{aligned} \alpha_m a &= m\pi, & m &= 1, 2, \dots \\ \beta_n b &= n\pi, & n &= 1, 2, \dots \end{aligned} \tag{2.54}$$

Take the results of equation 2.50, 2.52 and 2.54, the natural frequency ω_{mn} can be obtained as

$$\omega_{mn} = \lambda_{mn}^2 \sqrt{\frac{D}{\rho h}} = \pi^2 \left[\left(\frac{m}{a}\right)^2 + \left(\frac{n}{b}\right)^2 \right] \sqrt{\frac{D}{\rho h}} \tag{2.55}$$

while the normal modes $W_{mn}(x, y)$ are

$$W_{mn}(x, y) = C_{1mn} \sin\left(\frac{m\pi x}{a}\right) \sin\left(\frac{n\pi y}{b}\right), \quad m, n = 1, 2, \dots \tag{2.56}$$

Thus, the complete solution can be expressed as

$$w(x, y, t) = \sum_{m=1}^{\infty} \sum_{n=1}^{\infty} \sin\left(\frac{m\pi x}{a}\right) \sin\left(\frac{n\pi y}{b}\right) [A_{mn} \cos(\omega_{mnt}) + B_{mn} \sin(\omega_{mnt})] \tag{2.57}$$

Figure 2.8 shows the first few modes of a simply supported plate.

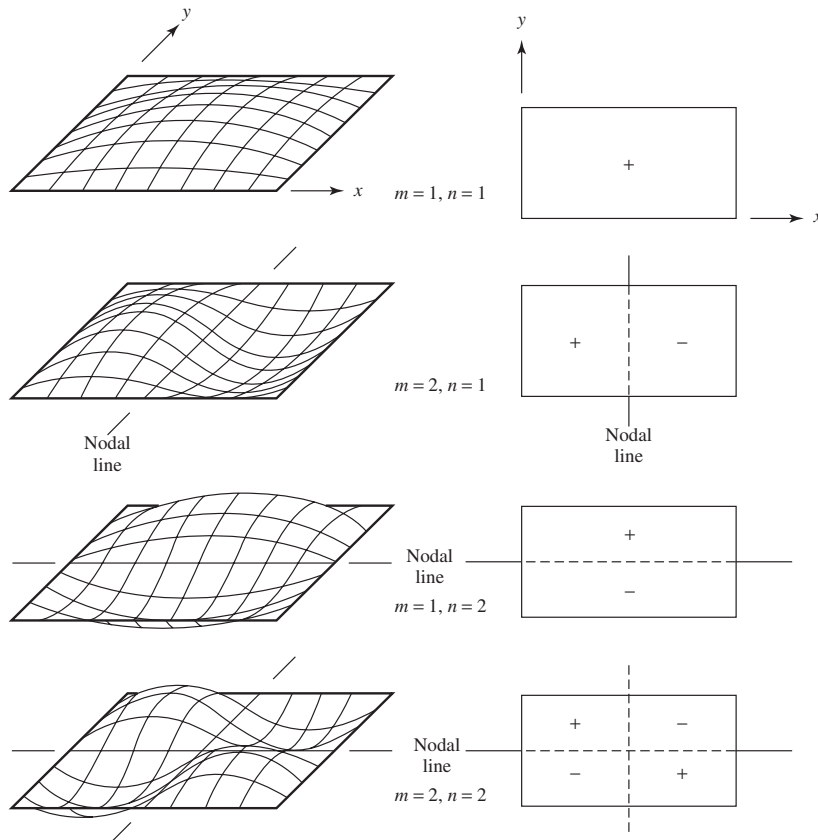


Figure 2.8: Mode shapes of a rectangular simply supported plate. Dashed lines denote nodal lines other than the edges. [10]

Figure 2.9 shows frequency equations and mode shapes of rectangular plate with other boundary conditions. It should be noted that in the boundary conditions mentioned below, $x = 0$ and $x = a$ are simply supported. In the figure, SS, C and F denote simply supported, clamped and free end respectively. Additionally, $\delta_1 = \sqrt{\lambda^2 - \alpha_m^2}$ and $\delta_2 = \sqrt{\lambda^2 + \alpha_m^2}$.

Case	Boundary conditions	Frequency equation	y-mode shape, $Y_n(y)$ without a multiplication factor, where $W_{mn}(x, y) = C_{mn} X_m(x) Y_n(y)$, with $X_m(x) = \sin \alpha_m x$
1	SS-SS-SS-SS	$\sin \delta_1 b = 0$	$Y_n(y) = \sin \beta_n y$
2	SS-C-SS-C	$2\delta_1 \delta_2 (\cos \delta_1 b \cosh \delta_2 b - 1) - \alpha_m^2 \sin \delta_1 b \sinh \delta_2 b = 0$	$Y_n(y) = (\cosh \delta_2 b - \cos \delta_1 b) (\delta_1 \sinh \delta_2 y - \delta_2 \sin \delta_1 y) - (\delta_1 \sinh \delta_2 b - \delta_2 \sin \delta_1 b) (\cosh \delta_2 y - \cos \delta_1 y)$
3	SS-F-SS-F	$\sinh \delta_2 b \sin \delta_1 b \{\delta_2^2 [\lambda^2 - \alpha_m^2 (1 - \nu)]^4 - \delta_1^2 [\lambda^2 + \alpha_m^2 (1 - \nu)]^4\} - 2\delta_1 \delta_2 [\lambda^4 - \alpha_m^4 (1 - \nu)^2]^2 (\cosh \delta_2 b \cos \delta_1 b - 1) = 0$	$Y_n(y) = -(\cosh \delta_2 b - \cos \delta_1 b) [\lambda^4 - \alpha_m^4 (1 - \nu)^2] \{\delta_1 [\lambda^2 + \alpha_m^2 (1 - \nu)] \sinh \delta_2 y + \delta_2 [\lambda^2 - \alpha_m^2 (1 - \nu)] \sin \delta_1 y\} + \{\delta_1 [\lambda^2 + \alpha_m^2 (1 - \nu)]^2 \sinh \delta_2 b - \delta_2 [\lambda^2 - \alpha_m^2 (1 - \nu)]^2 \sin \delta_1 b\} [\lambda^2 - \alpha_m^2 (1 - \nu)] \cosh \delta_2 y + [\lambda^2 + \alpha_m^2 (1 - \nu)] \cos \delta_1 y$
4	SS-C-SS-SS	$\delta_2 \cosh \delta_2 b \sin \delta_1 b - \delta_1 \sinh \delta_2 b \cos \delta_1 b = 0$	$Y_n(y) = \sin \delta_1 b \sinh \delta_2 y - \sinh \delta_2 b \sin \delta_1 y$
5	SS-F-SS-SS	$\delta_2 [\lambda^2 - \alpha_m^2 (1 - \nu)]^2 \cosh \delta_2 b \sin \delta_1 b - \delta_1 [\lambda^2 + \alpha_m^2 (1 - \nu)]^2 \sinh \delta_2 b \cos \delta_1 b = 0$	$Y_n(y) = [\lambda^2 - \alpha_m^2 (1 - \nu)] \sin \delta_1 b \sinh \delta_2 y + [\lambda^2 + \alpha_m^2 (1 - \nu)] \sinh \delta_2 b \sin \delta_1 y$
6	SS-F-SS-C	$\delta_1 \delta_2 [\lambda^4 - \alpha_m^4 (1 - \nu)^2] + \delta_1 \delta_2 [\lambda^4 + \alpha_m^4 (1 - \nu)^2] \cdot \cosh \delta_2 b \cos \delta_1 b + \alpha_m^2 [\lambda^4 (1 - 2\nu) - \alpha_m^4 (1 - \nu)^2] \cdot \sinh \delta_2 b \sin \delta_1 b = 0$	$Y_n(y) = \{[\lambda^2 + \alpha_m^2 (1 - \nu)] \cosh \delta_2 b + [\lambda^2 - \alpha_m^2 (1 - \nu)] \cos \delta_2 b\} \cdot (\delta_2 \sin \delta_1 y - \delta_1 \sinh \delta_2 y) + \{\delta_1 [\lambda^2 + \alpha_m^2 (1 - \nu)] \sinh \delta_2 b + \delta_2 [\lambda^2 - \alpha_m^2 (1 - \nu)] \sin \delta_1 b\} (\cosh \delta_2 y - \cos \delta_1 y)$

Figure 2.9: Frequency equations and mode shapes of rectangular plate with other boundary conditions [10]

Forced Vibration

The response of forced vibration of plate can be assumed as

$$w(x, y, t) = \sum_{m=1}^{\infty} \sum_{n=1}^{\infty} W_{mn}(x, y) \eta_{mn}(t) \quad (2.58)$$

where $W_{mn}(x, y)$ is mn th the mode shape given by equation 2.56 and $\eta_{mn}(t)$ is generalized coordinate. If the mode shape is normalized such as

$$\int_0^a \int_0^b \rho h W_{mn}^2 dy dx = 1 \quad (2.59)$$

then the coefficient C_{1mn} is obtained as $2/\sqrt{\rho h a b}$. Substitute equation 2.58 into equation of motion and premultiply it with mode shape, thereafter integrate the equation over the domain with the orthogonality condition, it yields to

$$\ddot{\eta}_{mn}(t) + \omega_{mn}^2 \eta_{mn}(t) = N_{mn}(t), \quad m, n = 1, 2, \dots \quad (2.60)$$

where N_{mn} is the generalized force and is given by

$$N_{mn}(t) = \int_0^a \int_0^b W_{mn} \cdot f(t) dy dx \quad (2.61)$$

Take the natural frequency ω_{mn} from equation 2.55, the solution for $\eta_{mn}(t)$ can be expressed as

$$\eta_{mn}(t) = \eta_{mn}(0) \cos(\omega_{mn} t) + \frac{\dot{\eta}_{mn}(0)}{\omega_{mn}} \sin(\omega_{mn} t) + \frac{1}{\omega_{mn}} \int_0^t N_{mn}(\tau) \sin[\omega_{mn}(t - \tau)] d\tau \quad (2.62)$$

Finally, the response $w(x, y, t)$ can be found by equation 2.58.

Chapter 3 Probability Theory

The basic concept of probability is to define a space with all possible outcomes (i.e. events or sets) and the probability of each event. If α_j is denoted as the j th possible outcome in the space Ω , an event is defined as a collection of some possible outcomes which meet a certain criteria. For example, event $A = \{\alpha : \text{displacement} \leq 0.1 \text{ (mm)}\}$ or event $B = \{\alpha : \text{displacement in z direction}\}$. The events must be Boolean so that $A \cup B$, $A \cap B$, A^c and B^c are also events, where $A \cup B = \{\alpha : \alpha \in A, \text{ or } \in B, \text{ or both}\}$, $A \cap B = \{\alpha : \alpha \in A \text{ and } \in B\}$, $A^c = \{\alpha : \alpha \notin A\}$ and $B^c = \{\alpha : \alpha \notin B\}$.

$P(\cdot)$ is denoted as the probability measure of an event. That is, $P(A) \geq 0$ for any event A and $P(\Omega) = 1$. The conditional probability is defined as the probability of the intersection of two events divided by the probability of the condition or given event. Equation 3.1 shows the conditional probability of A given B , where $P(AB) = P(A \cap B)$ is a commonly used simplification both in other literature and throughout this project.

$$P(A|B) = \frac{P(AB)}{P(B)} \quad (3.1)$$

While the product rule is shown in equation 3.2

$$P(AB) = P(B) P(A|B) = P(A) P(B|A) \quad (3.2)$$

and event A and B are said to be independent if

$$P(AB) = P(A) \cdot P(B) \quad (3.3)$$

When considering a random vibration problem, the input or excitation is often a random variable. That is, every measurement of the same input can have different result. This is often observed within natural environment such as wind load or wave, which can not be expressed as a simple time-dependent function. The considered random input in this project is the force that solar panels would experience during rocket launching.

Therefore, instead of finding a deterministic solution for vibration problem as shown in the previous chapter, it is necessary to bear the idea of "probability" in mind when dealing with random vibration problem. In this chapter, the concept of probability and random variable are introduced. Thereafter, time domain analysis of random variable is shown. Finally, the analysis in frequency domain, which is primarily used in the following analysis, is presented. The content of this chapter, including theory and equation, is mainly based on [6].

3.1 Random Variable

Consider a random variable $X(t)$, then a family of random variables is known as stochastic process and can be expressed as $\{X(t)\}$. For a given time t_0 , $X(t_0)$ can have different result every observation. That is, $X^{(1)}(t_0)$, $X^{(2)}(t_0)$, $X^{(3)}(t_0)$, ... can all be different, where $X^{(j)}(t)$ is the j th sample time history observed and $X^{(j)}(t_0)$ is the j th sample time history observed at time t_0 . If there is a sufficient number of observations, the characteristic of this stochastic process such as expected value or probability can be obtained.

Figure 3.1 shows a collection of sample time histories also known as ensemble. A section across this ensemble at time t_0 gives a statistical sample for the random variable corresponding to that t_0 value.

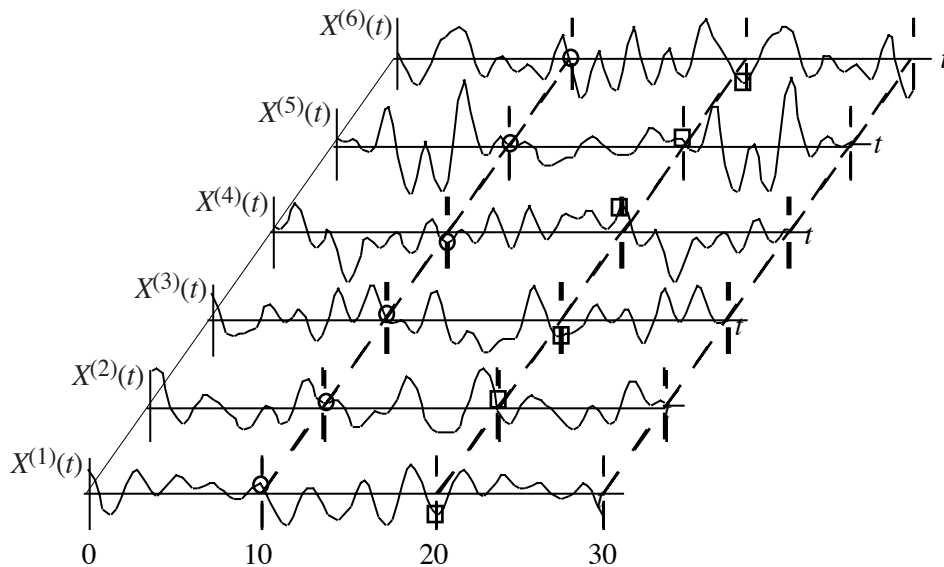


Figure 3.1: Ensemble of time histories of $\{X(t)\}$ [6]

A common way to describe the probability of a given random variable X is the cumulative distribution function $F_X(\cdot)$, which is shown in equation 3.4.

$$F_X(u) \equiv P(X \leq u) \quad (3.4)$$

where u is a arbitrary chosen real number and $P(X \leq u)$ is the probability of $X \leq u$. For example, if

$$P(X = 1) = P(X = 2) = P(X = 3) = P(X = 4) = 0.25 \quad (3.5)$$

then

$$\begin{aligned}
F_X(u) &= 0, & \text{for } -\infty < u < 1 \\
F_X(u) &= 0.25, & \text{for } 1 \leq u < 2 \\
F_X(u) &= 0.5, & \text{for } 2 \leq u < 3 \\
F_X(u) &= 0.75, & \text{for } 3 \leq u < 4 \\
F_X(u) &= 1, & \text{for } 4 \leq u < \infty
\end{aligned} \tag{3.6}$$

In the above example, the cumulative distribution function is not continuous. However, in other cases, the random variable X and cumulative distribution function such as $F_X(u) = 0.1 \cdot u$ are continuous. If the cumulative distribution function is continuous and differentiable everywhere, the probability density function $p_X(\cdot)$ can be defined as

$$p_X(u) = \frac{d}{du} F_X(u) \tag{3.7}$$

Thus, the probability that X lies within the interval $[a, b]$ is given by the integral of p_X over the interval as

$$P(a < X \leq b) = \int_a^b p_X(u) du = F_X(b) - F_X(a) \tag{3.8}$$

3.1.1 Expected Values

In order to describe the characteristic of a random variable, quantity that is the average over all possible outcomes is commonly used. One of such quantity is expected value which defined as

$$E(X) \equiv \int_{-\infty}^{\infty} u \cdot p_X(u) du \tag{3.9}$$

As it can be seen from equation [3.9](#), an expect value is a weighted average over all possible values of X , where the weighting function is probability density function $p_X(u)$. That is, u represents a value of X and $p_X(u) du$ is the probability of X being in the vicinity of u .

It should be noted that equation [3.9](#) should be normalized by an integral of weighting function for common approach, however the integral is found to be unity when the weighting function is probability density function. Therefore, the normalization integral is omitted in equation [3.9](#). Additionally, the expected value is also known as expectation or mean value of a random variable, which shows that expected value is not a value with highest probability, but a weighted average value.

For a function of random variable $g(X)$ such as X^2 or $\sin(3X)$, the expected value is given as

$$E[g(X)] \equiv \int_{-\infty}^{\infty} g(u) \cdot p_X(u) du \tag{3.10}$$

3.1.2 Moments of Random Variable

The moments of random variable are other characteristics of random variable and are actually special cases of expected value. The j th moment of X is defined as $E(X^j)$, where X^j can be viewed as a function of X and expressed as $g(X)$. The first moment of random variable, also known as mean value, is exactly the same as expected value but with a different notation μ_X and name. That is,

$$\text{First moment or mean value : } \mu_X \equiv E(X) = \int_{-\infty}^{\infty} u \cdot p_X(u) du \quad (3.11)$$

For two random variables X and Y , the cross moment of order (j, k) is defined as $E(X^j Y^k)$. The most common one is the cross product of random variables $E(XY)$. In addition to the moments defined above, there is also central moment which subtracts the mean value of random variable. The central moment is defined as $E[(X - \mu_X)^j]$ or for two random variables $E[(X - \mu_X)^j (Y - \mu_Y)^k]$. The three special central moments that are commonly used in analysis are

$$\text{Variance : } \sigma_X^2 \equiv E[(X - \mu_X)^2] = E(X^2) - \mu_X^2$$

$$\text{Covariance : } K_{XY} \equiv E[(X - \mu_X)(Y - \mu_Y)] = E(XY) - \mu_X \mu_Y \quad (3.12)$$

$$\text{Root-mean-square (RMS) value : } \sigma_X \equiv [E(X^2)]^{\frac{1}{2}}$$

while the normalized form of covariance known as correlation coefficient is defined as

$$\text{Correlation coefficient : } \rho_{XY} \equiv \frac{K_{XY}}{\sigma_X \sigma_Y} = E \left[\frac{(X - \mu_X)}{\sigma_X} \frac{(Y - \mu_Y)}{\sigma_Y} \right] \quad (3.13)$$

For two random variables from the same stochastic process $X(t)$ and $X(s)$, the cross product known as auto-correlation function is defined as

$$\begin{aligned} \text{Auto-correlation function: } \phi_{XX}(t, s) &\equiv E[X(t)X(s)] \\ &= \int_{-\infty}^{\infty} \int_{-\infty}^{\infty} uv p_{X(t)X(s)}(u, v) dudv \end{aligned} \quad (3.14)$$

The auto-correlation function is defined in a two-dimensional space with t and s varying over the index set of $\{X(t)\}$. On the other hand, for two random variables from different stochastic process $X(t)$ and $Y(s)$, the cross product known as cross-correlation function is defined as

$$\begin{aligned} \text{Cross-correlation function: } \phi_{XY}(t, s) &\equiv E[X(t)Y(s)] \\ &= \int_{-\infty}^{\infty} \int_{-\infty}^{\infty} uv p_{X(t)Y(s)}(u, v) dudv \end{aligned} \quad (3.15)$$

Similarly, cross-correlation function is also defined in a two-dimensional space with t varying over the index set of $\{X(t)\}$ and s varying over the index set of $\{Y(t)\}$.

Follow the same idea from auto-correlation and cross-correlation functions, the auto-covariance and cross-covariance functions are defined as

$$\begin{aligned}\text{Auto-variance : } K_{XX}(t, s) &\equiv E([X(t) - \mu_X(t)][X(s) - \mu_X(s)]) \\ &= \phi_{XX}(t, s) - \mu_X(t)\mu_X(s)\end{aligned}\tag{3.16}$$

$$\begin{aligned}\text{Cross-covariance : } K_{XY}(t, s) &\equiv E([X(t) - \mu_X(t)][Y(s) - \mu_Y(s)]) \\ &= \phi_{XY}(t, s) - \mu_X(t)\mu_Y(s)\end{aligned}\tag{3.17}$$

where can be seen that variance function is actually a special case of auto-variance function that $t = s$.

3.2 Time Domain Analysis

In time domain analysis of a general linear system, the input or excitation history can be considered as a combination of impulses. If the excitation $f(t)$ is a Dirac delta function $\delta(t)$, then the response $x(t)$ is defined as impulse response function $h_x(t)$. A brief introduction of Dirac delta function can be found in appendix C. In addition, the system considered is a casual system, which means $h_x(t) \equiv 0$ for $t < 0$. That is, the response to an excitation does not start until time $t = 0$. Thus, for a general linear system, the excitation can be expressed as a superposition of Dirac delta functions multiplied by their amplitudes

$$\begin{aligned}
 f(t) &= \int_{-\infty}^{\infty} f(s) \delta(t-s) ds \\
 &= \int_{-\infty}^{\infty} f(t-r) \delta(r) ds
 \end{aligned}
 \tag{3.18}$$

Similarly, the response can be expressed as

$$\begin{aligned}
 x(t) &= \int_{-\infty}^{\infty} f(s) h_x(t-s) ds \\
 &= \int_{-\infty}^{\infty} f(t-r) h_x(r) ds
 \end{aligned}
 \tag{3.19}$$

where equation 3.19 is known as Duhamel convolution integral. Figure 3.2 shows the schematic of time domain analysis for general linear system.

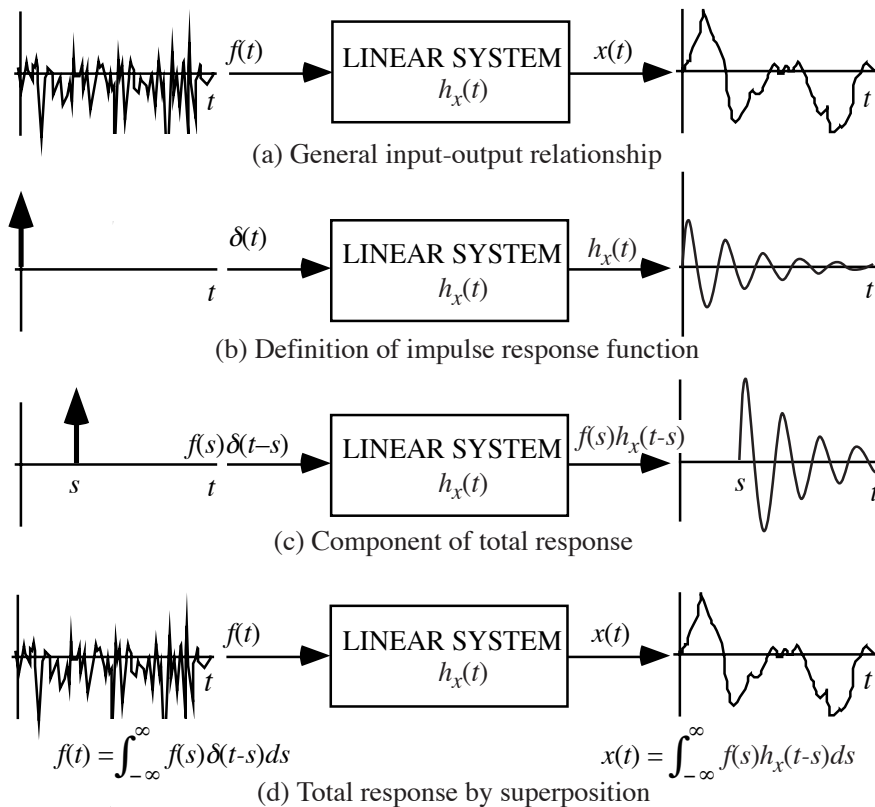


Figure 3.2: Schematic of general linear system [6]

It should be noted that the linear system stated above is a time-invariant system. That is, the system depends only indirectly on time domain, where the relationship between input and output is constant with respect to time t . In another word, for given input with time delay $f(t + \tau)$, the response is $x(t + \tau)$.

If the system is a time-varying system, then the response should be expressed as

$$x(t) = \int_{-\infty}^{\infty} f(s) h_{xf}(t, s) ds \quad (3.20)$$

where $h_{xf}(t, s)$ is a function of two time parameters.

Since the linear system considered in plate vibration is an ordinary differential equation, it is necessary to find the impulse response function for such system. A general form of n th order linear ordinary differential equation is given as

$$\sum_{j=0}^n a_j \frac{d^j x(t)}{dt^j} = f(t) \quad (3.21)$$

Thus, the corresponding impulse response function must satisfy

$$\sum_{j=0}^n a_j \frac{d^j h_x(t)}{dt^j} = \delta(t) \quad (3.22)$$

There are several difficulties encountered when solving equation [3.22](#). A brief review of the difficulties and solution can be found in appendix [C.2](#). The result is shown in equation [3.23](#).

$$\begin{aligned} \left(\frac{d^{n-1} h_x(t)}{dt^{n-1}} \right)_{t=0^+} &= a_n^{-1} \\ \left(\frac{d^j h_x(t)}{dt^j} \right)_{t=0^+} &= 0 \quad \text{for } j \leq n-2 \end{aligned} \quad (3.23)$$

For the stochastic analysis, simply replace the deterministic excitation $f(t)$ and response $x(t)$ with stochastic process $F\{t\}$ and $X\{t\}$ as

$$\begin{aligned} X(t) &= \int_{-\infty}^{\infty} F(s) h_x(t-s) ds \\ &= \int_{-\infty}^{\infty} F(t-r) h_x(r) ds \end{aligned} \quad (3.24)$$

The other characteristic functions such as mean value and auto-correlation function can also be found based on equation [3.24](#). However, since the frequency domain analysis is primarily used in this project, the other characteristic functions are not presented here.

3.3 Frequency Domain Analysis

By making use of Fourier transform, a time-dependent function can be decompose to its frequency component. The Fourier transform of a time-dependent function $f(t)$ is denoted by $\tilde{f}(\omega)$ and defined as

$$\tilde{f}(\omega) = \frac{1}{2\pi} \int_{-\infty}^{\infty} f(t) e^{-i\omega t} dt \quad (3.25)$$

while the inverse relation is

$$f(t) = \int_{-\infty}^{\infty} \tilde{f}(\omega) e^{i\omega t} d\omega \quad (3.26)$$

Equation [3.26](#) shows that the original time-dependent function is actually a summation of harmonic terms where $\tilde{f}(\omega) d\omega$ is the amplitude. However, since the amplitude is generally complex, it is necessary to consider the absolute value when determining the contribution from frequency ω to $f(t)$.

For a stochastic process $\{X(t)\}$, the Fourier transform is given by

$$\tilde{X}(\omega) = \frac{1}{2\pi} \int_{-\infty}^{\infty} X(t) e^{-i\omega t} dt \quad (3.27)$$

Other characteristic functions such as mean value and moments are also shown in the following equations. It should be noted that since $\tilde{X}(\omega)$ is complex, several terms are modified with complex conjugate denoted by $\tilde{X}^*(\omega)$.

$$\text{Mean value : } \mu_{\tilde{X}}(\omega) = \frac{1}{2\pi} \int_{-\infty}^{\infty} \mu_X(t) e^{-i\omega t} dt \quad (3.28)$$

$$\text{Second moment : } \phi_{\tilde{X}\tilde{X}}(\omega_1, \omega_2) = E[\tilde{X}(\omega_1) \tilde{X}^*(\omega_2)] \quad (3.29)$$

$$= \frac{1}{(2\pi)^2} \int_{-\infty}^{\infty} \int_{-\infty}^{\infty} \phi_{XX}(t_1, t_2) e^{-i(\omega_1 t_1 - \omega_2 t_2)} dt_1 dt_2 \quad (3.30)$$

$$\text{Auto-covariance : } K_{\tilde{X}\tilde{X}}(\omega_1, \omega_2) = E\left([\tilde{X}(\omega_1) - \mu_{\tilde{X}}(\omega_1)] [\tilde{X}(\omega_2) - \mu_{\tilde{X}}(\omega_2)]^*\right) \quad (3.31)$$

$$= \frac{1}{(2\pi)^2} \int_{-\infty}^{\infty} \int_{-\infty}^{\infty} K_{XX}(t_1, t_2) e^{-i(\omega_1 t_1 - \omega_2 t_2)} dt_1 dt_2 \quad (3.32)$$

Sometimes the auto-variance function $K_{XX}(t_1, t_2)$ is also written as

$$K_{XX}(t_1, t_2) = G_{XX}(t_1 - t_2) = G_{XX}(\tau) \quad (3.33)$$

3.3.1 Power Spectral Density

It should be noted that for a stationary stochastic process, the expressions shown above may not exist. Therefore, it is necessary to define other function that is applicable for stationary stochastic process. The function known as auto-spectral density function or power spectral density $S_{XX}(\omega)$ is defined as

$$S_{XX}(\omega) = \frac{1}{2\pi} \int_{-\infty}^{\infty} G_{XX}(\tau) e^{-i\omega\tau} d\tau \quad (3.34)$$

while the inverse relation gives

$$G_{XX}(\tau) = \int_{-\infty}^{\infty} S_{XX}(\omega) e^{i\omega\tau} d\omega \quad (3.35)$$

Similarly, the cross-spectral density is defined as

$$S_{XY}(\omega) = \frac{1}{2\pi} \int_{-\infty}^{\infty} G_{XY}(\tau) e^{-i\omega\tau} d\tau \quad (3.36)$$

There are three important properties of power spectral density function listed as follows

1. $S_{XX}(\omega)$ is always real for all values of ω
2. $S_{XX}(\omega)$ is greater or equal to 0 for all values of ω
3. $S_{XX}(\omega)$ is equal to $S_{XX}(-\omega)$ for all values of ω

Another important feature is the special case when setting $\tau = 0$ in equation [3.35](#) as

$$\sigma_X^2 = G_{XX}(0) = \int_{-\infty}^{\infty} S_{XX}(\omega) d\omega \quad (3.37)$$

which shows the area under power spectral density is equal to the variance of a random variable.

Furthermore, the derivatives of power spectral density can also be found as

$$S_{\dot{X}\dot{X}}(\omega) = \omega^2 S_{XX}(\omega) \quad (3.38)$$

and

$$S_{\ddot{X}\ddot{X}}(\omega) = \omega^4 S_{XX}(\omega) \quad (3.39)$$

Thus, if a displacement power spectral density is given, the corresponding velocity and acceleration spectral density can also be found based on equation [3.38](#) and [3.39](#) and vice versa. Additionally, the G_{rms} value is a very common expression known as root-mean-square acceleration. It can be obtained by calculating the square root of the area under an acceleration PSD curve such as $S_{\ddot{X}\ddot{X}}$. Similarly, the root-mean-square displacement, referred as D_{rms} in this project, is the square root of the area under an displacement spectral density curve S_{XX} as shown in equation [3.40](#)

$$D_{rms} = \sqrt{\int_{f_i}^{f_h} S_{ww} df} \quad (3.40)$$

The root-mean-square acceleration (or displacement) is also called one-sigma acceleration (or displacement), which is related to the statistical properties of the acceleration time history. That is,

- Within 66.8 % of time, the acceleration (or displacement) would not be exceed the range of ± 1 sigma acceleration (or displacement)
- Within 95.4 % of time, the acceleration (or displacement) would not be exceed the range of ± 2 sigma acceleration (or displacement)
- Within 99.7 % of time, the acceleration (or displacement) would not be exceed the range of ± 3 sigma acceleration (or displacement)

3.3.2 Frequency Response Function

In section 3.2 the idea of impulse response function $h_x(t)$ is introduced. The equivalent form in frequency domain analysis is known as frequency response function $H_x(\omega)$ and given as

$$\tilde{x}(\omega) = H_x(\omega) \tilde{f}(\omega) \quad (3.41)$$

where $\tilde{x}(\omega)$ and $\tilde{f}(\omega)$ is the Fourier transform of response $x(t)$ and excitation $f(t)$, respectively.

For the stochastic process response $\{X(t)\}$ and excitation $\{F(t)\}$, the equation simply becomes

$$\tilde{X}(\omega) = H_x(\omega) \tilde{F}(\omega) \quad (3.42)$$

Furthermore, the power spectral density is given as

$$S_{XX}(\omega) = H_x(\omega) H(-\omega) S_{FF}(\omega) = |H_x(\omega)|^2 S_{FF}(\omega) \quad (3.43)$$

Thus, the variance can be found by equation 3.37. One advantage for frequency domain analysis is that for a general n th order system as in time domain analysis

$$\sum_{j=0}^n a_j \frac{d^j x(t)}{dt^j} = f(t) \quad (3.44)$$

If $f(t) = e^{i\omega t}$ and $x(t) = H_x(\omega) e^{i\omega t}$, the equation gives

$$H_x(\omega) = \left(\sum_{j=0}^n a_j (i\omega)^j \right)^{-1} \quad (3.45)$$

which is relatively easy to solve compare to the initial condition and differential equations in time domain analysis. Based on equation 3.45, it can be seen that the frequency response function is highly related to the system characteristic. That is, the shape of response spectral density can be modified by adjusting the frequency transfer function (i.e. system characteristic). This makes the frequency transfer function can act in a way similar to a signal filter and produce the desire output spectral density.

Chapter 4 Analytical Analysis

This chapter focuses on building an analytical model for random vibration of a deployable solar panel. Beam models are used as a starting point in this project since they are relatively easy to analyze, the result can be seen in appendix B. Thereafter, plate models are considered in order to have a better representation of a solar panel. The equations used in this chapter are based on the previous chapters 2 and 3. Additionally, the approaches from [11], [1] and [5] are also adopted, a simple verification of [1] can be found in section 4.1. Some equations from the previous chapters are rewritten here to maintain the line of thought.

Recall the the detail of problem formulation in section 1.1, the solar panel system is divided into two subsystem and the one with random excitation is primary focus in this project. If the resultant force caused by random excitation is larger than pretension force, the support pins might loss contact and the system needs to be adjusted. Figure 1.4 is shown again here.

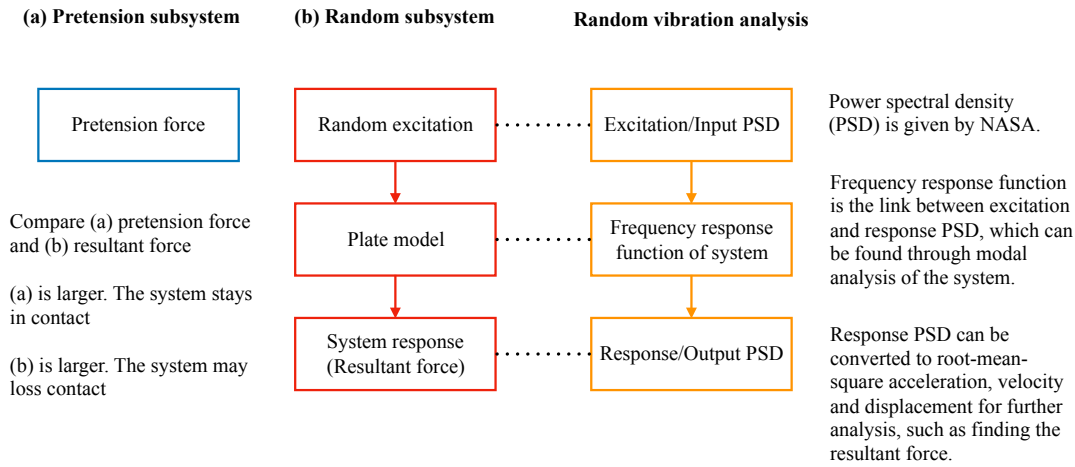


Figure 4.1: Illustration of approach

Random vibration analysis include three important elements, excitation, frequency response function and response. The excitation input used in this project is studied in section 1.1.1. The frequency response function of plate model based on the formulation in section 1.1 is studied in the following section 4.3. Section 4.3 presents three different studies including study of mode shape, location, damping and material. The resultant force from random excitation is found by multiplying plate mass with root-mean-square acceleration and compare with the pretension force. Finally, a short summary and discussion is given in section 4.4.

In addition, all analytical results are in company with numerical calculations, produced and plotted by commercial program Matlab and Maple, in order to give a better understanding of the system response. The data sheet used for numerical computations is shown

in table 4.1. It should be noted that the material property in data sheet is not the actual property of solar panel but an aluminum plate due to confidentiality concern.

Table 4.1: Data sheet for numerical calculations

	Symbol	Value	Unit
Young's modulus	E	70	GPa
Poisson's ration	ν	0.33	
Mass density	ρ	2700	$\frac{kg}{m^3}$
Excitation frequency	f	20 - 2000	Hz
Damping ratio	ζ	0.05	
Length in X direction of plate	a	0.4	m
Length in Y direction of plate	b	0.2	m
Thickness of plate	h	0.002	m

4.1 Verification of Previous Study

In [1], Chen, Zhou and Yang present several methods to evaluate response of thin plate subjected to random excitation. The article aims to accurately and efficiently achieve the benchmark solutions of stationary stochastic responses for rectangular thin plate. The approach is then adopted in this project since the problem considered is very similar. Before the approach is actually used, a simple verification is done through the same input data given in the article. A summary of the article is presented in the following paragraph. The approach detail and idea can be found in the complete article in appendix D.

The considered problem in the article is a rectangular thin plate subjected to white noise random excitation. The plate has length a , b and h along X , Y and Z coordinate, respectively. The differential equation of forced vibration of rectangular thin plate is given by

$$D\nabla^4 w(x, y, t) + c \frac{\partial w(x, y, t)}{\partial t} + \rho h \frac{\partial^2 w(x, y, t)}{\partial t^2} = p(x, y, t) \quad (4.1)$$

where

$$D = \frac{Eh^3}{12(1-\nu^2)}$$

$$\nabla^4 = \frac{\partial^4}{\partial x^4} + 2 \frac{\partial^4}{\partial x^2 \partial y^2} + \frac{\partial^4}{\partial y^4} \quad (4.2)$$

If the boundary condition has a couple of simply supported on the opposite edges, the mode shape are expressed as

$$\phi(x, y) = (A_1 \cos \lambda_1 y + A_2 \sin \lambda_1 y + A_3 \cosh \lambda_2 y + A_4 \sinh \lambda_2 y) \sin \mu x \quad (4.3)$$

where

$$\begin{aligned} \mu &= m\pi/a \\ \lambda_1 &= \sqrt{\mu^2 - \sqrt{\rho h \omega^2 / D}} \\ \lambda_2 &= \sqrt{\mu^2 + \sqrt{\rho h \omega^2 / D}} \end{aligned} \quad (4.4)$$

The constants A_1 to A_4 can be determinate according to the boundary condition. The transverse deflection $w(x, y, t)$ is then expressed as

$$w(x, y, t) = \sum_{m=1}^{\infty} \sum_{n=1}^{\infty} \phi_{mn}(x, y) \eta_{mn}(t) \quad (4.5)$$

where ϕ_{mn} is the m nth mode shape. The so-called pseudo random excitation $\tilde{p}(x, y, t)$ is used to replace the force $p(x, y, t)$ in the governing equation, where

$$\tilde{p}(x, y, t) = \sqrt{S_{pp}(x, y, t)} \exp(i\omega t) \quad (4.6)$$

and $S_{pp} = 0.5 (g^2 / \text{Hz})$ is the excitation PSD. By substituting above equation into governing equation and making use of the orthogonality of mode shape, it yields

$$\ddot{\tilde{\eta}}_{mn}(t) + 2\tilde{\xi}_{mn}\omega_{mn}\dot{\tilde{\eta}}_{mn}(t) + \omega_{mn}^2\tilde{\eta}_{mn}(t) = P_{mn} \cdot \exp(i\omega t) \quad (4.7)$$

where

$$\begin{aligned} P_{mn} &= \frac{1}{\gamma_{mn}} \int_0^a \int_0^b \sqrt{S_{pp}(x, y, t)} \phi_{mn}(x, y) dy dx \\ \gamma_{mn} &= \int_0^a \int_0^b \rho h \phi_{mn}^2(x, y) dy dx \end{aligned} \quad (4.8)$$

The relation between output and input is the frequency response function $H_{mn}(\omega)$. That is, $\tilde{\eta}_{mn}(t) = H_{mn}(\omega) P_{mn} \exp(i\omega t)$. For SDOF system it can be expressed as

$$H_{mn} = (\omega_{mn}^2 - \omega^2 + 2i\tilde{\xi}_{mn}\omega_{mn})^{-1} \quad (4.9)$$

Thus, the pseudo transverse deflection can be written as

$$\begin{aligned} \tilde{w}(x, y, t) &= \sum_{m=1}^{\infty} \sum_{n=1}^{\infty} \phi_{mn}(x, y) \tilde{\eta}_{mn}(t) \\ &= \sum_{m=1}^{\infty} \sum_{n=1}^{\infty} \phi_{mn}(x, y) H_{mn}(\omega) P_{mn} \exp(i\omega t) \end{aligned} \quad (4.10)$$

Finally, the transverse deflection response PSD can be obtained as

$$\begin{aligned}
 S_{ww}(x, y, \omega) &= \tilde{w}(x, y, t)^* \tilde{w}(x, y, t) \\
 &= \left(\sum_{m=1}^{\infty} \sum_{n=1}^{\infty} \phi_{mn}(x, y) H_{mn}(\omega) P_{mn} \right)^* \left(\sum_{m=1}^{\infty} \sum_{n=1}^{\infty} \phi_{mn}(x, y) H_{mn}(\omega) P_{mn} \right)
 \end{aligned} \tag{4.11}$$

where $\tilde{w}(x, y, t)^*$ is the complex conjugate value. The velocity and acceleration response PSD can also be obtained as

$$\begin{aligned}
 S_{\dot{w}\dot{w}} &= \tilde{\dot{w}}(x, y, t)^* \tilde{\dot{w}}(x, y, t) = \omega^2 \cdot S_{ww} \\
 S_{\ddot{w}\ddot{w}} &= \tilde{\ddot{w}}(x, y, t)^* \tilde{\ddot{w}}(x, y, t) = \omega^4 \cdot S_{ww}
 \end{aligned} \tag{4.12}$$

With the same input data including the plate geometry, material property and excitation PSD ... etc, the result can be seen in figure [4.2](#)

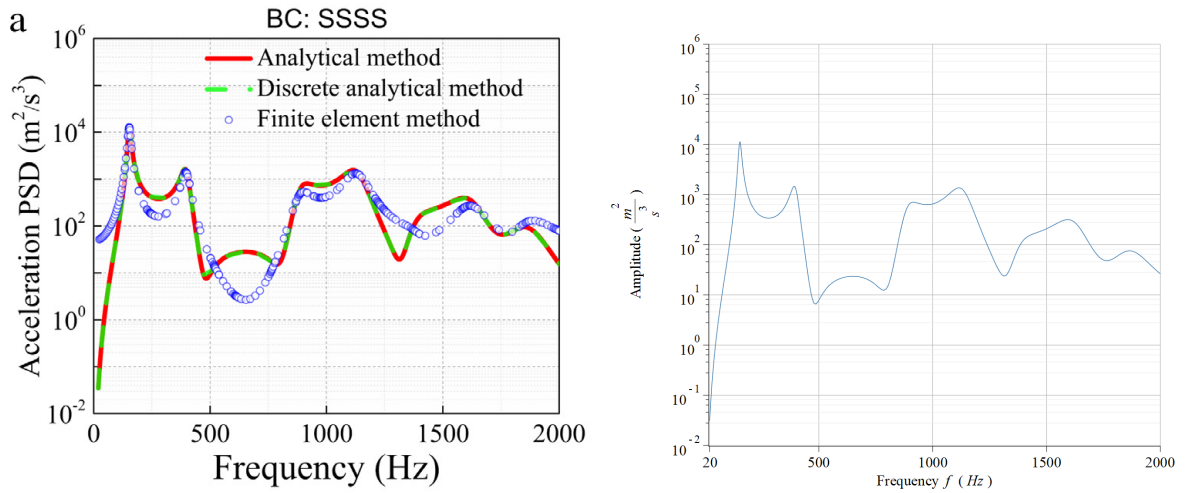


Figure 4.2: Result comparison

It can be seen that the results are the same and therefore this approach by [\[1\]](#) can be used in the following analysis.

4.2 Preliminary Study

To have a general idea of the plate vibration, a brief preliminary study is done in this section. The model is shown in figure 4.3. The harmonic base excitation is assumed to be $P \cos(\omega t)$.

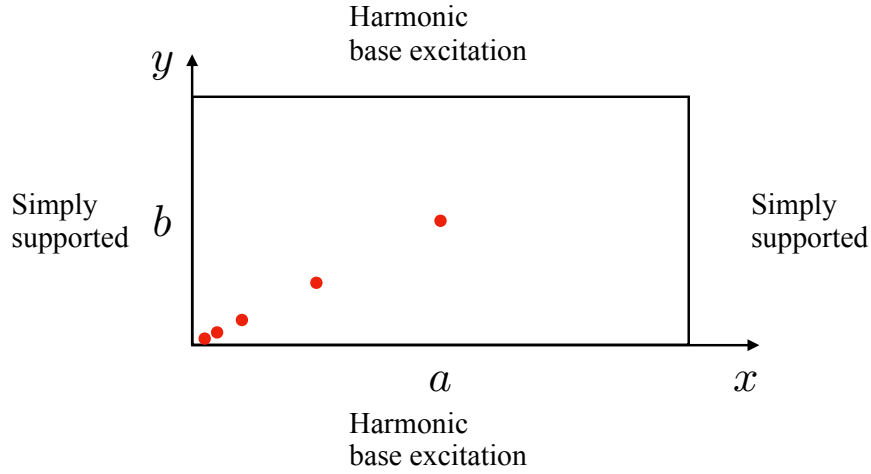


Figure 4.3: Model for preliminary study

For harmonic base excitation, it is equivalent to consider the excitation as boundary condition in free vibration. The differential equation for plate in free vibration is

$$D\nabla^4 w(x, y, t) + \rho h \frac{\partial^2 w(x, y, t)}{\partial t^2} = 0 \quad (4.13)$$

where the solution can be assumed as

$$\begin{aligned} w(x, y, t) &= W(x, y) T(t) \\ &= X(x) Y(y) \cos(\omega t) \end{aligned} \quad (4.14)$$

By substituting it in the differential equation, it yields

$$X''''Y + 2X''Y'' + Y'''' - \lambda^4 XY = 0 \quad (4.15)$$

where

$$\lambda^4 = \frac{\omega^2}{\beta_1^2} = \frac{\rho h \omega^2}{D} \quad (4.16)$$

If the boundary condition is simply supported along $x = 0$ and $x = a$ as shown in the model, $X(x)$ can be obtained as

$$X(x) = A \sin(\alpha_m x) \quad (4.17)$$

where A is a constant and $\alpha_m = m\pi/a$. While the equation becomes

$$Y''''(y) - 2\alpha_m^2 Y''(y) - (\lambda^4 - \alpha_m^4) Y(y) = 0 \quad (4.18)$$

Assuming $Y(y) = \exp^{sy}$, it gives

$$s^4 - 2s^2\alpha_m^2 - (\lambda^4 - \alpha_m^4) = 0 \quad (4.19)$$

By solving above equation, $Y(y)$ can be obtained as

$$Y(y) = C_1 \sin \delta_1 y + C_2 \cos \delta_1 y + C_3 \sinh \delta_2 y + C_4 \cosh \delta_2 y \quad (4.20)$$

where

$$\begin{aligned} \delta_1 &= \sqrt{\lambda^2 - \alpha_m^2} \\ \delta_2 &= \sqrt{\lambda^2 + \alpha_m^2} \end{aligned} \quad (4.21)$$

and the constants C_1 to C_4 can be obtained by the following boundary conditions

1. $W(x, 0) = P$
2. $W(x, b) = P$
3. $M_y(x, 0) = -D \left(\frac{\partial^2 W}{\partial y^2} + \nu \frac{\partial^2 W}{\partial x^2} \right) \Big|_{(x,0)} = 0$
4. $M_y(x, b) = -D \left(\frac{\partial^2 W}{\partial y^2} + \nu \frac{\partial^2 W}{\partial x^2} \right) \Big|_{(x,b)} = 0$

Once the constants C_1 TO C_4 are obtained, $Y(y)$ can also be obtained and hence the displacement $w(x, y, t)$. To compare the force caused by harmonic excitation, the acceleration is calculated by taking the second derivative of $w(x, y, t)$ and multiply with the plate mass. That is,

$$F = \frac{\partial^2 w(x, y, t)}{\partial t^2} \cdot M_{plate} \quad (4.22)$$

Finally, the result can be seen in figure 4.4. It should be noted that all the numerical data are the same in table 4.1, while the amplitude of harmonic excitation P is take as 0.01 (mm) in the analysis.

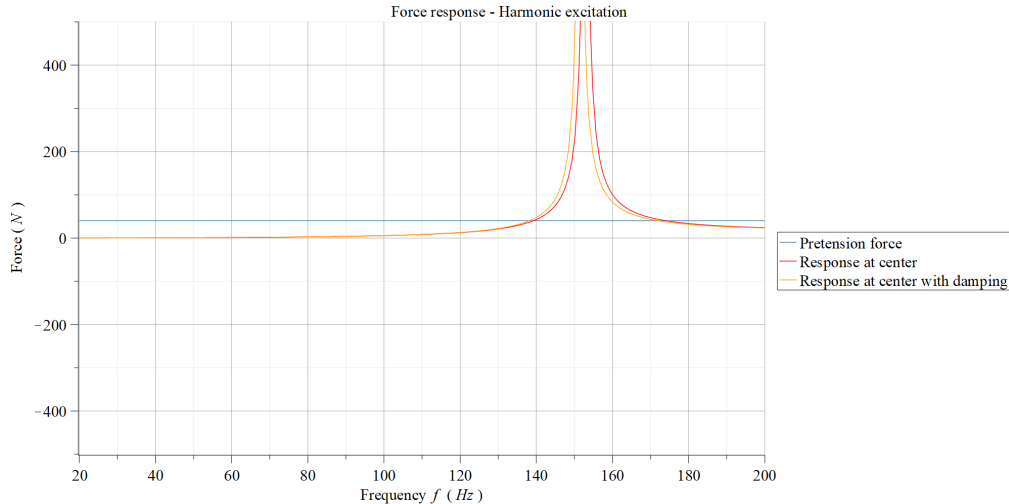


Figure 4.4: Harmonic excitation

Noted that the figure is shown in absolute value with the pretension force line so it is easier to find the admissible range of frequency. It can be seen that the harmonic excitation does not cause much force to most of the frequency. However, when the excitation frequency gets closer to the resonance frequency (in this case, it is 152 Hz for the first mode), the force becomes really large and will most likely to make the support pins loss contact with solar panel since the pretension force is only 40 Newtons. It can also be seen that the result with damping is very similar to the one without it, the only change is the resonance frequency is slightly shifted to the other one. From the above results, it can be concluded that if the plate is subjected to the harmonic excitation only instead of random excitation, the support pins will indeed loss contact near the resonance frequency.

4.3 Plate Model

In order to find the frequency response function of the plate model, modal analysis need to be performed first. The equation of motion of plate is shown in equation 4.23.

$$D\nabla^4 w(x, y, t) + c \frac{\partial w(x, y, t)}{\partial t} + \rho h \frac{\partial^2 w(x, y, t)}{\partial t^2} = f(t) \quad (4.23)$$

where

$$D = \frac{Eh^3}{12(1-\nu^2)} \quad (4.24)$$

$$\nabla^4 = \frac{\partial^4}{\partial x^4} + 2 \frac{\partial^4}{\partial x^2 \partial y^2} + \frac{\partial^4}{\partial y^4}$$

In the above equations, E , ρ , ν , c and h are the Young's modulus, mass density, Poisson's ration, damping coefficient and thickness of the plate, respectively. The transverse displacement of plate at location (x, y) and time t is $w(x, y, t)$, while $f(t)$ represents the time-varying force applied on the plate.

As explained in section 1.1, the plate model used is a simply supported aluminum plate subjected to random excitation. Follow the same procedure described in section 2.3, it can be assumed that equation 4.23 has the solution in the form of

$$w(x, y, t) = \sum_{m=1}^{\infty} \sum_{n=1}^{\infty} W_{mn}(x, y) \eta_{mn}(t) \quad (4.25)$$

where $W_{mn}(x, y)$ is the mode shape and $\eta_{mn}(t)$ is generalized coordinate. The mode shape is normalized in order to satisfy orthogonality as follows

$$\int_0^a \int_0^b \rho h \cdot W_{mn}^2 dy dx = 1 \quad (4.26)$$

Consider the boundary condition of plate as simply supported plate along four edges, the mode shape and natural frequency are given as

$$\begin{aligned}
W_{mn} &= \frac{2}{\sqrt{\rho h a b}} \cdot \sin\left(\frac{m\pi x}{a}\right) \sin\left(\frac{n\pi y}{b}\right) \\
\omega_{mn} &= \pi^2 \sqrt{\frac{D}{\rho h}} \cdot \left[\left(\frac{m}{a}\right)^2 + \left(\frac{n}{b}\right)^2 \right]
\end{aligned} \tag{4.27}$$

Substitute equation 4.25 into equation 4.23 and integrate it over the surface domain, a series decoupled equations can be obtained as shown in equation 4.28.

$$\ddot{\eta}_{mn}(t) + 2\xi_{mn}\omega_{mn}\dot{\eta}_{mn}(t) + \omega_{mn}^2\eta_{mn}(t) = N_{mn} \cdot f(t) \tag{4.28}$$

where

$$N_{mn} = \int_0^a \int_0^b W_{mn}(x, y) dy dx \tag{4.29}$$

By making use of frequency response function $H(\omega)$, the solution for equation 4.28 is assumed to be

$$\tilde{\eta}_{mn}(\omega) = H_{\eta, mn}(\omega) \cdot N_{mn} \cdot \tilde{f}(\omega) \tag{4.30}$$

Furthermore, according to equation 3.45, the frequency response function $H_{\eta, mn}$ for damped plate can be found as

$$H_{\eta, mn}(\omega) = \frac{1}{\omega_{mn}^2 + 2i\omega\xi_{mn}\omega_{mn} - \omega^2} \tag{4.31}$$

Finally, substitute equation 4.30 into 4.25, the solution of $w(x, y, t)$ or $\tilde{w}(x, y, \omega)$ can be expressed as

$$\begin{aligned}
w(x, y, t) &= \sum_{m=1}^{\infty} \sum_{n=1}^{\infty} W_{mn}(x, y) \eta_{mn}(t) \\
\tilde{w}(x, y, \omega) &= \sum_{m=1}^{\infty} \sum_{n=1}^{\infty} W_{mn}(x, y) \tilde{\eta}_{mn}(\omega) \\
&= \sum_{m=1}^{\infty} \sum_{n=1}^{\infty} W_{mn}(x, y) H_{\eta, mn}(\omega) N_{mn} \cdot \tilde{f}(\omega) \\
&= H_w(\omega) \cdot \tilde{f}(\omega)
\end{aligned} \tag{4.32}$$

The displacement response power spectral density (PSD) S_{ww} of the plate model with an acceleration excitation PSD S_{ff} can be found by

$$S_{ww} = |H_w|^2 \cdot S_{ff} \tag{4.33}$$

while the velocity and acceleration PSD are given by

$$\begin{aligned}
S_{\dot{w}\dot{w}} &= \omega^2 \cdot S_{ww} \\
S_{\ddot{w}\ddot{w}} &= \omega^4 \cdot S_{ww}
\end{aligned}
\tag{4.34}$$

Once the acceleration PSD is found, the root-mean-square acceleration A_{rms} can be calculated through the area under the PSD curve as shown in equation 4.35. Thereafter the resultant force caused by random excitation F_{random} can be found by multiplying the mass of plate M_{plate} with A_{rms} . It should be noted that normally the acceleration PSD has an unit of g^2/Hz and hence the root-mean square acceleration has an unit of g , which is commonly referred as G_{rms} value. However in order to find out the resultant force, the unit of acceleration should be m/s^2 . Thus the root-mean-square acceleration here is referred as A_{rms} for the unit is different from G_{rms} . It can be seen that the relation is $A_{rms} = G_{rms} \cdot 9.81$.

$$A_{rms} = \sqrt{\int_{f_l}^{f_h} S_{\ddot{w}\ddot{w}} df} \cdot 9.81
\tag{4.35}$$

$$F_{random} = M_{plate} \cdot A_{rms}$$

The following analysis is categorized as four studies, namely the study of mode shape, location, damping and material. Each study focus on one variable only in order to have a better understanding on the system behavior.

4.3.1 Study of Mode Shape

In equation 4.32, the upper limit of summation for modes m and n are infinity, however it is not necessary to find a convergent result. The study of mode shape focuses on determine the system response with different number of mode shape. By making use of this study, it can be seen that how many mode shapes should be included for the following analysis. Thus, the upper limit for mode m and n are set to be M and N , respectively. That is, M and N are the number of modes included. The location chosen for analysis is the middle of the plate. The result can be seen in figure 4.5.

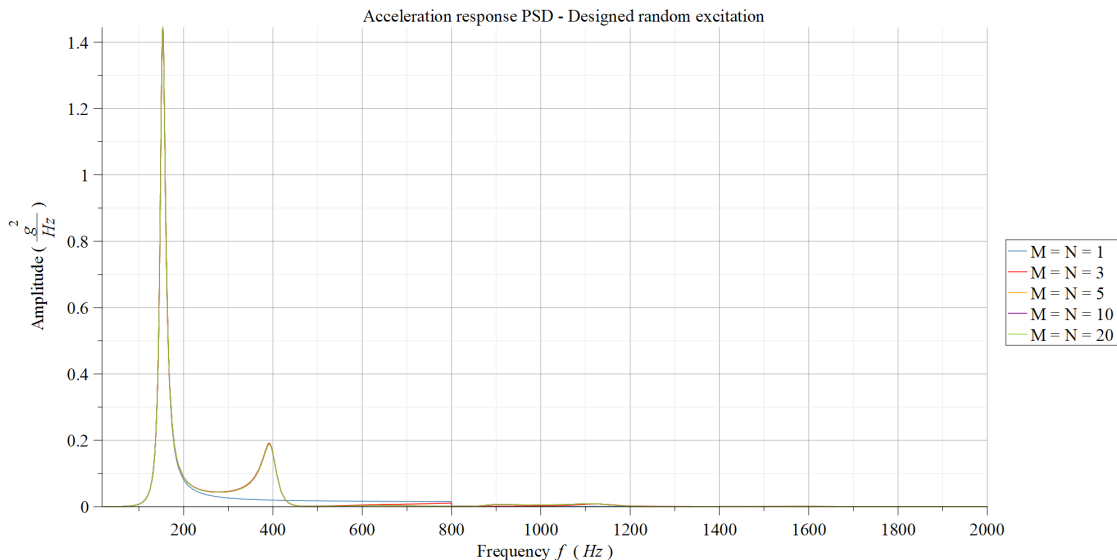


Figure 4.5: Acceleration response PSD - Designed random excitation

The A_{rms} values of different number of mode shape is shown in table [4.3](#).

Table 4.2: A_{rms} value of different condition

Number of mode shape	$A_{rms} (m/s^2)$	$F_{random} (N)$
$M = N = 1$	66.31	28.64
$M = N = 3$	70.69	30.54
$M = N = 5$	70.69	30.54
$M = N = 10$	70.69	30.54
$M = N = 20$	70.69	30.54

It can be seen from the result above, the resultant force does not change above $M = N = 3$. Therefore, to be more conservative, the number of mode shapes for following studies is chosen as $M = N = 5$.

4.3.2 Study of Location

The study of location focuses on determine the system response in different location of the plate. The most relevant location in this project is the center of the plate, where the pretension force is applied. The location chosen for analysis can be seen in figure [4.6](#).

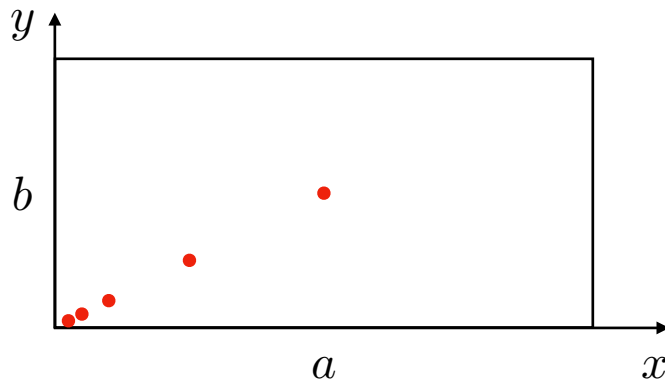


Figure 4.6: Location chosen for analysis

The result can be seen in figure [4.7](#).

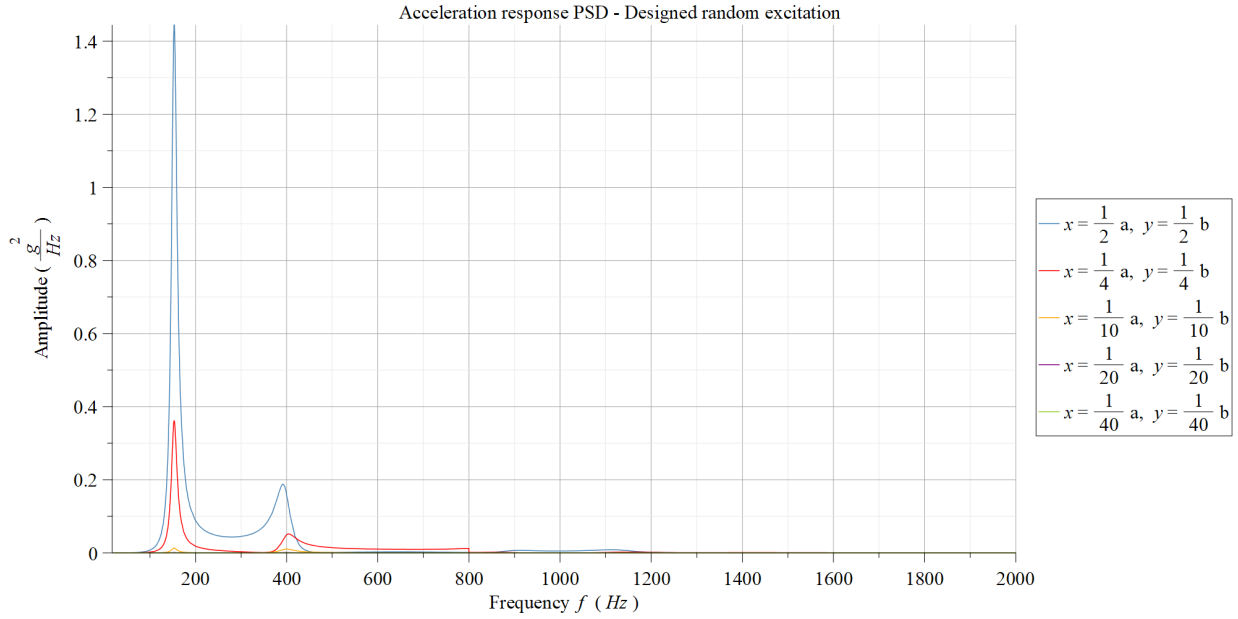


Figure 4.7: Acceleration response PSD - Designed random excitation

The A_{rms} values of different location (x, y) is shown in table [4.3](#).

Table 4.3: A_{rms} value of different condition

Location	$A_{rms} (m/s^2)$	$F_{random} (N)$
$x = \frac{a}{2}, y = \frac{b}{2}$	70.69	30.54
$x = \frac{a}{4}, y = \frac{b}{4}$	39.57	17.09
$x = \frac{a}{10}, y = \frac{b}{10}$	10.79	4.66
$x = \frac{a}{20}, y = \frac{b}{20}$	3.04	1.31
$x = \frac{a}{40}, y = \frac{b}{40}$	0.78	0.34

It can be seen from the result above, the resultant force caused by random excitation at center of the plate is 30.54 (N). The resultant force is smaller than the pretension force and hence the support pins should remain contact. However, it should be bear in mind that the A_{rms} used here is one sigma value as explained in chapter [3](#). It means that the result is assumed to be valid only within 68% of time. If three sigma value (i.e. 99.7%) is taken into account, the resultant force would be 91.7 (N). Therefore, it is recommended to increase the pretension force for keeping the support pins in contact.

The other result from above study is that the A_{rms} value decreases when the location is closer to the edge. This is a reasonable result since the boundary condition is set to be simply supported. That is, the boundaries do not have any displacement and hence acceleration.

4.3.3 Study of Damping

The study of damping focuses on determine the system response with different damping of the plate. The location is chosen at the middle of the plate, where the largest resultant force is. Since the real damping of the system is difficult to measure, a damping ratio 0.05 is used as a start point. However, it can be seen from the study of location that the pretension force is not enough if three sigma acceleration is used. Thus, a study of damping is essential and also offer a general idea when adjusting the system. The result can be seen in figure 4.8.

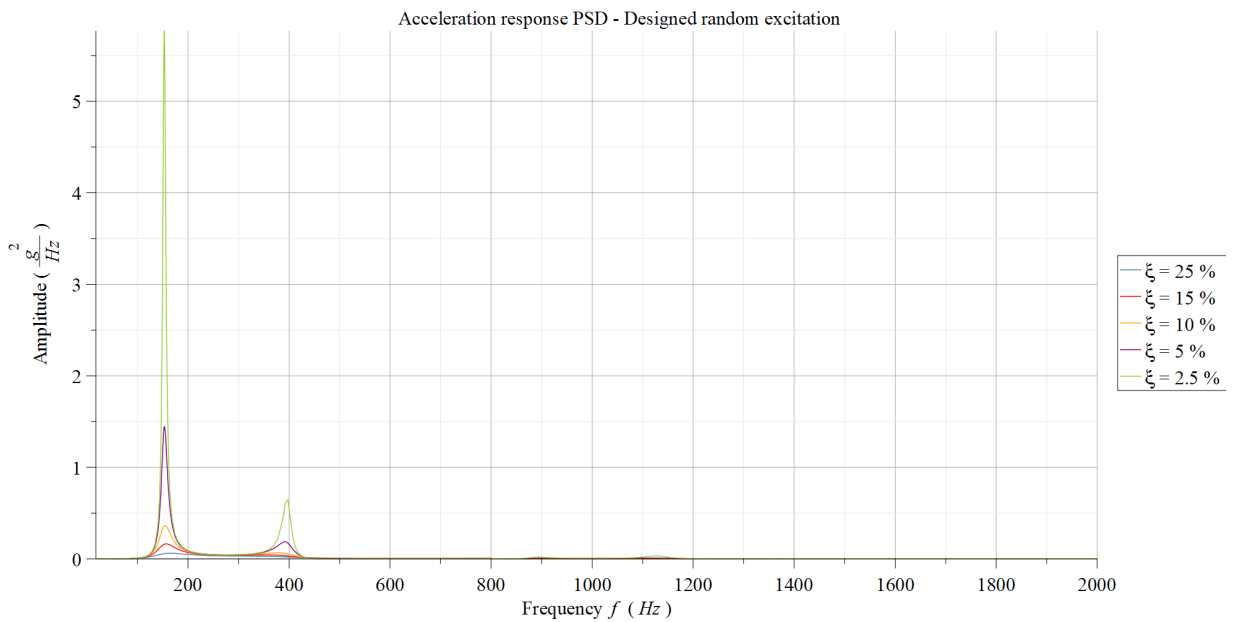


Figure 4.8: Acceleration response PSD - Designed random excitation

The A_{rms} values of different damping ratio ζ is shown in table 4.4.

Table 4.4: A_{rms} value of different damping ratio

Location	$A_{rms} (m/s^2)$	$F_{random} (N)$
$\zeta = 25\%$	36.33	15.69
$\zeta = 15\%$	44.06	19.03
$\zeta = 10\%$	52.04	22.48
$\zeta = 5\%$	70.69	30.54
$\zeta = 2.5\%$	97.66	42.19

If three sigma acceleration is used, the resultant force should be lower than 13.34 (N) for a pretension force of 40 (N). However, it can be seen from the result above, even a 25% damping ratio is not enough to reach it. A 25% damping ratio is not very realistic in a common system. Thus, an increase of pretension force is recommended more than increase the damping system. Thus, an increase of pretension force is recommended more than increase the damping ratio to a very high value in order to keep the support pins in contact.

4.3.4 Study of Material

Due to confidentiality concern, the previous studies are done with the property of aluminum plate. However, the influence of material property is also helpful in order to find out the deviation between the analysis here and the real system. According to the result in [8], the overall Young's modulus of the Al-Si solar cells is estimated to be 43 GPa. The mass density is not changed in this study since the mass density of silicon is close to aluminum. The result can be seen in figure 4.9.

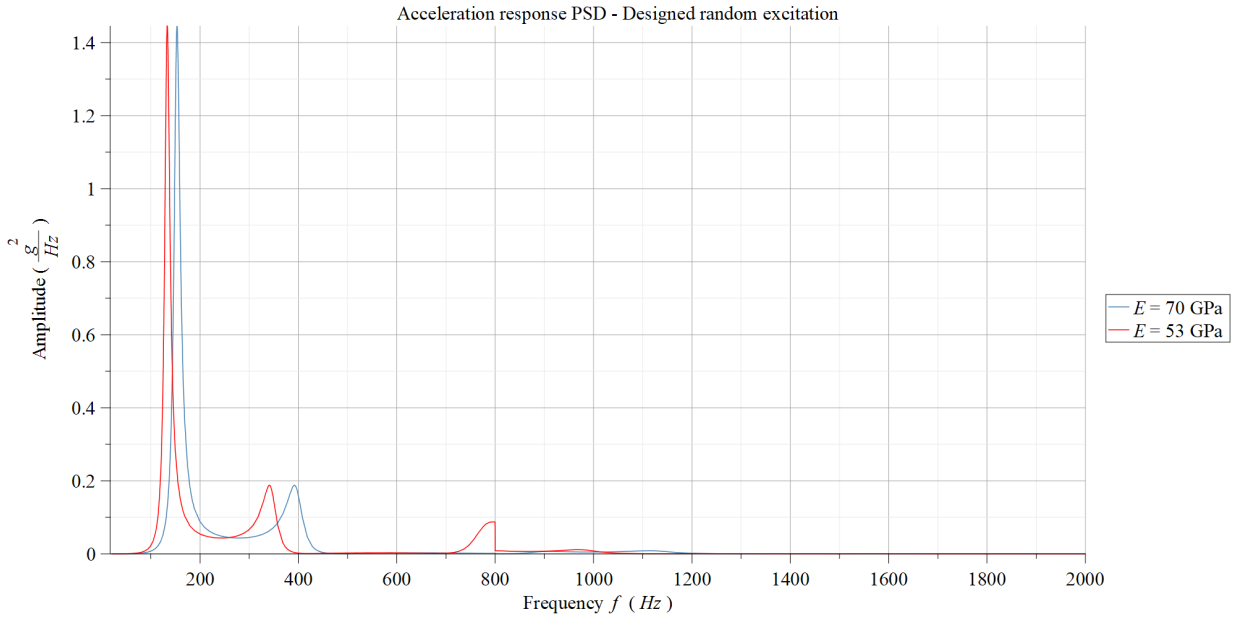


Figure 4.9: Acceleration response PSD - Designed random excitation

The A_{rms} values of different damping ratio ζ is shown in table 4.5.

Table 4.5: A_{rms} value of different Young's modulus

Location	$A_{rms} (m/s^2)$	$F_{random} (N)$
$E = 70GPa$	70.69	30.54
$E = 53GPa$	68.84	29.74

It can be seen from the result that the resultant forces are close. Thus the influence for the contact is not obvious. However, it can also be noticed that the frequency of amplitude peaks are changed. That is, the system behavior (i.e. frequency response function) and resonance frequency are changed slightly.

4.4 Summary and Discussion

Consider all the results presents in section 4.3, a brief summary and discussion is presented here. The figures of response spectral density contain several information, one of which is the peaks that distributed along the frequency. The peaks show the resonance frequencies of the system. When a system is excited by its resonance frequency, the response would

be much greater than it being excited with other frequency. It can also be seen that the number of peaks is related to the number of mode shapes included in the analysis. As the number of mode shape included increases, more peaks appear.

Moreover, it can be seen from the results that the number of mode shape does not have a great effect on the A_{rms} value. On the other hand, the location has larger influence. The center part of the plate has the largest A_{rms} value and the vicinity of plate edge has much lower one. This is a reasonable result since the boundary is simply supported, which means there should be no transverse deflection at the end of plate. In other words, the acceleration should be very small compare to other part of the plate given the same probability (one sigma value, see detail in section 3.3).

Another result worth noticing is the effect of damping. The A_{rms} values are lower in the plate model with larger damping ratio. That is, the damping indeed reduces the acceleration. It should be noted that the fundamental difference between the plates with different damping ratio during random vibration analysis takes place in the frequency response function $H(\omega)$. Since other component of equation 4.32 are the same, the frequency response function is the critical part where the difference appears. This result is also corresponding what was mentioned in section 3.3 that the frequency response function can be used to manipulate system response.

Additionally, the effect of damping can also be seen directly from the figure, especially in the range where excitation PSD is constant (50Hz to 800Hz). Since the excitation PSD is only a constant, the response spectral density is essentially the plot of $|H_w|^2$. Thus, due to the correlation between damping and frequency response function, the damping effect can also be seen directly from the figures. To be more clear, the width of each peak appears to be wider when damping is larger.

Finally, the problem regarding if the pretension force is enough to hold the solar panels in random excitation needs to be addressed. It can be clearly seen from the results that the resultant force (30.54N) caused by random excitation is smaller than the presentation force (40N) for one sigma value (68%). However, if three sigma value (99.7%) is considered, the resultant force (91.7N) would be larger than pretension force. It results that the support pins should remain in contact within only part of the time during launching. Therefore, it is recommended to increase the pretension force to a level such that it is larger than 91.7N.

It should be emphasized that the results are only valid for the given conditions. That is, the solar panels are made of aluminum and the boundaries are simply supported. However, neither of these conditions are completely true for the real solar panels on nano-satellite. This result only gives the basic understanding of how the system would behave and should not be used directly in design. Instead, the result can be adopted for further analysis in order to build a more realistic analytical model.

Chapter 5 Conclusion

The deployable solar panels attached on nano-satellites are folded into several layers during the launch of a rocket. Afterwards, they will unfold when the correct orbit is reached. Consider the forces originated from rocket, the folded solar panels would indeed experience random vibration during launching. Therefore, it is necessary to understand the characteristic of a solar panel subjected to random vibration in order to build a better design. This project focuses on providing a basic understanding of random vibration and analytical solutions of several relevant models.

The random vibration analysis consists in two major parts, namely the analysis of vibration and random variable. Firstly, the theory of vibration is reviewed in chapter [2](#) including single degree of freedom model, multiple degree of freedom model and plate vibration. The associate topic modal analysis is also reviewed and plays an important role in the following analysis. Beam vibration can also be found in appendix [A](#). Secondly, the theory of probability regarding random variable analysis is introduced in chapter [3](#). In random vibration, the excitation can not be modeled as a single time function and needs to be expressed by random variable. Thus, the idea of probability and corresponding time and frequency domain analysis method are introduced. Finally, the analytical analysis of several models based on the theories stated above is presented in chapter [4](#).

In analytical analysis, a verification of previous study and a preliminary study are conducted first. It verifies the approach used and provides the general idea of harmonic base excitation of plate. Thereafter, four plate studies are utilized for a better representation of a solar panel. Beam models subjected to base excitation and white noise random excitation can also be found in appendix [B](#), in the beginning of the project they served as a starting point since they are relatively simple to analyze.

The four studies include study of mode, location, damping and material. Each of them focuses on changing one variable only and determine change of system response. The results of above studies are summarized and discussed in section [4.4](#). Several notes are given on how the characteristic of the system is changed when adjusting the analysis settings. The figures of response spectral density contain several information. For instance, the response spectral density gives some rough estimation regarding how large is the damping of the system and where the resonance frequencies are. The root-mean-square acceleration A_{rms} results serve as an important factor when determining if the contact would loss between solar panels and support pins. Compare the maximum force in the middle of the plate (30.54 Newtons) with the pretension force (40 Newtons), it is thereafter concluded that the pretension force can hold the solar panels from losing contact with support pins for one-sigma value.

For future analysis on this topic, more boundary conditions and material property are recommended to consider. Due to the lack of time, the scope of this project is very limited. Since the solar panels are actually supported by only four to six support pins, the boundary condition considered in this project may not be accurate enough. More boundary conditions of the models could be utilized and try to simulate the actual condition the best possible way. Additionally, the material property used should be adjusted to the one of solar panels. Another commonly used estimation tool known as Mile's equation is also worth noticing. [11]

Bibliography

- [1] Guohai Chen, Jilei Zhou, and Dixiong Yang. “Benchmark solutions of stationary random vibration for rectangular thin plate based on discrete analytical method”. In: *Probabilistic Engineering Mechanics* 50 (2017), pp. 17–24.
- [2] Clive L. Dym and Irving H. Shames. *Solid Mechanics : A Variational Approach*. Augmented ed. Springer New York, 2013.
- [3] GomSpace. *GomSpace*. URL: <https://gomspace.com/home.aspx>.
- [4] NASA Finite Element Modeling Continuous Improvement group. *FEMCI Book*. URL: <https://femci.gsfc.nasa.gov/index.html>.
- [5] Ashkan Haji Hosseinloo, Fook Fah Yap, and Nader Vahdati. “Analytical Random Vibration Analysis of Boundary-excited thin Rectangular Plates”. In: *International Journal of Structural Stability and Dynamics* 13 (2013).
- [6] Loren D. Lutes and Shahram Sarkani. *Random Vibrations : Analysis of Structural and Mechanical Systems*. 1st ed. Elsevier Inc., 2004.
- [7] NASA. *General Environmental Verification Standard (GEVS)*. Tech. rep. 2013.
- [8] V. A. Popovich et al. “Understanding the Properties of Silicon Solar Cells Aluminium Contact Layers and Its Effect on Mechanical Stability”. In: *Materials Sciences and Applications* 4 (2013), pp. 118–127.
- [9] Singiresu S. Rao. *Mechanical Vibrations*. 5th ed. Pearson Education Inc., 2010.
- [10] Singiresu S. Rao. *Vibration of Continuous Systems*. John Wiley and Sons Inc, 2007.
- [11] Jaap Wijker. *Miles’ Equation in Random Vibrations : Theory and Applications in Spacecraft Structures Design*. Springer, 2018.

Appendix A Beam Vibration

The equation of motion of beam is firstly derived and followed by the description of various boundary conditions in this section. The boundary condition is not introduced in the previous sections since it only influences the discrete system in an indirect way. Finally, the analysis of free and forced vibration of beam is demonstrated.

A.1 Equation of Motion and Boundary Condition

Consider a beam subjected to distributed load $f(x, t)$ as shown in figure [A.1](#). $M(x, t)$, $V(x, t)$ and $w(x, t)$ represents the bending moment, shear force and lateral deflection of the beam, respectively.

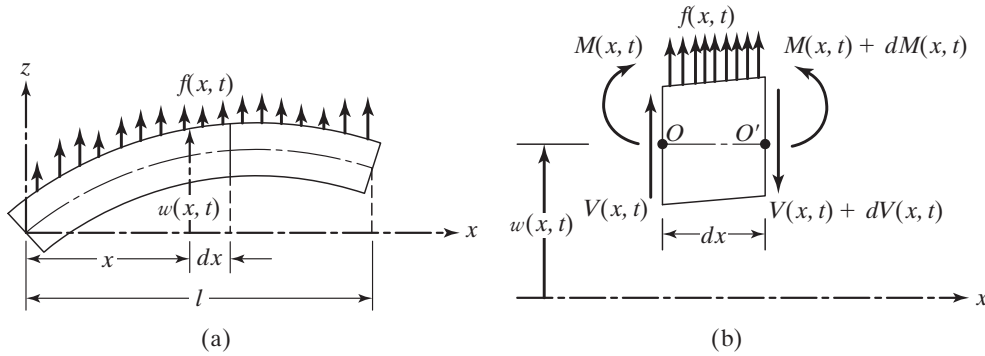


Figure A.1: (a) A beam subjected to distributed load. (b) Free body diagram of the beam [\[9\]](#)

By making use of force and moment equilibrium with the relation between shear force and moment $V = \partial M / \partial x$, it gives

$$-\frac{\partial^2 M}{\partial x^2}(x, t) + f(x, t) = \rho A(x) \frac{\partial^2 w}{\partial t^2}(x, t) \quad (\text{A.1})$$

where ρ and $A(x)$ are the mass density and cross section area of the beam, respectively. The moment M can be found by Euler-Bernoulli thin beam theory

$$M(x, t) = EI(x) \frac{\partial^2 w}{\partial x^2}(x, t) \quad (\text{A.2})$$

where E and $I(x)$ are the Young's modulus and moment of inertia of the beam. Substitute equation [A.2](#) into [A.1](#), it yields

$$\frac{\partial^2}{\partial x^2} \left[EI(x) \frac{\partial^2 w}{\partial x^2}(x, t) \right] + \rho A(x) \frac{\partial^2 w}{\partial t^2}(x, t) = f(x, t) \quad (\text{A.3})$$

For a uniform beam, which $I(x) = I$ and $A(x) = A$, equation [A.3](#) becomes

$$EI \frac{\partial^4 w}{\partial x^4} (x, t) + \rho A \frac{\partial^2 w}{\partial t^2} (x, t) = f(x, t) \quad (\text{A.4})$$

or for free vibration

$$c^2 \frac{\partial^4 w}{\partial x^4} (x, t) + \frac{\partial^2 w}{\partial t^2} (x, t) = 0 \quad (\text{A.5})$$

where

$$c = \sqrt{\frac{EI}{\rho A}} \quad (\text{A.6})$$

There are three commonly used boundary conditions, namely free end, simply supported and fixed, for beam vibration as listed below

1. Free end :

(a) Bending moment : $EI \frac{\partial^2 w}{\partial x^2} = 0$

(b) Shear force : $\frac{\partial}{\partial x} \left(EI \frac{\partial^2 w}{\partial x^2} \right) = 0$

2. Simply supported (pinned) end :

(a) Deflection : $w = 0$

(b) Bending moment : $EI \frac{\partial^2 w}{\partial x^2} = 0$

3. Fixed (clamped) end :

(a) Deflection : $w = 0$

(b) Slope (angle) : $\frac{\partial w}{\partial x} = 0$

A.2 Free and Forced Vibration of Beam

A.2.1 Free Vibration

The response for free vibration of beam can be obtained by making use of the method separation of variables, that is

$$w(x, t) = W(x) \cdot T(t) \quad (\text{A.7})$$

where $W(x)$ is known as mode shape or normal mode and $T(t)$ is a time dependent function. Substitute equation [A.7](#) into [A.5](#) and rewritten as

$$\frac{c^2}{W(x)} \frac{d^4 W(x)}{dx^4} = -\frac{1}{T(t)} \frac{d^2 T(t)}{dt^2} = \omega^2 \quad (\text{A.8})$$

Since each part of the equation depends on different variable, they much equal to a constant, which is assumed to be the square of natural frequency ω^2 . Thus, equation [A.8](#) can be rewritten as

$$\begin{aligned}\frac{d^2T(t)}{dt^2} + \omega^2T(t) &= 0 \\ \frac{d^4W(x)}{dx^4} - \beta^4W(x) &= 0\end{aligned}\tag{A.9}$$

where

$$\beta^4 = \frac{\omega^2}{c^2} = \frac{\rho A \omega^2}{EI}\tag{A.10}$$

The solution of the first part of equation [A.9](#) can be assumed as

$$T(t) = A \cos(\omega t) + B \sin(\omega t)\tag{A.11}$$

where A and B are constants and can be found with initial condition. While the solution of the second part of equation [A.9](#) can be assumed as

$$W(x) = C \cdot e^{sx}\tag{A.12}$$

where C and s are constants. By substituting equation [A.12](#) into [A.9](#), the normal mode $W(x)$ and frequency ω can be found as

$$\begin{aligned}W(x) &= C_1 \cos(\beta x) + C_2 \sin(\beta x) + C_3 \cosh(\beta x) + C_4 \sinh(\beta x) \\ \omega &= \beta^2 \sqrt{\frac{EI}{\rho A}}\end{aligned}\tag{A.13}$$

where C_1, C_2, C_3 and C_4 are constants and can be determined by the boundary conditions. For a fixed-simply supported uniform beam with length l , equation [A.13](#) becomes

$$\begin{aligned}C_1 [\cos(\beta l) - \cosh(\beta l)] + C_2 [\sin(\beta l) - \sinh(\beta l)] &= 0 \\ -C_1 [\cos(\beta l) + \cosh(\beta l)] - C_2 [\sin(\beta l) + \sinh(\beta l)] &= 0\end{aligned}\tag{A.14}$$

In order to find a non-trivial solution, the determinant of equation [A.14](#) must be zero. Thus,

$$\cos(\beta l) \sinh(\beta l) - \sin(\beta l) \cosh(\beta l)\tag{A.15}$$

or

$$\tan(\beta l) = \tanh(\beta l)\tag{A.16}$$

Equation [A.16](#) is known as frequency equation, since the roots of this equation $\beta_n l$ gives the natural frequencies ω_n . Equation [A.10](#) is now rewritten as

$$\omega_n = \beta_n^2 \sqrt{\frac{EI}{\rho A}}\tag{A.17}$$

Therefore, the corresponding lateral displacement $w_n(x, t)$ can be expressed as

$$w_n(x, t) = W_n(x) [A_n \cos(\omega_n t) + B_n \sin(\omega_n t)] \quad (\text{A.18})$$

Finally, the complete solution of $w(x, t)$ is given by

$$w(x, t) = \sum_{n=1}^{\infty} W_n(x) [A_n \cos(\omega_n t) + B_n \sin(\omega_n t)] \quad (\text{A.19})$$

It should be noted that the normal mode W_n also has the property orthogonality for the domain (i.e. from 0 to l) as shown in equation [A.20](#).

$$\int_0^l \rho A W_n^2 dx = 1 \quad (\text{A.20})$$

Additionally, figure [A.2](#) by [\[9\]](#) shows the common boundary conditions, frequency equations and mode shapes for the transverse vibration of a beam.

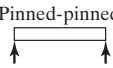
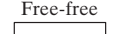
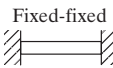
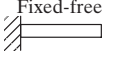
End Conditions of Beam	Frequency Equation	Mode Shape (Normal Function)	Value of $\beta_n l$
 Pinned-pinned	$\sin \beta_n l = 0$	$W_n(x) = C_n [\sin \beta_n x]$	$\beta_1 l = \pi$ $\beta_2 l = 2\pi$ $\beta_3 l = 3\pi$ $\beta_4 l = 4\pi$
 Free-free	$\cos \beta_n l \cdot \cosh \beta_n l = 1$	$W_n(x) = C_n [\sin \beta_n x + \sinh \beta_n x + \alpha_n (\cos \beta_n x + \cosh \beta_n x)]$ where $\alpha_n = \left(\frac{\sin \beta_n l - \sinh \beta_n l}{\cosh \beta_n l - \cos \beta_n l} \right)$	$\beta_1 l = 4.730041$ $\beta_2 l = 7.853205$ $\beta_3 l = 10.995608$ $\beta_4 l = 14.137165$ ($\beta l = 0$ for rigid-body mode)
 Fixed-fixed	$\cos \beta_n l \cdot \cosh \beta_n l = 1$	$W_n(x) = C_n [\sin \beta_n x - \sinh \beta_n x + \alpha_n (\cosh \beta_n x - \cos \beta_n x)]$ where $\alpha_n = \left(\frac{\sinh \beta_n l - \sin \beta_n l}{\cos \beta_n l - \cosh \beta_n l} \right)$	$\beta_1 l = 4.730041$ $\beta_2 l = 7.853205$ $\beta_3 l = 10.995608$ $\beta_4 l = 14.137165$
 Fixed-free	$\cos \beta_n l \cdot \cosh \beta_n l = -1$	$W_n(x) = C_n [\sin \beta_n x - \sinh \beta_n x - \alpha_n (\cos \beta_n x - \cosh \beta_n x)]$ where $\alpha_n = \left(\frac{\sin \beta_n l + \sinh \beta_n l}{\cos \beta_n l + \cosh \beta_n l} \right)$	$\beta_1 l = 1.875104$ $\beta_2 l = 4.694091$ $\beta_3 l = 7.854757$ $\beta_4 l = 10.995541$
 Fixed-pinned	$\tan \beta_n l - \tanh \beta_n l = 0$	$W_n(x) = C_n [\sin \beta_n x - \sinh \beta_n x + \alpha_n (\cosh \beta_n x - \cos \beta_n x)]$ where $\alpha_n = \left(\frac{\sin \beta_n l - \sinh \beta_n l}{\cos \beta_n l - \cosh \beta_n l} \right)$	$\beta_1 l = 3.926602$ $\beta_2 l = 7.068583$ $\beta_3 l = 10.210176$ $\beta_4 l = 13.351768$
 Pinned-free	$\tan \beta_n l - \tanh \beta_n l = 0$	$W_n(x) = C_n [\sin \beta_n x + \alpha_n \sinh \beta_n x]$ where $\alpha_n = \left(\frac{\sin \beta_n l}{\sinh \beta_n l} \right)$	$\beta_1 l = 3.926602$ $\beta_2 l = 7.068583$ $\beta_3 l = 10.210176$ $\beta_4 l = 13.351768$ ($\beta l = 0$ for rigid-body mode)

Figure A.2: Common boundary conditions for the transverse vibration of a beam. [\[9\]](#)

A.2.2 Forced Vibration

The analysis of forced vibration of beam follows very similar procedure as described earlier. The deflection $w(x, t)$ is assumed as

$$w(x, t) = \sum_{n=1}^{\infty} W_n(x) q_n(t) \quad (\text{A.21})$$

where W_n is taken from the second part of equation [A.9](#) with ω_n from equation [A.17](#). q_n is the n -th generalized coordinate. Substitute equation [A.21](#) into [A.4](#), it becomes

$$EI \sum_{n=1}^{\infty} \frac{d^4 W_n(x)}{dx^4} q_n(t) + \rho A \sum_{n=1}^{\infty} W_n(x) \frac{d^2 q_n(t)}{dt^2} = f(x, t) \quad (\text{A.22})$$

or rewritten as

$$\sum_{n=1}^{\infty} \omega_n^2 W_n(x) q_n(t) + \sum_{n=1}^{\infty} W_n(x) \frac{d^2 q_n(t)}{dt^2} = \frac{1}{\rho A} f(x, t) \quad (\text{A.23})$$

Premultiply equation [A.23](#) by $W_m(x)$ and integrate it from 0 to l , i.e. the domain, and use the orthogonality condition shown in equation [A.20](#), it yields to

$$\frac{d^2 q_n(t)}{dt^2} + \omega_n^2 q_n(t) = \frac{1}{\rho A B} Q_n(t) \quad (\text{A.24})$$

where $Q_n(t)$ is the generalized force and B is a constant given by

$$Q_n(t) = \int_0^l f(x, t) W_n(x) dx$$

$$B = \int_0^l W_n^2(x) dx \quad (\text{A.25})$$

It can be seen from equation [A.24](#) that it is essentially the same as undamped single degree of freedom vibration system. Thus, the solution is given by

$$q_n(t) = A_n \cos(\omega_n t) + B_n \sin(\omega_n t) + \frac{1}{\rho A B \omega_n} \int_0^t Q_n(\tau) \sin[\omega_n(t - \tau)] d\tau \quad (\text{A.26})$$

It should be noted that the first two terms of equation [A.26](#) resulting from initial conditions give transient state of the system. On the other hand, the last term gives the steady-state solution of the system.

Appendix B Analytical Beam Model

The equation of motion of beam is shown in equation [A.4](#) and rewritten here. The boundary conditions can be found in appendix [A](#).

$$EI \frac{\partial^4 w}{\partial x^4}(x, t) + \rho A \frac{\partial^2 w}{\partial t^2}(x, t) = f(x, t) \quad (\text{B.1})$$

where E , I , ρ and A are Young's modulus, moment of inertia of the beam, mass density and cross section area of the beam, respectively. The data used for numerical calculations are shown in table [B.1](#).

Table B.1: Data sheet for numerical calculations

	Symbol	Value	Unit
Young's modulus	E	70	GPa
Poisson's ration	ν	0.33	
Mass density	ρ	2700	$\frac{kg}{m^3}$
Frequency range of excitation	f	20 - 2000	Hz
Damping ratio	ζ	0.05	
Length of beam	L	0.4	m
Moment of inertia of beam	I	$1 \cdot 10^{-9}$	m^4
Cross section area of beam	A	0.01	m^2

B.1 Harmonic Base Excitation

A harmonic base excitation beam model with length L is shown in figure [B.1](#) and can be used in comparison with other models. Since there is no external force acting on the beam, $f(x, t)$ becomes 0 in equation [B.1](#).

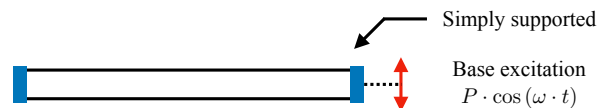


Figure B.1: Sketch of harmonic base excitation beam model

The boundaries are simply supported at $x = 0$ and $x = L$ while the harmonic base excitation is at right hand boundary $x = L$ as

$$w(L, t) = P \cdot \cos(\omega t) \quad (\text{B.2})$$

where the amplitude P is taken from 0.1 to 0.5 (mm). Substitute equation [B.2](#) into the equation of motion with other boundary conditions and apply separation of variables as $w(x, t) = W(x)T(t)$, it becomes

$$\begin{aligned} W(x) &= C_1 (\cos(\beta x) - \cosh(\beta x)) + C_2 (\sin(\beta x) - \sinh(\beta x)) \\ T(t) &= \cos(\omega t) \end{aligned} \quad (\text{B.3})$$

where β is given by equation [A.10](#) and

$$\begin{aligned} \beta^4 &= \frac{\rho A \omega^2}{EI} \\ C_1 &= \frac{P}{2} \cdot \frac{-\sin(\beta L) + \sinh(\beta L)}{\sinh(\beta L) \cos(\beta L) + \sin(\beta L) \cosh(\beta L)} \\ C_2 &= \frac{P}{2} \cdot \frac{\cos(\beta L) + \cosh(\beta L)}{\sinh(\beta L) \cos(\beta L) + \sin(\beta L) \cosh(\beta L)} \end{aligned} \quad (\text{B.4})$$

Thus, the solution of $w(x, t)$ can be found as shown in equation [B.5](#).

$$\begin{aligned} w(x, t) &= \frac{P}{2} \cdot \frac{1}{\sinh(\beta L) \cos(\beta L) + \sin(\beta L) \cosh(\beta L)} \cdot \\ & [(\sin(\beta L) - \sinh(\beta L)) \cdot (\cos(\beta x) - \cosh(\beta x)) + \\ & (\cos(\beta L) + \cosh(\beta L)) \cdot (\sin(\beta x) - \sinh(\beta x))] \cdot \cos(\omega t) \end{aligned} \quad (\text{B.5})$$

The results are shown in figure [B.2](#) and [B.3](#). In the following figures, the only time-dependent part of solution $\cos(\omega t)$ is taken as 1 in order to find out the maximum displacement (or shear force). Additionally, the figures also show the influence from different amplitude P and location of beam x .

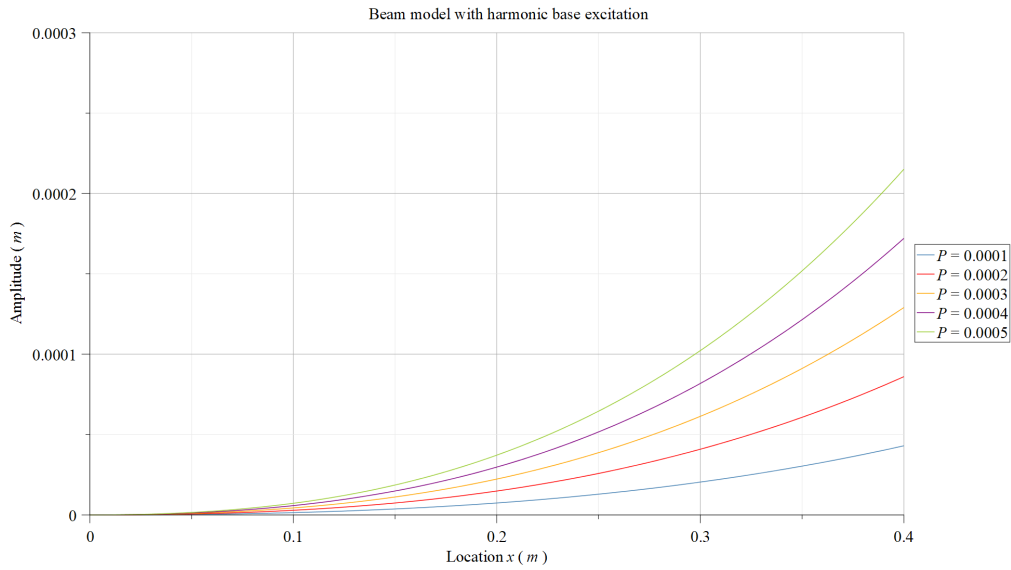


Figure B.2: Harmonic base excitation beam model result with various amplitude P and location x

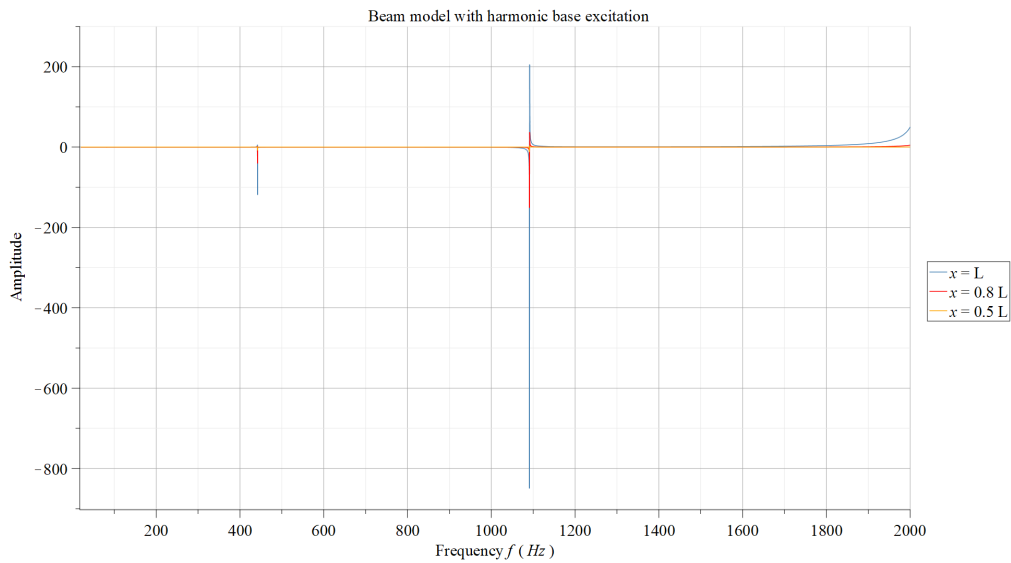


Figure B.3: Harmonic base excitation beam model result with various frequency f and location x

B.2 White Noise Random Excitation

Consider a simply supported beam subjected to a white noise random excitation. A sketch of such model is shown in figure B.4.



Figure B.4: Sketch of random excitation beam model

Recall modal analysis and forced vibration of beam described in chapter 2. The transverse deflection can be expressed as

$$w(x, t) = \sum_{n=1}^{\infty} W_n(x) q_n(t) \quad (\text{B.6})$$

where the mode shape $W_n(x)$ is given by

$$\begin{aligned} W_n(x) &= C_n [\sin(\beta_n x)] \\ \beta_n &= \frac{n\pi}{L}, \quad n = 1, 2, \dots \end{aligned} \quad (\text{B.7})$$

Substitute equation B.6 into the equation of motion with the orthogonality of mode shapes, it becomes

$$\frac{d^2 q_n(t)}{dt^2} + \omega_n^2 q_n(t) = \frac{1}{\rho AB} Q_n(t) = N_n(t) \quad (\text{B.8})$$

where

$$\begin{aligned} Q_n(t) &= \int_0^L W_n(x) dx \cdot f(t) \\ B &= \int_0^L W_n^2(x) dx \\ \omega_n &= \beta_n^2 \sqrt{\frac{EI}{\rho A}} \end{aligned} \quad (\text{B.9})$$

Recall the frequency domain analysis in chapter 3 and the definition of frequency response function $H(\omega)$ for a general n th-order linear system. If the general n th order linear system is expressed as

$$\sum_{j=0}^n a_j \frac{d^j x(t)}{dt^j} = f(t) \quad (\text{B.10})$$

then frequency response function $H(\omega)$ is given as

$$H(\omega) = \left(\sum_{j=0}^n a_j (i\omega)^j \right)^{-1} \quad (\text{B.11})$$

Thus, in this case, the frequency response function can be found as

$$H_{q,n}(\omega) = \frac{1}{\omega_n^2 - \omega^2} \quad (\text{B.12})$$

Take the above results and substitute into equation B.6, it yields

$$\begin{aligned}
w(x, t) &= \sum_{n=1}^{\infty} W_n(x) q_n(t) \\
&= \sum_{n=1}^{\infty} W_n(x) H_{q,n}(\omega) N_n(t) \\
&= H_w(\omega) f(t)
\end{aligned} \tag{B.13}$$

The acceleration response power spectral density (PSD) $S_{\ddot{w}\ddot{w}}$ of the beam model with an acceleration excitation PSD S_{ff} can be found by

$$S_{\ddot{w}\ddot{w}} = |H_w|^2 \cdot S_{ff} \tag{B.14}$$

while the velocity and displacement PSD are given by

$$\begin{aligned}
S_{\dot{w}\dot{w}} &= \frac{1}{\omega^2} \cdot S_{\ddot{w}\ddot{w}} \\
S_{ww} &= \frac{1}{\omega^4} \cdot S_{\ddot{w}\ddot{w}}
\end{aligned} \tag{B.15}$$

The root-mean-square(RMS) displacement is thereafter calculated from the area below displacement response PSD curve.

$$D_{rms} = \sqrt{\int_{20}^{2000} S_{ww} df} \tag{B.16}$$

If the beam is subjected to a white noise $0.1(g^2/Hz)$ from 20 to 2000 Hertz as described in section 1.1.1, the acceleration response results are shown in figure B.5 and B.6. It should be noted that the figures are semi-log plot. In addition, the location x is $\frac{l}{2}$ in figure B.5 and B.7 and the number of mode shape n is taken as 5 in figure B.6 and B.8.

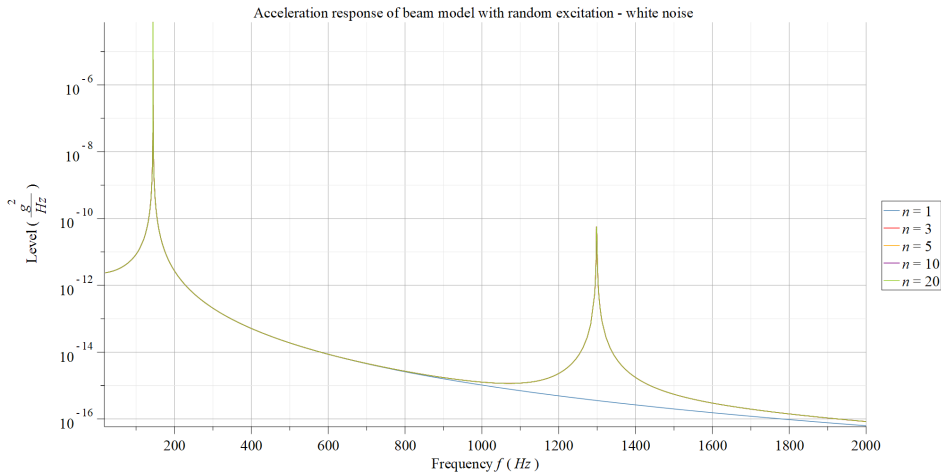


Figure B.5: White noise beam model result with various frequency f and number of mode shapes n

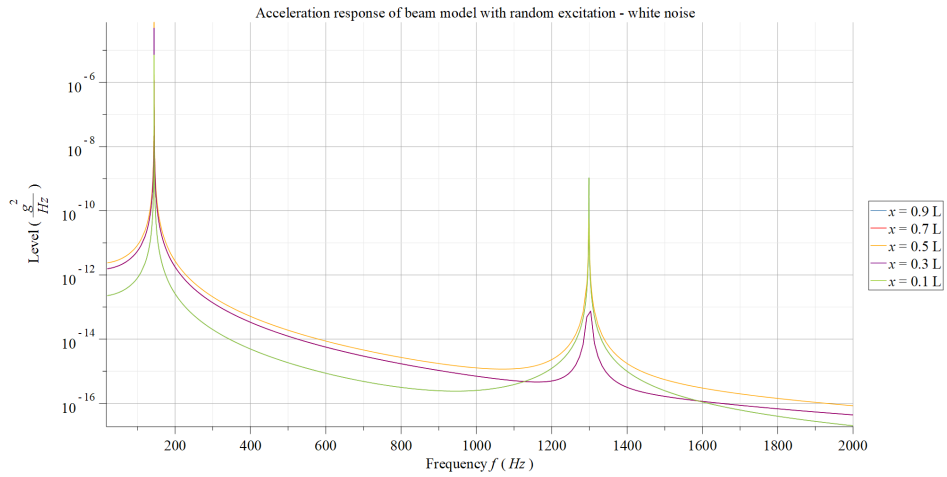


Figure B.6: White noise beam model result with various frequency f and location x

The displacement response results are shown in figure [B.7](#) and [B.8](#).

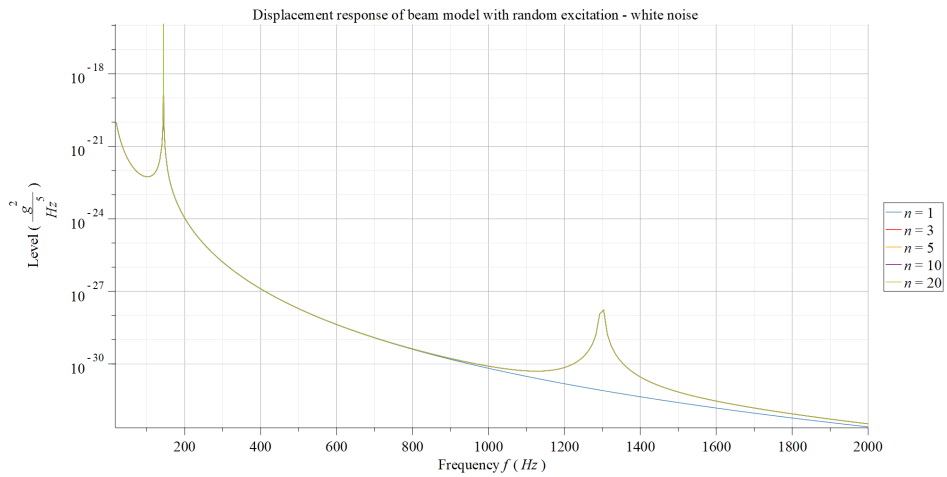


Figure B.7: White noise beam model result with various frequency f and number of mode shapes n

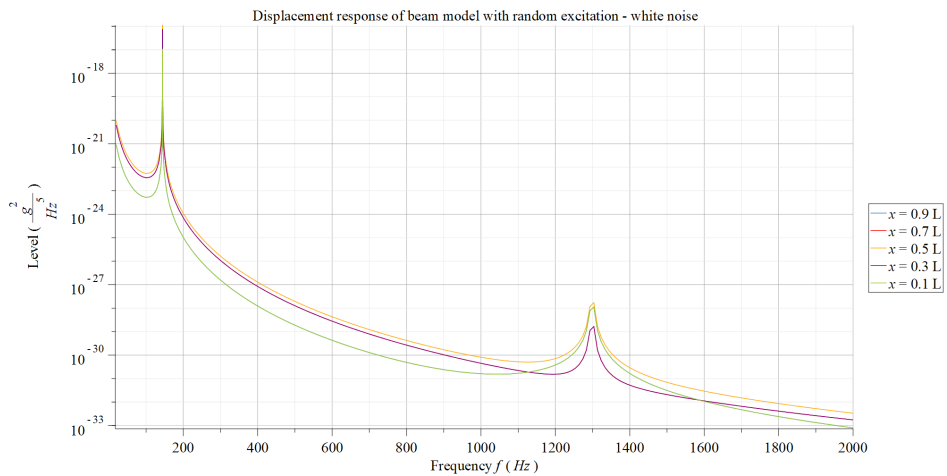


Figure B.8: White noise beam model result with various frequency f and location x

The D_{rms} values of different location x and number of mode shape n are shown in table

B.2

Table B.2: D_{rms} value of different condition

Location	n	$D_{rms} (mm)$	Location	n	$D_{rms} (mm)$
$x = \frac{L}{2}$	1	0.0510	$x = 0.9 L$	5	0.0158
	3	0.0509	$x = 0.7 L$		0.0413
	5	0.0509	$x = 0.5 L$		0.0509
	10	0.0509	$x = 0.3 L$		0.0413
	20	0.0509	$x = 0.1 L$		0.0158

Appendix C Dirac Delta Function

Dirac delta function was introduced by the physicist Paul Dirac for modeling the density of an idealized point mass or point charge. It is equal to zero everywhere except at zero as shown in figure [C.1](#).

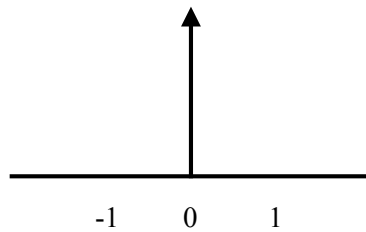


Figure C.1: Schematic representation of the Dirac delta function

C.1 Properties of Dirac Delta Function

Dirac delta function can be thought as a function on the real line which is zero everywhere and infinite at zero, that is

$$\delta(t) = \begin{cases} +\infty & t = 0 \\ 0 & t \neq 0 \end{cases} \quad (\text{C.1})$$

while the integration is defined as

$$\int_{-\infty}^{\infty} \delta(t) dt = 1 \quad (\text{C.2})$$

Dirac delta function also follows translation property as

$$\int_{-\infty}^{\infty} f(t) \delta(t - T) dt = f(T) \quad (\text{C.3})$$

C.2 Solution to Ordinary Differential Equation

Equation [3.22](#) is rewritten here as

$$\sum_{j=0}^n a_j \frac{d^j h_x(t)}{dt^j} = \delta(t) \quad (\text{C.4})$$

As stated in section [3.2](#), $h_x(t)$ is zero for $t < 0$, the problem left is the situation that time is equal or greater than zero. For the time greater than zero, the equation becomes

$$\sum_{j=0}^n a_j \frac{d^j h_x(t)}{dt^j} = 0 \quad \text{for } t > 0 \quad (\text{C.5})$$

To have a unique solution for a n th order ordinary differential equation such as equation [C.5](#), n initial conditions or boundary conditions are needed. The values used are the initial value of $h_x(t)$ and its first derivatives at time $t = 0^+$.

Reconsider equation [C.4](#), it shows that the left hand side of equation should have at least one term to be infinity since Dirac delta function is infinity at time $t = 0$. Assume the j th order term is infinity as

$$\frac{d^j h_x(t)}{dt^j} = b \delta(t) \quad (\text{C.6})$$

where b is an arbitrary value and the first derivative is

$$\frac{d^{j+1} h_x(t)}{dt^{j+1}} = b \frac{d\delta(t)}{dt} = b \delta'(t) \quad (\text{C.7})$$

Figure [C.2](#) shows the possible approximations for the Dirac delta function and its derivative. As it can be seen from the figure, $|\delta'(t)|/\delta(t) \rightarrow \infty$ as $\Delta \rightarrow 0$.

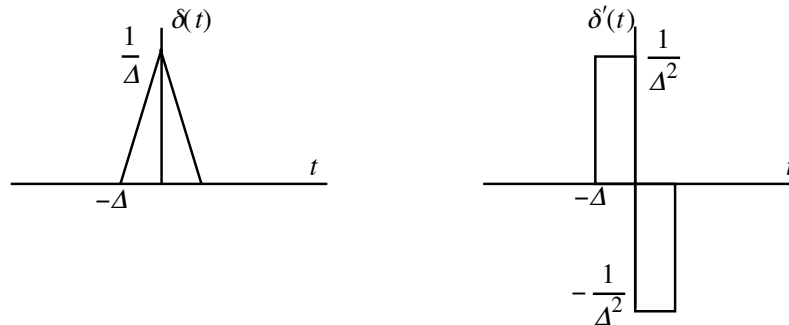


Figure C.2: Possible approximations for the Dirac delta function and its derivative. [\[6\]](#)

It indicates that the magnitude of $\delta'(t)$ is infinitely larger than that of $\delta(t)$. Therefore, if the j th order derivative of $h_x(t)$ is equivalent to $\delta(t)$ and the $(j+1)$ th order derivative of $h_x(t)$ also appears in equation [C.4](#), then the boundary condition can not be satisfied. However, if the n th order derivative of $h_x(t)$ in the vicinity of origin is $b\delta(t)$, then all other terms in left hand side of equation [C.4](#) would be finite. That is, the equation would be satisfied at the origin if $b = a_n^{-1}$ as

$$\frac{d^n h_x(t)}{dt^n} = a_n^{-1} \delta(t) \quad \text{for very small } |t| \quad (\text{C.8})$$

which gives the initial condition for equation [C.5](#) at time $t = 0^+$ and the integral gives

$$\frac{d^{n-1} h_x(t)}{dt^{n-1}} = a_n^{-1} U(t) \quad \text{for very small } |t| \quad (\text{C.9})$$

where $U(t)$ is unit step function. Thus,

$$\left(\frac{d^{n-1} h_x(t)}{dt^{n-1}} \right)_{t=0^+} = a_n^{-1} \quad (\text{C.10})$$

and the integral gives

$$\left(\frac{d^j h_x(t)}{dt^j} \right)_{t=0^+} = 0 \quad \text{for } j \leq n-2 \quad (\text{C.11})$$

Finally, equation [C.10](#) and [C.11](#) give the initial conditions that are necessary to find the solution of $h_x(r)$.

Appendix D Reference Article

The article primary used in this project is "Benchmark solutions of stationary random vibration for rectangular thin plate based on discrete analytical method" [1] by Guohai Chen, Jilei Zhou and Dixiong Yang. The complete article can be seen in the following pages.



Benchmark solutions of stationary random vibration for rectangular thin plate based on discrete analytical method



Guohai Chen^a, Jilei Zhou^b, Dixiong Yang^{a,*}

^a State Key Laboratory of Structural Analysis for Industrial Equipment, Department of Engineering Mechanics, International Research Center for Computational Mechanics, Dalian University of Technology, Dalian 116024, China

^b School of Traffic and Vehicle Engineering, Shandong University of Technology, Zibo 255049, China

ARTICLE INFO

Keywords:

Stationary random vibration
Rectangular thin plate
Discrete analytical method
Benchmark solutions
Pseudo excitation method

ABSTRACT

This paper aims to accurately and efficiently achieve the benchmark solutions of stationary stochastic responses for rectangular thin plate. Firstly, the exact solutions of free vibration for thin plate with SSSS, SSSC, SCSC, SFSF, SSSF and SCSF boundary conditions are introduced to random vibration analysis. Based on pseudo excitation method (PEM), the analytical power spectral density (PSD) functions of the transverse deflection, velocity, acceleration and stress responses for thin plate under random base acceleration excitation are derived. Subsequently, to enhance computational efficiency, the discrete analytical method (DAM) that realizes the discretization for the modal coordinates and frequency domain is proposed. Finally, the efficiency of DAM and the accuracy of benchmark solutions are scrutinized by comparison with the analytical solutions and finite element solutions.

© 2017 Elsevier Ltd. All rights reserved.

1. Introduction

As a basic structural member, the plate is widely applied to practical engineering. Usually, the plate structure is subjected to various excitations such as the earthquakes, winds, waves, turbulent boundary and jet noise, etc., which commonly present the randomness both in temporal and spatial domain. Random vibration analysis for a plate structure involves two types of model. The first is the continuous model based on the high-order partial differential equation, from which the analytical solution of random vibration response may be achieved. The second is the discrete model in which the continuum structure with infinite degrees of freedom is discretized to a multiple degrees of freedom (MDOF) system, by means of the numerical technique such as the popular finite element method (FEM). The discrete model can be utilized to approximately obtain the stochastic dynamical responses of structure. However, the continuous model can describe accurately its mechanical behavior, and is suitable to achieve the credible benchmark solutions of structures for verifying the discrete model and associated numerical methods. This work attempts to address the problem that there is a lack of benchmark solutions of random vibration responses, especially the stress solutions of thin plate.

In the past fifty years, the progresses on random vibration analysis based on the continuous model have been made. By virtue of

normal mode method and the time domain Green function method, Lin [1] investigated the transient displacement responses for continuous structures subjected to stationary random excitations. Crandall and his colleagues [2,3] pointed out that, with exception for enhanced response in small zones and narrow lanes, the mean square velocity response of plate under stationary wide-band point random excitation presents uniform spatial distribution. Rosa and Franco [4,5] carried out the random vibration analysis for the rectangular thin plate subjected to the turbulent boundary layer excitation. However, only the simple supported edges for the beam or plate was tackled in their works. In fact, the boundary condition has considerable effect on the stochastic response of the structure, because its frequencies and mode shapes are completely different under different boundary conditions. Hosseinloo et al. [6] examined the effects of modal damping and excitation frequency range on the root mean square (rms) of acceleration response and the maximum deflection of thin plates with CCSS, SCCC, CCCC boundary conditions subjected to the base acceleration random excitation, and indicated that these responses decrease with the increasing of the modal damping ratio and the excitation frequency range. Nevertheless, it is difficult to achieve the benchmark solutions in their study, since the approximate frequencies and modal shapes were adopted. Moreover, the complete quadratic combination (CQC) based analytical approach might require

* Corresponding author.

E-mail address: yangdx@dlut.edu.cn (D. Yang).

the large computational efforts with the widening of frequency band of random excitation.

On the other hand, to balance the computational accuracy and efficiency, the significance of the modal cross-correlation was also intensively investigated. Crandall et al. [2,7–9] examined the effects of modal overlap ratio on the mean square response for various structures, and pointed out that the bandwidth of random excitation and the damping ratio of structures are the main influence factor on stochastic response, as well as suggested the modal-sum and image-sum approaches to decrease the approximate evaluation error of the sum of a large number of integral [10]. Elishakoff et al. [11–14] performed a series of researches on different structures such as curved panel and shell, to elaborate the dramatic effects of modal cross-correlation on the mean square responses. Meanwhile, the similar works for discrete MDOF systems were also conducted. In order to decrease the computational effort of stochastic dynamical analysis, an approximate square root of sum square (SRSS) method was applied by omitting modal cross-correlation terms [15]. Wilson et al. [16] developed a CQC method to reduce the numerical errors of SRSS rule, but at the expense of efficiency. Accordingly, Lin et al. [17–20] proposed a highly efficient and accurate algorithm named as pseudo excitation method (PEM), which promotes the engineering application of random vibration theory. The extensive application of the PEM is dependent on the development of finite element method. It is well known that the numerical errors of FEM will nonlinearly increase with the increasing frequency [21]. For obtaining the benchmark solutions, the analytical solutions of free vibration can be adopted to eliminate the errors in the band-wide random vibration analysis for the plate. In this paper, the benchmark solutions are achieved efficiently, when the plate is subjected to band-wide random excitation up to 20 kHz with the proposed PEM-based discrete analytical method.

For the free vibration analysis of plates, Leissa, Leissa and Qatu [22,23] reviewed the free vibration for rectangular thin plate with various boundary conditions, and pointed out that there are exact solutions of free vibration for only the 6 Lévy boundary conditions (SSSS, SSSC, SCSC, SFSF, SSSF, SCSF) with two opposite edges simply supported among 21 cases, which involve the possible combinations of clamped (C), simply-supported (S), and free edge (F) condition. Due to the difficulty of solving the fourth-order partial differential governing equation, the other 15 cases must be solved by the approximate approaches, such as FEM [24], finite difference method [25], finite strip method [26], boundary element method [27], differential quadrature method [28], Rayleigh–Ritz method [29], superposition method [30], symplectic superposition method [31,32] etc.

In this paper, the analytical PSD functions of stationary stochastic responses for rectangular thin plate with the 6 Lévy boundary conditions (SSSS, SSSC, SCSC, SFSF, SSSF and SCSF) are obtained. Therein, the exact solutions of free vibration of thin plate are introduced, and the pseudo excitation method based on the continuous model is employed. Through integrating the corresponding PSD functions, the rms of the displacement, velocity and acceleration responses as well as the stress components are achieved, whose results are also termed as benchmark solutions. Moreover, the discrete analytical method (DAM) is developed to improve computational efficiency without reducing the precision by discretizing the modal space coordinate and frequency domain.

The remainder of this paper is organized as follows. Section 2 revisits the exact Lévy solutions of free vibration for rectangular plate under 6 boundary conditions, which provides a foundation of benchmark solutions of stationary random responses. In Section 3, the analytical response PSD functions are derived by employing the PEM-based analytical method and discrete analytical method. Moreover, an approach to calculate the rms of stationary random response of thin plate is presented in Section 4. Then, two examples in Section 5 illustrate the benchmark solutions of stationary random vibration for the 6 cases under base wide-band white noise excitation and filtered white noise excitation. Comparison between the analytical solutions and finite element solutions verifies the high accuracy and efficiency of DAM. Section 6 draws some conclusions.

2. Exact solutions of free vibration of rectangular thin plate

2.1. Differential equation of forced vibration of rectangular thin plate

The differential equation of forced vibration for rectangular thin plate is given by [22,23]

$$D\nabla^4 w(x, y, t) + c \frac{\partial w(x, y, t)}{\partial t} + \rho h \frac{\partial^2 w(x, y, t)}{\partial t^2} = p(x, y, t) \quad (1)$$

where $D = Eh^3/12(1 - \nu^2)$ is the bending rigidity of the plate; E the Young's modulus and ν the Poisson's ratio; $\nabla^4 = \frac{\partial^4}{\partial x^4} + 2\frac{\partial^4}{\partial x^2 \partial y^2} + \frac{\partial^4}{\partial y^4}$ is the bi-harmonic operator; $w(x, y, t)$ is the transverse deflection; c indicates the viscous damping coefficient of the plate; ρ is the volume density of the plate; h indicates the plate thickness; $p(x, y, t)$ is an excitation.

As shown in Fig. 1, the three classical boundary conditions for the rectangular plate, namely simply supported (S), clamped (C) and free (F) can be described by

$$\text{Simply supported (S): } w = 0, \quad M_x = 0$$

$$\text{Clamped (C): } w = 0, \quad \frac{\partial w}{\partial x} = 0 \quad (2)$$

$$\text{Free (F): } M_x = 0, \quad V_x = Q_x + \frac{\partial M_{xy}}{\partial y} = 0$$

where $\frac{\partial w}{\partial x}$ is the rotation angle in the xz plane; M_x denotes the bending moment in the xz plane; Q_x represents the shear force; M_{xy} is the torsional moment in the yz plane; V_x is the equivalent shear force.

2.2. Exact solutions of free vibration under 6 boundary conditions

The undamped free vibration differential equation of thin plate is formulated as [22]

$$D\nabla^4 w(x, y, t) + \rho h \frac{\partial^2 w(x, y, t)}{\partial t^2} = 0 \quad (3)$$

The transverse deflection in Eq. (3) is expressed as $w(x, y, t) = \phi(x, y) \exp(i\omega t)$, in which ω indicates the angular frequency of free vibration, and $\phi(x, y)$ represents the corresponding modal shape. Substituting the transverse deflection formulation $w(x, y, t)$ into Eq. (3) can yield the differential equation about the modal shape function

$$D\nabla^4 \phi(x, y) - \rho h \omega^2 \phi(x, y) = 0 \quad (4)$$

For the 6 cases with a couple of simply supported boundary conditions on the opposite edge in Fig. 1(b), the Lévy solutions [22,23] of modal shape are expressed as

$$\phi(x, y) = (A_1 \cos \lambda_1 y + A_2 \sin \lambda_1 y + A_3 \cosh \lambda_2 y + A_4 \sinh \lambda_2 y) \sin \mu x \quad (5)$$

where $\mu = m\pi/a$, and m is the number of half-wave; a is the length of plate along the y coordinate; $\lambda_1 = \sqrt{\mu^2 - \sqrt{\rho h \omega^2 / D}}$, and $\lambda_2 = \sqrt{\mu^2 + \sqrt{\rho h \omega^2 / D}}$ can be calculated according to the corresponding frequency equations (see Table A in Appendix); $A_1 \sim A_4$ will be determined in terms of the boundary conditions.

Note that an assumption $\sqrt{\rho h \omega^2 / D} > \mu^2$ is taken in Eq. (5), and frequency equations are listed in Table A. If $\sqrt{\rho h \omega^2 / D} < \mu^2$, it must be replaced $\sin \lambda_1 y$ and $\cos \lambda_1 y$ with $\sinh \lambda_1 y$ and $\cosh \lambda_1 y$, respectively.

3. Discrete analytical method for stationary random responses

In this section, at first, the analytical procedure of stationary random vibration responses for rectangular thin plate is derived by combining the mode superposition method with the pseudo excitation method. Actually, it is not restricted by the form of random excitation, such as the point excitation, the distributed excitation or the base acceleration excitation.

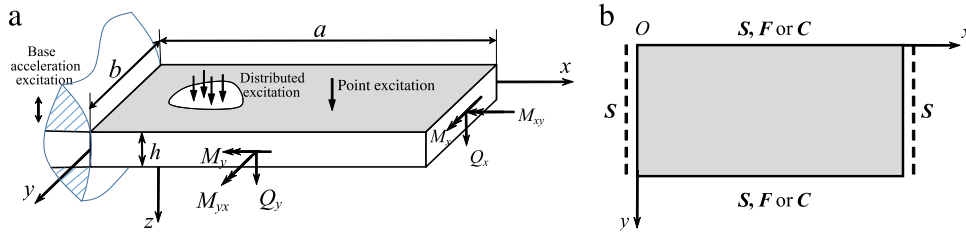


Fig. 1. Rectangular thin plate (a) subjected to various random excitations; (b) with boundary conditions.

3.1. Analytical method based on PEM

Herein, the pseudo excitation method is introduced briefly, and a more detailed description of PEM is referred to [17–20]. There is a 2D elastic thin plate subjected to stationary random excitation with a power spectral density $S_{pp}(x, y, \omega)$. $S_{uu}(x, y, \omega)$, $S_{vv}(x, y, \omega)$ and $S_{uv}(x, y, \omega)$ denote the auto-PSD and the cross-PSD of two arbitrary stationary response $u(x, y, t)$ and $v(x, y, t)$ at location (x, y) , respectively. Assume the following pseudo harmonic excitation [17,19,20] to replace the Gaussian random excitation $p(x, y, t)$ in Eq. (1)

$$\tilde{p}(x, y, t) = \sqrt{S_{pp}(x, y, \omega)} \exp(i\omega t) \quad (6)$$

Subsequently, the pseudo responses $u(x, y, t)$ and $v(x, y, t)$ can be calculated as

$$\begin{aligned} \tilde{u}(x, y, t) &= \sqrt{S_{pp}(x, y, \omega)} H_u(x, y, \omega) \exp(i\omega t) \\ \tilde{v}(x, y, t) &= \sqrt{S_{pp}(x, y, \omega)} H_v(x, y, \omega) \exp(i\omega t) \end{aligned} \quad (7)$$

where $H_u(x, y, \omega)$, $H_v(x, y, \omega)$ is the corresponding frequency response function at location (x, y) . Multiplying the pseudo response $\tilde{u}(x, y, t)$ or $\tilde{v}(x, y, t)$ by its conjugate quantity $\tilde{u}(x, y, t)^*$ or $\tilde{v}(x, y, t)^*$, the corresponding auto-PSD and cross-PSD functions can be obtained

$$\begin{aligned} S_{uu}(x, y, \omega) &= \tilde{u}(x, y, t)^* \tilde{u}(x, y, t) = |H_u(x, y, \omega)|^2 S_{pp}(x, y, \omega) \\ S_{uv}(x, y, \omega) &= \tilde{u}(x, y, t)^* \tilde{v}(x, y, t) = H_u(x, y, \omega)^* S_{xx}(x, y, \omega) H_v(x, y, \omega) \end{aligned} \quad (8)$$

It is seen from Eqs. (7) and (8) that the stationary random vibration analysis for elastic thin plate is simplified to a deterministic harmonic vibration analysis. Actually, the pseudo excitation method is also termed as fast CQC method [17]. The reason is that its accuracy is consistent with CQC, but it is unnecessary to explicitly calculate the modal cross-correlation coefficient. Consequently, the computational efficiency of PEM is enhanced significantly, say to two or three orders of magnitude [19,33]. Hence, the PEM is incorporated into the following analytical methods to achieve the benchmark solutions of stationary random response for rectangular thin plate efficiently and accurately.

3.1.1. Analytical PSD functions of deflection and acceleration responses

In this section, the exact response PSD functions are derived by the analytical method. In Eq. (1), the right-hand item about the external load is considered to be random with respect to the time t . The transverse deflection $w(x, y, t)$ of the plate is expressed as

$$w(x, y, t) = \sum_{m=1}^{\infty} \sum_{n=1}^{\infty} \phi_{mn}(x, y) \eta_{mn}(t) \quad (9)$$

where $\phi_{mn}(x, y)$ is the m th modal shape of the plate, m, n denotes the half-wave number in x and y direction, respectively; $\eta_{mn}(t)$ is the normal coordinate corresponding to the m th mode.

The orthogonality of modal shapes is written as follows

$$\int_0^a \int_0^b \rho h \phi_{mn}(x, y) \phi_{kl}(x, y) dx dy = \gamma_{mn} \delta_{mn,kl} \quad (10)$$

$$\int_0^a \int_0^b c \phi_{mn}(x, y) \phi_{kl}(x, y) dx dy = c_{mn} \delta_{mn,kl} \quad (11)$$

where

$$\gamma_{mn} = \int_0^a \int_0^b \rho h \phi_{mn}(x, y)^2 dx dy \quad (12)$$

indicates the m th modal mass; $c_{mn} = c \gamma_{mn} / \rho h$ for homogeneous plate is modal damping, or is expressed as $c_{mn} = 2 \zeta_{mn} \omega_{mn} \gamma_{mn}$ by introducing the m th modal damping ratio ζ_{mn} ; $\delta_{mn,kl} = 1$ ($mn = kl$) or $\delta_{mn,kl} = 0$ ($mn \neq kl$) is the Kronecker delta function.

Eq. (9) is substituted to Eq. (1) and the orthogonality (Eqs. (10) and (11)) of modal shapes is introduced. Then multiplying the l th modal shape $\phi_{lk}(x, y)$ in the two sides of equation, and integrating it over the surface domain Ω of the plate yields

$$\begin{aligned} \ddot{\eta}_{mn}(t) + 2 \zeta_{mn} \omega_{mn} \dot{\eta}_{mn}(t) + \omega_{mn}^2 \eta_{mn}(t) \\ = \frac{1}{\gamma_{mn}} \int_0^a \int_0^b p(x, y, t) \phi_{mn}(x, y) dx dy \end{aligned} \quad (13)$$

Then, assuming the pseudo harmonic excitation shown in Eq. (6) and substituting into Eq. (13), the random vibration analysis for rectangular thin plate is transformed into the deterministic stationary vibration analysis of a series of uncoupled SDOF systems

$$\ddot{\tilde{\eta}}_{mn}(t) + 2 \zeta_{mn} \omega_{mn} \dot{\tilde{\eta}}_{mn}(t) + \omega_{mn}^2 \tilde{\eta}_{mn}(t) = P_{mn} \exp(i\omega t) \quad (14)$$

$$P_{mn} = \frac{1}{\gamma_{mn}} \int_0^a \int_0^b \sqrt{S_{pp}(x, y, \omega)} \phi_{mn}(x, y) dx dy \quad (15)$$

in which, P_{mn} means the amplitude of generalized harmonic excitation. There is a relationship between output and input: $\tilde{\eta}_{mn}(t) = H_{mn}(\omega) P_{mn} \exp(i\omega t)$ for a SDOF system subjected to harmonic excitation, and $H_{mn}(x, y, \omega) = (\omega_{mn}^2 - \omega^2 + 2i\omega \zeta_{mn} \omega_{mn})^{-1}$ is the m th frequency response function. According to Eq. (9), the pseudo transverse deflection can be written as

$$\begin{aligned} \tilde{w}(x, y, t) &= \sum_{m=1}^{\infty} \sum_{n=1}^{\infty} \phi_{mn}(x, y) \tilde{\eta}_{mn}(t) \\ &= \sum_{m=1}^{\infty} \sum_{n=1}^{\infty} \phi_{mn}(x, y) H_{mn}(\omega) P_{mn} \exp(i\omega t) \end{aligned} \quad (16)$$

According to the PEM, the exact auto-PSD functions of transverse deflection responses can be obtained as

$$\begin{aligned} S_{ww}(x, y, \omega) &= \tilde{w}(x, y, t)^* \tilde{w}(x, y, t) \\ &= \left(\sum_{m=1}^{\infty} \sum_{n=1}^{\infty} \phi_{mn}(x, y) H_{mn}(\omega) P_{mn} \right)^* \\ &\quad \times \left(\sum_{k=1}^{\infty} \sum_{s=1}^{\infty} \phi_{ks}(x, y) H_{ks}(\omega) P_{ks} \right) \end{aligned} \quad (17)$$

Also, the auto-PSD functions of velocity and acceleration response can be formulated by

$$S_{\dot{w}\dot{w}}(x, y, \omega) = \dot{\tilde{w}}(x, y, t)^* \dot{\tilde{w}}(x, y, t) = \omega^2 S_{ww}(x, y, \omega) \quad (18)$$

$$S_{\ddot{w}\ddot{w}}(x, y, \omega) = \ddot{\tilde{w}}(x, y, t)^* \ddot{\tilde{w}}(x, y, t) = \omega^4 S_{ww}(x, y, \omega) \quad (19)$$

where the superscript $(\bullet)^*$ denotes the complex conjugate of concerned quantity (\bullet) .

3.1.2. Analytical PSD function of stress components

For the elastic thin plate, the relationships between strain and deflection are given by

$$\varepsilon_x = -z \frac{\partial^2 w}{\partial x^2}, \quad \varepsilon_y = -z \frac{\partial^2 w}{\partial y^2}, \quad \gamma_{xy} = -2z \frac{\partial^2 w}{\partial x \partial y} \quad (20)$$

By introducing the constitutive relationship between stress and strain, one can obtain the pseudo stresses of plate

$$\begin{aligned} \tilde{s}_x(x, y, t) &= -\frac{zE \exp(i\omega t)}{1 - \nu^2} \\ &\quad \times \sum_{m=1}^{\infty} \sum_{n=1}^{\infty} \left(\frac{\partial^2 \phi_{mn}(x, y)}{\partial x^2} + \nu \frac{\partial^2 \phi_{mn}(x, y)}{\partial y^2} \right) H_{mn}(\omega) P_{mn} \\ \tilde{s}_y(x, y, t) &= -\frac{zE \exp(i\omega t)}{1 - \nu^2} \\ &\quad \times \sum_{m=1}^{\infty} \sum_{n=1}^{\infty} \left(\frac{\partial^2 \phi_{mn}(x, y)}{\partial y^2} + \nu \frac{\partial^2 \phi_{mn}(x, y)}{\partial x^2} \right) H_{mn}(\omega) P_{mn} \\ \tilde{s}_{xy}(x, y, t) &= -\frac{zE \exp(i\omega t)}{1 + \nu} \sum_{m=1}^{\infty} \sum_{n=1}^{\infty} \frac{\partial^2 \phi_{mn}(x, y)}{\partial x \partial y} H_{mn}(\omega) P_{mn} \end{aligned} \quad (21)$$

Similarly, the exact PSD functions of stress responses are calculated by

$$\mathbf{S}_s(x, y, \omega) = \begin{pmatrix} S_{s_x s_x} & S_{s_x s_y} & S_{s_x s_{xy}} \\ S_{s_y s_x} & S_{s_y s_y} & S_{s_y s_{xy}} \\ S_{s_{xy} s_x} & S_{s_{xy} s_y} & S_{s_{xy} s_{xy}} \end{pmatrix} = \begin{pmatrix} \tilde{s}_x^* \tilde{s}_x & \tilde{s}_x^* \tilde{s}_y & \tilde{s}_x^* \tilde{s}_{xy} \\ \tilde{s}_y^* \tilde{s}_x & \tilde{s}_y^* \tilde{s}_y & \tilde{s}_y^* \tilde{s}_{xy} \\ \tilde{s}_{xy}^* \tilde{s}_x & \tilde{s}_{xy}^* \tilde{s}_y & \tilde{s}_{xy}^* \tilde{s}_{xy} \end{pmatrix} \quad (22)$$

where the principal diagonal elements denote auto-spectral density of normal stress s_x , s_y and shear stress s_{xy} , and other elements indicates cross-spectral density of stress components.

In above analysis, a series of analytical PSD functions of stationary random responses are achieved by introducing the exact frequencies and modal shape functions of thin plate and using the PEM-based analytical method with the aid of MATLAB Symbolic Math Toolbox. In fact, however, such an analytical method may take much computing time, particularly for the case of the wide-band excitation.

3.2. Discrete analytical method

To improve the computational efficiency of the analytical method without losing the accuracy, the discrete analytical method is suggested by discretizing the modal space coordinate and the frequency domain to transform symbol operations into matrix operations.

By adopting discretization treatment, the vector form of transverse deflection can be written as

$$\mathbf{w} = \mathbf{\Phi} \boldsymbol{\eta} = \begin{bmatrix} \Phi_1^1 & \Phi_2^1 & \dots & \Phi_{NF}^1 \\ \Phi_1^2 & \Phi_2^2 & \dots & \Phi_{NF}^2 \\ \vdots & \vdots & \ddots & \vdots \\ \Phi_1^{NG} & \Phi_2^{NG} & \dots & \Phi_{NF}^{NG} \end{bmatrix} \begin{Bmatrix} \eta_1 \\ \eta_2 \\ \vdots \\ \eta_{NF} \end{Bmatrix} \quad (23)$$

where $\mathbf{w}_{NG \times 1}$ indicates the transverse deflection matrix; Φ_i^j is the i th mode shape at j th node; $\boldsymbol{\eta}_{NF \times 1}$ is the normal coordinate vector; NG represents the number of nodes; NF is the number of modes participating in vibration. Therefore, according to Eq. (6), the pseudo excitations are written as a vector form

$$\tilde{\mathbf{p}} = \left\{ \sqrt{S_{p,1}(\omega)} \sqrt{S_{p,2}(\omega)} \dots \sqrt{S_{p,NF}(\omega)} \right\}^T \exp(i\omega t) \quad (24)$$

in which $S_{p,j}(\omega)$ denotes the input PSD in the j th SDOF system. According to Eq. (16), the vector form of pseudo transverse deflection can be expressed as follows

$$\tilde{\mathbf{w}} = \mathbf{\Phi} \tilde{\boldsymbol{\eta}} = \mathbf{\Phi} \mathbf{H} \mathbf{P} \tilde{\boldsymbol{\eta}} \exp(i\omega t) \quad (25)$$

where $\mathbf{\Phi}_{NG \times NF}$ is the modal shape matrix; $\mathbf{H}_{NF \times NF}$ means the frequency response function matrix; $\mathbf{P}_{NF \times 1}$ is the amplitude matrix of

generalized harmonic excitation. The pseudo stress response vectors of the plate are reformulated from Eq. (21)

$$\tilde{\mathbf{s}}_x = \lambda (\mathbf{\Phi}_{,xx} \mathbf{H} \mathbf{P} + \nu \mathbf{\Phi}_{,yy} \mathbf{H} \mathbf{P}) \exp(i\omega t) \quad (26)$$

$$\tilde{\mathbf{s}}_y = \lambda (\mathbf{\Phi}_{,yy} \mathbf{H} \mathbf{P} + \nu \mathbf{\Phi}_{,xx} \mathbf{H} \mathbf{P}) \exp(i\omega t) \quad (27)$$

$$\tilde{\mathbf{s}}_{xy} = \kappa (\mathbf{\Phi}_{,xy} \mathbf{H} \mathbf{P}) \exp(i\omega t) \quad (28)$$

where $\mathbf{\Phi}_{,rs} = \frac{\partial^2 \mathbf{\Phi}}{\partial r \partial s}$ ($r, s = x$ or y), which can be obtained by taking derivatives of the closed-form modal shape function $\phi(x, y)$ in Eq. (21) with respect to x or y , then substituting the coordinates of nodes into the derivatives functions realizes the discretization; $\lambda = -zE/(1-\nu^2)$, $\kappa = -zE/(1+\nu)$, z is the coordinate along the direction of thickness from the middle plane of rectangular plate. Obviously, the maximum or the minimum of the stress components in Eqs. (26)–(28) occurs in the upper or lower surface of the plate ($z = \pm h/2$), respectively.

Furthermore, the auto-PSD matrices of the stationary random response for the plate can be obtained as

$$\mathbf{S}_{\mathbf{w}\mathbf{w}}(\omega) = \tilde{\mathbf{w}}^* \tilde{\mathbf{w}}^T = (\mathbf{\Phi} \mathbf{H} \mathbf{P})^* (\mathbf{\Phi} \mathbf{H} \mathbf{P})^T \quad (29)$$

$$\mathbf{S}_{s_x, s_x}(\omega) = \tilde{s}_x^* \tilde{s}_x^T = \lambda^2 (\mathbf{\Phi}_{,xx} \mathbf{H} \mathbf{P} + \nu \mathbf{\Phi}_{,yy} \mathbf{H} \mathbf{P})^* (\mathbf{\Phi}_{,xx} \mathbf{H} \mathbf{P} + \nu \mathbf{\Phi}_{,yy} \mathbf{H} \mathbf{P})^T \quad (30)$$

$$\mathbf{S}_{s_y, s_y}(\omega) = \tilde{s}_y^* \tilde{s}_y^T = \lambda^2 (\mathbf{\Phi}_{,yy} \mathbf{H} \mathbf{P} + \nu \mathbf{\Phi}_{,xx} \mathbf{H} \mathbf{P})^* (\mathbf{\Phi}_{,yy} \mathbf{H} \mathbf{P} + \nu \mathbf{\Phi}_{,xx} \mathbf{H} \mathbf{P})^T \quad (31)$$

$$\mathbf{S}_{s_{xy}, s_{xy}}(\omega) = \tilde{s}_{xy}^* \tilde{s}_{xy}^T = \kappa^2 (\mathbf{\Phi}_{,xy} \mathbf{H} \mathbf{P})^* (\mathbf{\Phi}_{,xy} \mathbf{H} \mathbf{P})^T \quad (32)$$

In Eqs. (29)–(32), the PSD matrices of the transverse deflection, stress responses are achieved accurately and efficiently at given nodes in the rectangular thin plate by the discrete analytical method. Moreover, the accuracy of DAM is independent on the mesh number of plate structure, because the exact modal shape $\phi(x, y)$ and its analytical derivative are adopted directly before the discretization.

4. Root mean square of stationary responses of rectangular thin plate

By integrating the response PSD curve over the interested frequency range and taking square root, the root mean square (i.e., standard deviation $\sigma_u(x, y)$) of arbitrary stochastic response $u(x, y, t)$ (e.g., deflection or stress components) of the rectangular thin plate can be calculated

$$\sigma_u(x, y) = \sqrt{\int_{\omega_L}^{\omega_U} G_{uu}(x, y, \omega) d\omega} = \sqrt{\sum_{j=1}^{NF} G_{uu}^{(i,j)} \Delta\omega} \quad (33)$$

where ω_L, ω_U denotes the lower or upper cutoff frequency; $G_{uu}(x, y, \omega)$ is the one-sided PSD of response $u(x, y, t)$. By means of MATLAB Symbolic Toolbox, the analytical integral of PSD function with respect to ω can be easily carried out. Nevertheless, a numerical integration shown in Eq. (33) must be implemented for the DAM, because the formula of PSD is vector form instead of analytic form. Actually, the results in the next section indicate that the precision of the DAM is still high as long as the interval $\Delta\omega$ is small enough.

5. Numerical examples for benchmark solutions of stationary random responses

This section demonstrates the high accuracy and efficiency of DAM by two examples under the band-limited and filtered white noise random excitation. As benchmark solutions, the rms of the deflection, velocity, acceleration and stress responses are exhibited for the rectangular thin plate with the 6 boundary conditions, respectively.

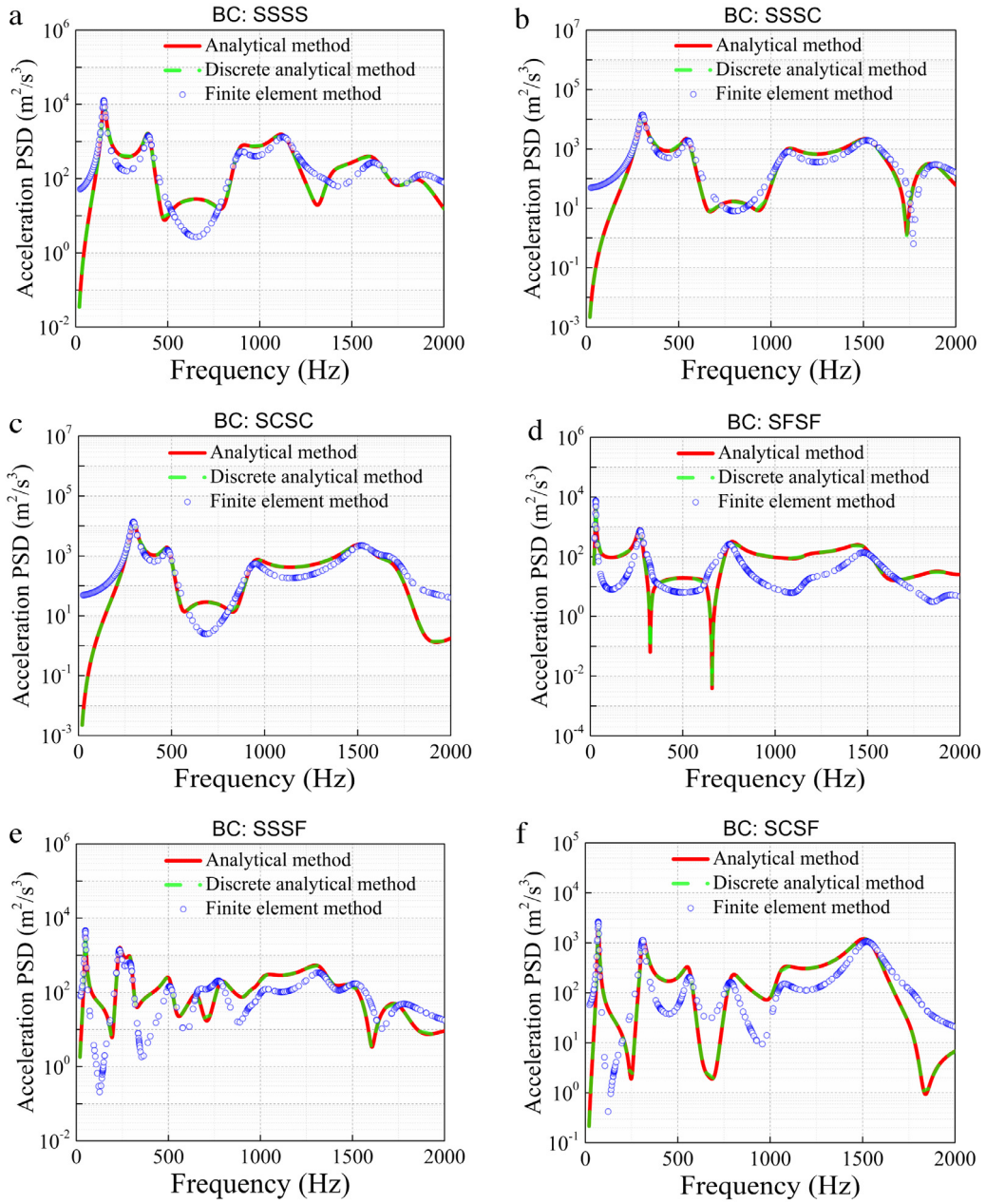


Fig. 2. Acceleration response PSD at the central point for (a) SSSS; (b) SSSC; (c) SCSC; (d) SFSF; (e) SSSF; (f) SCSF boundary condition within 20–2000 Hz.

5.1. Example 1

5.1.1. Verification of accuracy and efficiency

A rectangular thin plate [6] with $a = 0.4$ m, $b = 0.2$ m, $h = 0.002$ m, elastic modulus $E = 70$ GPa, Poisson's ratio $\nu = 0.33$, $\rho = 2700$ kg/m³ and modal damping ratio $\zeta = 0.05$ is considered, which is subjected to a band-limited white noise excitation of base acceleration with PSD $S_0 = 0.5$ g²/Hz within [20,2000] Hz. In this example, the FEM is also performed by ANSYS software. To ensure relatively accurate results for FEM, the plate is divided to 5000 (100 × 50) elements.

Fig. 2 indicates the PSD curves of acceleration response at the central point of thin plate with 6 boundary conditions, respectively. It is observed that, the PSD curves of acceleration responses obtained by DAM are in good agreement with the analytical solutions, but the results by FEM appear large errors even if the mesh number reaches to 5000. As a result, FEM cannot predict accurately the PSD of acceleration

response of rectangular plate due to its numerical error resulting from the approximate discretization of spatial domain.

On the other hand, for the 6 boundary conditions the acceleration response of plate is dominated by the first mode, and the higher order modes also present remarkable contribution as shown in Fig. 2. Moreover, the rms of the deflection, velocity, acceleration and normal stress along x direction are listed in Table 1. The root mean square of random stationary responses by the DAM is well consistent with the counterparts of the analytical method, while FEM produces errors for various boundary conditions compared to the analytical solutions as a reference in Table 1.

In addition, the CPU time taken by the three methods is also displayed in Table 1. For the convenience of comparison, the same number of points is adopted for computation with DAM and FEM, but just one point is selected to calculate its analytical responses owing to its inefficiency. Therefore, the CPU time is real for the analytical method,

Table 1
The rms of responses under 6 boundary conditions within 20–2000 Hz.

Boundary condition	Modes ^a	Nodes ^b	Method	Root mean square of responses				CPU Time (s)
				Def. ^c (m)	Vel. ^d (m/s)	Acc. ^e (m/s ²)	s_x ^f (MPa)	
SSSS	20	1	Analytical	5.966×10^{-4}	0.591	929.13	7.207	22.071
	20	5151	DAM	5.966×10^{-4}	0.591	929.13	7.207	0.003
			ϵ_{DAM} ^g (%)	0.000	0.000	0.000	0.000	—
			FEM	5.970×10^{-4}	0.591	929.07	7.216	0.003
SSSC	17	1	Analytical	3.523×10^{-4}	0.491	989.22	5.122	24.176
	17	5151	DAM	3.523×10^{-4}	0.491	989.22	5.122	0.003
			ϵ_{DAM} (%)	0.000	0.000	0.000	0.000	—
			FEM	3.523×10^{-4}	0.491	989.12	5.131	0.003
SCSC	17	1	Analytical	2.320×10^{-4}	0.447	1220.66	4.284	23.907
	17	5151	DAM	2.320×10^{-4}	0.447	1220.66	4.284	0.003
			ϵ_{DAM} (%)	0.000	0.000	0.000	0.000	—
			FEM	2.320×10^{-4}	0.447	1220.26	4.294	0.005
SFSF	30	1	Analytical	5.290×10^{-3}	1.004	478.53	22.597	101.119
	30	5151	DAM	5.290×10^{-3}	1.004	478.53	22.597	0.005
			ϵ_{DAM} (%)	0.000	0.000	0.000	0.000	—
			FEM	5.290×10^{-3}	1.004	478.76	23.901	0.004
SSSF	25	1	Analytical	1.931×10^{-3}	0.631	600.96	10.144	75.754
	25	5151	DAM	1.931×10^{-3}	0.631	600.96	10.144	0.006
			ϵ_{DAM} (%)	0.000	0.000	0.000	0.000	—
			FEM	1.931×10^{-3}	0.631	601.03	10.146	0.003
SCSF	24	1	Analytical	8.629×10^{-4}	0.405	702.84	3.279	110.299
	24	5151	DAM	8.629×10^{-4}	0.405	702.84	3.279	0.007
			ϵ_{DAM} (%)	0.000	0.000	0.000	0.000	—
			FEM	8.629×10^{-4}	0.405	703.48	3.281	0.003
		ϵ_{FEM} (%)	0.000	0.000	0.091	0.040	—	

^a Modes denotes the number of modes participating in vibration;

^b Nodes indicates the number of nodes need to be calculated;

^c Def. means the transverses deflection response;

^d Vel. denotes the velocity response;

^e Acc. means the acceleration response;

^f s_x indicates the normal stress along x direction;

^g $\epsilon_{DAM} = \frac{|r_{rmsDAM} - r_{rmsAnalytical}|}{r_{rmsAnalytical}} \times 100\%$ denotes the error of the DAM solution;

^h $\epsilon_{FEM} = \frac{|r_{rmsFEM} - r_{rmsAnalytical}|}{r_{rmsAnalytical}} \times 100\%$ denotes the error of the FEM solution.

while it is average for DAM and FEM by dividing the total CPU time to the number of nodes. It is seen that, the CPU time taken by DAM is close to that by FEM, but far less than that of analytical method. Thus, the DAM is not only a high precision method compared to FEM but an efficient method to the analytical method and FEM.

5.1.2. Effect of excitation bandwidth on acceleration PSD

In practice, the thin plate may be excited by wide-band random loads, such as the acoustic loads during launch of the spacecraft, which result in high frequency random vibration in a broad frequency spectrum from 20–10000 Hz [34]. In such a situation, the FEM is difficult to calculate exactly all of the natural frequencies. Fig. 3 illustrates that the error of the acceleration response PSD increases as the frequency increases gradually. Meanwhile, the rms of random responses by DAM and FEM are exhibited in Table 2. It is found that the results of FEM are close to DAM as the number of nodes increases from 861 (41×21) to 5151 (101×51).

Note that the CPU time increases rapidly with the increasing of node number and frequency bandwidth. The above analysis indicates that the accuracy and efficiency of DAM is superior to those of FEM. Moreover, it is seen from Table 2, the frequency bandwidth has a remarkable effect on the rms of acceleration response for SSSS edge case, followed by the velocity response. Whereas, it presents little influence on the rms of deflection response, which is coincide with the observation in [6]. The main reason is that the acceleration PSD has a higher order effect on the frequency than velocity PSD, followed by deflection PSD, as shown in Eqs. (18) and (19).

5.2. Example 2

In Section 5.1, the rectangular plate is subjected to the band-limited white noise random excitation. Nevertheless, the stationary random excitation is generally not this case, such as the Kanai–Tajimi spectrum and the modified Kanai–Tajimi spectrum with a high-pass filter, and its PSD function is expressed as

$$S(\omega) = \frac{\omega^{2N}}{\omega^{2N} + \omega_h^{2N}} \frac{\omega_g^4 + 4\omega^2\omega_g^2\zeta_g^2}{(\omega^2 - \omega_g^2)^2 + 4\omega^2\omega_g^2\zeta_g^2} S_0 \quad (34)$$

To present the benchmark solutions of stationary response under filtered white noise excitation by the analytical methods, another example is illustrated for the rectangular thin plate with $6 \text{ m} \times 4 \text{ m} \times 0.12 \text{ m}$, $E = 36.2 \text{ GPa}$, $\nu = 0.2$, $\rho = 2400 \text{ kg/m}^3$, and $\zeta = 0.05$. The base acceleration excitation is also considered with the input PSD (see Fig. 4(a)) as shown in Eq. (34), which is parameterized by $\omega_g = 2.41 \text{ rad/s}$, $\zeta_g = 2.47$, $\omega_h = 1.18 \text{ rad/s}$, $N = 2$, $S_0 = 3.03 \text{ m}^2/\text{s}^3$ [35] and over the frequency range [0, 25] Hz.

Herein, the SCSF plate is considered to be subjected to a filtered white noise base acceleration excitation as shown in Fig. 4(a). In Fig. 4(b), the PSD curves of the acceleration response at central point of thin plate are illustrated. Note that DAM can obtain the coincident results with the analytical method, while the PSD values nearby the input PSD peak frequency solved by FEM have remarkable errors. Further, the maximum rms of acceleration responses are listed in Table 3. According to the discussion in Section 5.1, the maximum rms of the deflection,

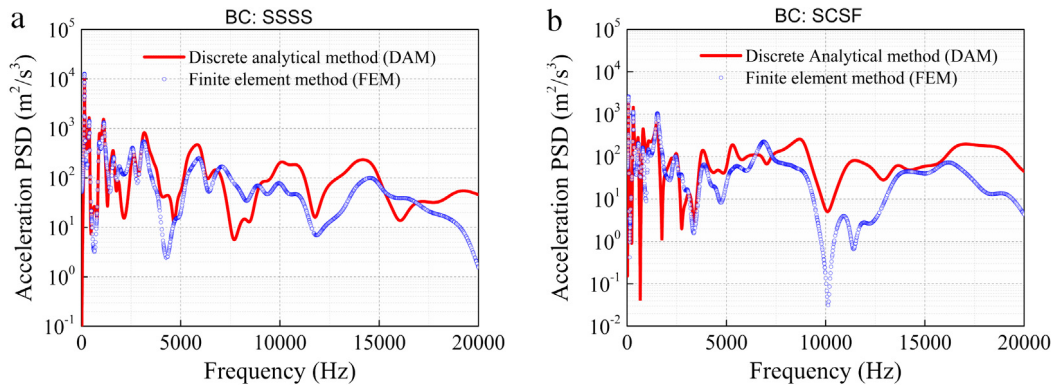


Fig. 3. Acceleration response PSD at the central point for (a) SSSS; (b) SCSF boundary condition within 20–20000 Hz.

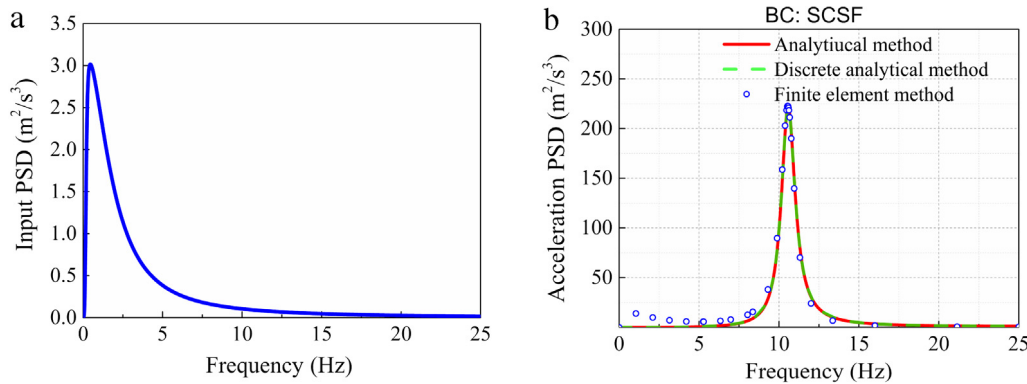


Fig. 4. PSD of (a) input acceleration of filtered white noise excitation; (b) acceleration response at central point of plate with SCSF boundary condition.

Table 2
The rms of responses for the SSSS plate under excitation with different frequency band-width.

Frequency range (Hz)	Modes	Nodes	Method	Root mean square of responses			CPU Time (s)
				Def. (m)	Vel. (m/s)	Acc. (m/s ²)	
20–2000	20	1	DAM	5.966×10^{-4}	0.591	929.13	1.323
	20	861	FEM-1	5.969×10^{-4}	0.591	928.95	7.828
	20	3321	FEM-2	5.967×10^{-4}	0.591	929.07	13.047
	20	5151	FEM-3	5.967×10^{-4}	0.591	929.09	17.078
				ϵ_{FEM-3} (%)	0.067	0.000	0.006
20–20000	237	1	DAM	5.966×10^{-4}	0.592	1702.08	9.992
	248	861	FEM-1	5.969×10^{-4}	0.592	1685.70	66.484
	247	3321	FEM-2	5.967×10^{-4}	0.592	1697.00	210.953
	247	5151	FEM-3	5.967×10^{-4}	0.592	1698.80	334.766
				ϵ_{FEM-3} (%)	0.017	0.000	0.193

Table 3
The maximum rms of stationary responses of plate under filtered white noise excitation with SCSF by the analytical method, DAM and FEM.

Method	Maximum root mean square of responses		
	Def. $l_{(a/2,b)}$ (m)	Vel. $l_{(a/2,b)}$ (m/s)	Acc. $l_{(a/2,b)}$ (m/s ²)
Analytical method	5.266×10^3	0.286	19.053
DAM	5.266×10^3	0.286	19.053
ϵ_{DAM} (%)	0.000	0.000	0.000
FEM	5.230×10^3	0.287	19.297
ϵ_{FEM} (%)	0.684	0.367	1.280

velocity and acceleration occur at the point $(a/2, b)$ in free edge (F). As can be seen from Table 3, the results calculated by DAM are consistent with the analytical ones, but FEM produces greater errors because of its inaccurate representation for input PSD. Consequently, the proposed DAM is flexibly applicable to stochastic excitations with more complex PSD function.

6. Conclusions

The exact analytical benchmark solutions of random vibration for rectangular thin plate with simply supported, clamped and free boundary conditions are not available in the literature to the authors' knowledge. In this paper, firstly, the analytical PSD functions of stationary random vibration for rectangular plate are derived. The analytical method incorporates the exact solution of free vibration of the 6 cases with one opposite simply supported boundary condition (e.g., SSSS, SSSC, SCSF, SFSF, SSSF and SCSF) and performs a large number of symbol operations based on PEM which takes a lot of computing time. Further, by discretizing the modal coordinate and frequency domain, the discrete analytical method is proposed to efficiently obtain the exact solutions of stochastic responses for rectangular thin plate subjected to stationary random excitation. Those exact solutions can be taken as benchmark solution to verify numerical methods.

Numerical examples are performed to demonstrate the high precision and efficiency of the proposed DAM. In addition, the influences

Table A

Exact frequency equations and the modal shape functions of rectangular plate under 6 boundary conditions ($\sqrt{\rho h \omega^2 / D} > \mu^2$).

Boundary condition	Frequency equation	Mode shape function
SSSS	$\sin \lambda_1 b = 0$	$\phi(x, y) = \sin \lambda_1 y \sin \mu x$
SCSC	$2\lambda_1 \lambda_2 (\cos \lambda_1 b \cosh \lambda_2 b - 1) + (\lambda_1^2 - \lambda_2^2) \sin \lambda_1 b \sinh \lambda_2 b = 0$	$\phi(x, y) = (A_1 \cos \lambda_1 y + A_2 \sin \lambda_1 y + A_3 \cosh \lambda_2 y + A_4 \sinh \lambda_2 y) \sin \mu x$ $A_1 = \lambda_1 \sinh \lambda_2 b \sin \lambda_1 b; \quad A_2 = \lambda_2 (\cos \lambda_1 b - \cosh \lambda_2 b)$ $A_3 = -A_1; \quad A_4 = -\lambda_1 / \lambda_2 A_2$
SSSC	$\lambda_2 \tan \lambda_1 b = \lambda_1 \tanh \lambda_2 b$	$\phi(x, y) = (A_1 \cos \lambda_1 y + A_2 \sin \lambda_1 y + A_3 \cosh \lambda_2 y + A_4 \sinh \lambda_2 y) \sin \mu x$ $A_1 = A_3 = 0; \quad A_2 = -\sinh \lambda_2 b; \quad A_4 = \sin \lambda_1 b$
SFSF	$\{\lambda_2^2 [(k/\mu)^2 - (1-\nu)]^4 - \lambda_1^2 [(k/\mu)^2 + (1-\nu)]^4\} \sin \lambda_1 b \sinh \lambda_2 b = 2\lambda_1 \lambda_2 [(k/\mu)^4 - (1-\nu)^2]^2 (\cos \lambda_2 b \cosh \lambda_1 b - 1)$	$\phi(x, y) = (A_1 \cos \lambda_1 y + A_2 \sin \lambda_1 y + A_3 \cosh \lambda_2 y + A_4 \sinh \lambda_2 y) \sin \mu x$ $A_1 = \{\lambda_1 [(k/\mu)^2 + (1-\nu)]^2 \sinh \lambda_2 b - \lambda_2 [(k/\mu)^2 - (1-\nu)]^2 \sin \lambda_1 b\} [(k/\mu)^2 + (1-\nu)]$ $A_2 = -\lambda_2 (\cosh \lambda_2 b - \cos \lambda_1 b) [(k/\mu)^4 - (1-\nu)^2] [(k/\mu)^2 - (1-\nu)]$ $A_3 = \frac{(k/\mu)^2 - (1-\nu)}{(k/\mu)^2 + (1-\nu)} A_1; \quad A_4 = \frac{\lambda_1 [(k/\mu)^2 + (1-\nu)}{\lambda_2 [(k/\mu)^2 - (1-\nu)]} A_2$
SSSF	$\lambda_2 [(k/\mu)^2 - (1-\nu)]^2 \tan \lambda_1 b = \lambda_1 [(k/\mu)^2 + (1-\nu)]^2 \tan h \lambda_2 b$	$\phi(x, y) = (A_1 \cos \lambda_1 y + A_2 \sin \lambda_1 y + A_3 \cosh \lambda_2 y + A_4 \sinh \lambda_2 y) \sin \mu x$ $A_1 = 0; \quad A_2 = [(k/\mu)^2 + (1-\nu)] \sinh \lambda_2 b$ $A_3 = 0; \quad A_4 = (k/\mu)^2 - (1-\nu)$
SCSF	$2\lambda_1 \lambda_2 [(k/\mu)^4 - (1-\nu)^2] + 2\lambda_1 \lambda_2 [(k/\mu)^4 + (1-\nu)^2] \cos \lambda_1 b \cosh \lambda_2 b + (\lambda_2^2 - \lambda_1^2) \sin \lambda_1 b \sinh \lambda_2 b \times [(k/\mu)^4 (1-2\nu) - (1-\nu)^2] = 0$	$\phi(x, y) = (A_1 \cos \lambda_1 y + A_2 \sin \lambda_1 y + A_3 \cosh \lambda_2 y + A_4 \sinh \lambda_2 y) \sin \mu x$ $A_1 = -\lambda_1 [(k/\mu)^2 + (1-\nu)] \sinh \lambda_2 b + \lambda_2 [(k/\mu)^2 - (1-\nu)] \sin \lambda_1 b;$ $A_2 = \lambda_2 [(k/\mu)^2 + (1-\nu)] \cosh \lambda_2 b + [(k/\mu)^2 - (1-\nu)] \cos \lambda_1 b;$ $A_3 = -A_1; \quad A_4 = -A_2 \lambda_1 / \lambda_2$

of boundary conditions and frequency range of excitation on the acceleration response PSD and the rms of the responses are investigated. Computational results show that the first-order mode dominates the acceleration response. For stationary filtered white noise excitation called as the modified Kanai–Tajimi spectrum model, DAM also obtains the exact benchmark solutions identical with the analytical solutions and possesses good applicability, while FEM presents some numerical errors.

Finally, it is pointed out that, the proposed DAM can be extended to obtain the benchmark solutions of the thin or middle-thick plate subjected to the point and surface stationary random excitation or the non-stationary random excitation, which will be studied in future.

Acknowledgments

The supports of the National Natural Science Foundation of China (Grant Nos. 51478086 and 11772079) and the National Key Research Development Program of China (Grant No. 2016YFB0201601) are gratefully acknowledged.

Appendix

See Table A.

References

- [1] Y.K. Lin, Nonstationary response of continuous structures to random loading, *J. Acoust. Soc. Am.* 35 (1963) 222–227.
- [2] S.H. Crandall, L.E. Wittig, Chladni's patterns for random vibration of a plate, in: G. Herrmann, N. Perrone (Eds.), *Dynamic Response of Structures*, Pergamon Press, New York, 1972.
- [3] S.H. Crandall, Random vibration of one-and two-dimensional structures, in: R. Krishnaiah (Ed.), *Developments in Statistics*, vol.2, Academic Press, New York, 1979.
- [4] F. Franco, S. De Rosa, E. Ciappi, Numerical approximations on the predictive responses of plates under stochastic and convective loads, *J. Fluids Struct.* 42 (2013) 296–312.
- [5] S. De Rosa, F. Franco, E. Ciappi, A simplified method for the analysis of the stochastic response in discrete coordinates, *J. Sound Vib.* 339 (2015) 359–375.
- [6] A.H. Hosseinloo, F.F. Yap, N. Vahdati, Analytical random vibration analysis of boundary-excited thin rectangular plates, *Int. J. Struct. Stab. Dyn.* 13 (2013) 1250062.
- [7] S.H. Crandall, A. Yildiz, Random vibration of beams, *J. Appl. Mech.* 29 (1962) 267–275.
- [8] K. Itao, S. Crandall, Wide-band random vibration of circular plates, *J. Mech. Des.* 100 (1978) 690–695.
- [9] S.H. Crandall, W.Q. Zhu, Wide band random vibration of an equilateral triangular plate, *Probab. Eng. Mech.* 1 (1986) 5–12.
- [10] S.H. Crandall, Modal-sum and image-sum procedures for estimating wide-band random response of structures, *Probab. Eng. Mech.* 8 (1993) 187–196.
- [11] I. Elishakoff, On the role of cross-correlations in the random vibrations of shells, *J. Sound Vib.* 50 (1977) 239–252.
- [12] I. Elishakoff, A.T. Van Zanten, S.H. Crandall, Wide-band random axisymmetric vibration of cylindrical shells, *J. Appl. Mech.* 46 (1979) 417–422.
- [13] I. Elishakoff, B. Ducreux, Dramatic effect of cross-correlations in random vibration of point-driven spherically curved panel, *Arch. Appl. Mech.* 84 (2014) 473–490.
- [14] I. Elishakoff, R. Santoro, Random vibration of a point-driven two-span beam on an elastic foundation, *Arch. Appl. Mech.* 84 (2014) 355–374.
- [15] D.E. Newland, *An Introduction To Random Vibrations, Spectral and Wavelet Analysis*, Longman Scientific and Technical, Essex, England, 1993.
- [16] E.L. Wilson, A. Der Kiureghian, E. Bayo, A replacement for the SRSS method in seismic analysis, *Earthq. Eng. Struct. Dyn.* 9 (1981) 187–192.
- [17] J.H. Lin, A fast CQC algorithm of PSD matrices for random seismic responses, *Comput. Struct.* 44 (1992) 683–687.
- [18] J.H. Lin, W. Zhang, F.W. Williams, Pseudo-excitation algorithm for nonstationary random seismic responses, *Eng. Struct.* 16 (1994) 270–276.
- [19] J.H. Lin, Y. Zhao, Y.H. Zhang, Accurate and highly efficient algorithms for structural stationary/non-stationary random responses, *Comput. Methods Appl. Mech. Engrg.* 191 (2001) 103–111.
- [20] J.H. Lin, Y.H. Zhang, Y. Zhao, Pseudo excitation method and some recent developments, *Procedia Eng.* 14 (2011) 2453–2458.
- [21] T.J.R. Hughes, *The Finite Element Method: Linear Static and Dynamic Finite Element Analysis*, Dover Publications Inc., New York, 2000.
- [22] A.W. Leissa, *Vibration of plates*, in: NASA SP-160, NASA Special Publication, 1969.
- [23] A.W. Leissa, M.S. Qatu, *Vibration of Continuous Systems*, McGraw-Hill Inc., New York, 2011.
- [24] T. Rock, E. Hinton, Free vibration and transient response of thick and thin plates using the finite element method, *Earthq. Eng. Struct. Dyn.* 3 (1974) 51–63.
- [25] G. Aksu, R. Ali, Free vibration analysis of stiffened plates using finite difference method, *J. Sound Vib.* 48 (1976) 15–25.
- [26] M. Cheung, M. Chan, Static and dynamic analysis of thin and thick sectorial plates by the finite strip method, *Comput. Struct.* 14 (1981) 79–88.
- [27] D. Nardini, C.A. Brebbia, A new approach to free vibration analysis using boundary elements, *Appl. Math. Model.* 7 (1983) 157–162.
- [28] C.W. Bert, M. Malik, The differential quadrature method for irregular domains and application to plate vibration, *Int. J. Mech. Sci.* 38 (1996) 589–606.
- [29] R.B. Bhat, Natural frequencies of rectangular plates using characteristic orthogonal polynomials in Rayleigh-Ritz method, *J. Sound Vib.* 102 (1985) 493–499.
- [30] D.J. Gorman, Free vibration analysis of the completely free rectangular plate by the method of superposition, *J. Sound Vib.* 57 (1978) 437–447.
- [31] Y.M. Liu, R. Li, Accurate bending analysis of rectangular plates with two adjacent edges free and the others clamped or simply supported based on new symplectic approach, *Appl. Math. Model.* 34 (2010) 856–865.
- [32] R. Li, Y. Zhong, B. Tian, On new symplectic superposition method for exact bending solutions of rectangular cantilever thin plates, *Mech. Res. Commun.* 38 (2011) 111–116.
- [33] Y.L. Xu, W.S. Zhang, J.M. Ko, J.H. Lin, Pseudo-excitation method for vibration analysis of wind-excited structures, *J. Wind Eng. Ind. Aerodyn.* 83 (1999) 443–454.
- [34] J.J. Wijker, *Random Vibrations in Spacecraft Structures Design: Theory and Applications*, Springer, New York, 2009.
- [35] D.X. Yang, J.L. Zhou, A stochastic model and synthesis for near-fault impulsive ground motions, *Earthq. Eng. Struct. Dyn.* 44 (2015) 243–264.